NASA Technical Memorandum 87663

High Reynolds Number Tests of a Douglas DLBA 032 Airfoil in the Langley 0.3-Meter Transonic Cryogenic Tunnel

Charles B. Johnson, David A. Dress,
and Acquilla S. Hill
Langley Research Center
Hampton, Virginia

Peter A. Wilcox and Minh H. Bui
Douglas Aircraft Company
Long Beach, California

National Aeronautics
and Space Administration

**Scientific and Technical
Information Branch**

1986

Use of trademarks or names of manufacturers in this report does not constitute an official endorsement of such products or manufacturers, either expressed or implied, by the National Aeronautics and Space Administration.

SUMMARY

In a cooperative effort with the U.S. manufacturers of large transport aircraft, NASA has conducted an extensive program to provide a systematic study of well-known conventional and advanced-technology airfoil design concepts over a wide range of Reynolds numbers. This airfoil program, referred to as the Advanced Technology Airfoil Test (ATAT) program, was conducted in the 8- by 24-inch two-dimensional test section of the Langley 0.3-Meter Transonic Cryogenic Tunnel (0.3-m TCT).

The results presented in this report are from a NASA/U.S. industry airfoil investigation conducted as a part of the ATAT program. The industry participant for this investigation was the Douglas Aircraft Company, and the airfoil tested was their DLBA 032. Test temperature was varied from 227 K (409°R) to 100 K (180°R) at pressures ranging from about 159 kPa (1.57 atm) to about 514 kPa (5.07 atm). Mach number was varied from 0.50 to 0.78. These variables provided a Reynolds number range (based on airfoil model chord) from 6.0×10^6 to 30.0×10^6. The tests were conducted with and without sidewall-boundary-layer removal, and removal rates varied from 1 to 2 percent of the test-section mass flow. This investigation was specifically designed to (1) test a Douglas airfoil from moderately low to flight-equivalent Reynolds numbers; and (2) systematically evaluate the effects of sidewall boundary interference by using the sidewall-boundary-layer removal system.

All the objectives of the investigation were met. The aerodynamic results are presented as integrated force and moment coefficients. These data show the expected changes in the airfoil characteristics with increasing Mach number, such as increased normal-force slope, increased drag force, and increased nose-down pitching moment. The data also show that increasing Reynolds number results in increased normal force, increased nose-down pitching moment, and, generally, decreased drag force. Additional data are included which show the effects of fixing transition and sidewall-boundary-layer removal. Model design, model structural integrity, and the overall test experience are discussed.

INTRODUCTION

Research on advanced-technology airfoils has been stimulated in recent years by the interest in developing energy-efficient transport aircraft for the subsonic flight regime. In support of this airfoil research, the National Aeronautics and Space Administration (NASA) has recently completed an extensive program to provide a systematic study of both conventional and advanced-technology airfoil concepts over a wide range of Reynolds numbers. This airfoil testing program, described in reference 1, is referred to as the Advanced Technology Airfoil Tests (ATAT). References 2 through 27 report some of the results obtained from other investigations during the ATAT program.

Much of the advanced-airfoil testing portion of the ATAT program has been carried out in cooperation with the U.S. aircraft industry. Three of the major U.S. manufacturers of large commercial transport aircraft (Boeing (ref. 5), Lockheed (ref. 10), and Douglas) have participated in the advanced-airfoil phase of the program by providing technical personnel, airfoil design concepts, and airfoil models. The overall objectives of the ATAT program are (1) to provide the industry

participants with the opportunity to test and compare their advanced airfoils with the latest NASA designs at high Reynolds numbers in the same facility; (2) to provide industry with experience in cryogenic wind-tunnel model design, construction, and testing techniques; (3) to expand the high Reynolds number airfoil data base; and (4) to provide each participant with the opportunity to evaluate their current level of airfoil technology.

The results presented in this report are from an investigation of a Douglas Aircraft Company (Douglas) advanced-technology airfoil conducted as part of the ATAT program. The model was designed and fabricated by Douglas, and some details of the model design, fabrication techniques, and operational experience are included herein. The tests were conducted in the Langley 0.3-Meter Transonic Cryogenic Tunnel (0.3-m TCT) with a two-dimensional 8- by 24-inch test section installed. A description of the design and operating characteristics of the facility are given in reference 28. Test total temperature was varied from 227 K (409°R) to 100 K (180°R) at pressures ranging from about 159 kPa (1.57 atm) to 514 kPa (5.07 atm). Mach number was varied from 0.50 to 0.78. The tests were conducted at Reynolds numbers (based on chord) of 6×10^6, 15×10^6, and 30×10^6. Sidewall-boundary-layer removal ranged from 1.0 to 2.0 percent of the test-section mass flow. Aerodynamic results are presented as integrated forces and moments. Detailed pressure distributions and airfoil coordinates are not included in this report.

The Douglas objectives of the ATAT program were somewhat different from other ATAT participants, because they already had experience in the testing of transonic airfoils at cryogenic conditions in the Douglas transonic, blowdown One-Foot (1-CWT) Cryogenic Wind Tunnel. (See ref. 29.) Also, they already had a good high Reynolds number data base on the airfoil selected for this ATAT program from extensive testing, with and without sidewall-boundary-layer removal, in the National Aeronautical Establishment (NAE) facility in Ottawa, Canada. Consequently, the Douglas ATAT program focused on evaluating sidewall-boundary-layer effects on transonic airfoil performance characteristics through a systematic variation of sidewall-boundary-layer removal. An interesting aspect to consider in the evaluation of sidewall-boundary-layer effects is that in the NAE facility the sidewall boundary layer is removed from around the model through a porous plate and turntable. (See ref. 30.) In the 0.3-m TCT, however, the sidewall boundary layer is removed from a porous plate upstream of the model. (See ref. 11.) Therefore, the results from the 0.3-m TCT have also been used to establish a data base to compare with the data base obtained for the same airfoil configuration in the NAE facility for the two different methods of sidewall-boundary-layer removal.

SYMBOLS

The measurements are presented in the International System of Units (SI), with the U.S. Customary Units in parentheses when needed for clarity.

BL boundary layer

b airfoil model span, 20.32 cm (8.0 in.)

c airfoil model chord, 15.24 cm (6.0 in.)

c_d section drag-force coefficient from wake measurements

c_m	section pitching-moment coefficient about model quarter-chord point
c_n	section normal-force coefficient from airfoil pressures
M	free-stream Mach number (downstream of perforated sidewall plates)
$\bar{M}$	mean value of Mach number for a given angle-of-attack polar (a polar is defined as an angle-of-attack sweep for nominally constant M, R, and $\dot{m}_{bl}$)
$\dot{m}_{bl}$	sidewall-boundary-layer removal, percent of test-section mass-flow rate
R	Reynolds number based on airfoil chord
x	chordwise distance from leading edge of model (positive measured aft), cm (in.)
y	spanwise distance from centerline of tunnel and model (positive measured toward right-hand side), cm (in.)
α	uncorrected angle of attack (positive measured from tunnel centerline up to airfoil reference line), deg
σ	standard deviation from mean value of Mach number $\bar{M}$
σ_m	maximum deviation from mean value of Mach number $\bar{M}$

WIND TUNNEL AND MODEL

Wind Tunnel

The tests of the Douglas Aircraft Company DLBA 032 airfoil were made in the 8- by 24-inch two-dimensional test section of the 0.3-Meter Transonic Cryogenic Tunnel (TCT). Figure 1(a) is a photograph of the tunnel, and figure 1(b) is a schematic of the tunnel. The passive system of boundary-layer removal is described in reference 3. A photograph of a typical test section setup with boundary-layer removal is shown in figure 2(a). In this photograph, the plenum lid and test-section ceiling have been removed to show the model installation. For the tests presented in this paper, the boundary-layer rakes shown in figure 2(a) were not installed. A side-view schematic of the test section is shown in figure 2(b), including the traversing survey probe which holds the momentum rake. This tunnel is a continuous-flow, fan-driven, transonic tunnel which uses nitrogen gas as the test medium. For this test, 5-percent open-slotted walls were installed on the floor and ceiling to reduce model blockage. The tunnel is capable of operating at stagnation temperatures from about 80 K (144°R) to about 327 K (589°R) and stagnation pressures from slightly greater than 101.3 kPa (1 atm) to 607.8 kPa (6 atm). Test-section Mach number can be varied from about 0.2 to 0.85. The ability to operate at cryogenic temperatures and 607.8 kPa (6 atm) pressure provides an extremely high Reynolds number capability at relatively low model loadings.

The two-dimensional test section contains computer-driven angle-of-attack and momentum-rake systems. The angle-of-attack system is capable of varying the angle of attack over a range of about 40°. The momentum rake, located just downstream of the airfoil (see fig. 2(b)), provides up to five total-pressure measurements across

half the width of the tunnel. These pressures are converted to drag levels and provide a mechanism for determining the extent of two-dimensionality in the flow. The momentum-rake system is designed to traverse automatically through the wake, determine the boundaries of the wake, and then step through the wake at a selected rate and number of steps. Both the angle-of-attack and momentum-rake systems have a manual override capability. Additional design features and characteristics regarding the cryogenic-tunnel concept, in general, and the 0.3-m TCT, in particular, are presented in references 28 and 31 through 33.

Model

The airfoil model used in this test was a 12.28-percent-thick supercritical airfoil with a chord of 15.24 cm (6.0 in.). The model was designed and fabricated by Douglas in accordance with NASA aerodynamic and structural requirements for the ATAT program models. Aerodynamic tolerances as specified by the ATAT program were generally satisfied with airfoil contour accuracies of ±0.00254 cm (0.0010 in.), a surface finish of 1.016×10^{-4} mm (4.0×10^{-6} in.) root mean square, and closely spaced chordwise distribution static-pressure orifices. The structural requirements were satisfied for the specified model chord and span dimensions. A material was selected that was cryogenically acceptable, with safety factors of at least 3 at all operating conditions and Charpy impact strengths greater than 93.55 J (69.00 ft-lbf).

Instrumentation in the airfoil model included 76 static-pressure orifices distributed in 3 chordwise rows near the midspan, 15 spanwise pressures distributed in 3 spanwise rows (see table 1), and 19 thermocouples (see table 2) distributed throughout the airfoil. The thermocouples were used to ensure that model temperatures had stabilized prior to taking data. Figure 3 is a schematic which indicates the locations of the orifices and thermocouples. A photograph of the Douglas model installed in the sidewall inserts of the 0.3-m TCT test section is shown in figure 4.

Model fabrication.- The model was fabricated at Douglas from Armco Nitronic 40 stainless steel, a cryogenically acceptable material. Two-piece construction was used with the split line of the two halves beginning at a point approximately 5 percent aft of the leading edge on the lower surface and bisecting the trailing edge. The contouring was performed in stages to allow for material stabilization and to reduce the possibility of model distortion. A wire EDM (electrical discharge machining) process was utilized because of the excellent accuracies provided by this method. Thermal cycling of the model in liquid nitrogen and surface inspection prior to and following rough EDM machining was performed. Instrumentation grooves and trenches for the pressures and thermocouples were then EDM machined in the separated pieces. Figure 5 is a photograph of the inside surfaces of the model at this stage of construction. The next steps were to temporarily bolt the halves together with the 3M Company EC-2216 B/A adhesive used to bond the trailing-edge section of the model. The final airfoil contour was EDM machined to 0.00254 cm (0.001 in.) and hand polished to the required finish. The model parts were again separated, holes for the pressure orifices were drilled, and the instrumentation was installed. Pressure tubing, with a 0.0787-cm (0.0031-in.) outside diameter, was located inside the trenches and glued in place with Dexter Corporation Hysol 9309, a cryogenically acceptable epoxy. In the final assembly, the two halves were bolted together using Loctite Corp. Locklite 262 (RED) on the threads, and EC-2216 B/A adhesive was used to bond the trailing-edge joint. The exposed bolt holes on the lower surface were filled with a mixture of Hysol 9309 and type S-100 carbospheres (100-μm diameter carbon powder purchased from Versar Manufacturing, Inc.).

Model stress analysis.- The Douglas stress analysis used a conservative loading distribution based on a maximum model normal force of 6672 N (1500 lbf). Stress calculations in the various critical regions were performed for ambient-temperature model conditions (conservative) and accounted for stress concentration factors using Nitronic 40 material properties. Classical structural analysis methods were used, which resulted in safety factors of three or greater. Consideration was also given to the cryogenic effects on the shear pins and mechanical fasteners used in the assembly of the model. Results indicated satisfactory compliance with safety factors for the temperature range to be tested. The decambering effect of trailing-edge movement under load was calculated to be 0.00762 cm (0.0030 in.); therefore, extensive aeroelastic studies during the wind-tunnel test were considered unnecessary.

Model accuracy and integrity.- Contour inspection of the model was performed with a Zeiss coordinate measuring machine. The contour was generally within the specified tolerance near the centerline of the model, with the exception of two extreme points which measured within 0.00508 cm (0.0020 in.) and -0.00381 cm (-0.0015 in.) of the nominal airfoil contour. Seven spanwise inspection stations were chosen with 33 chordwise locations inspected on each of the upper and lower surfaces. The locations of the pressure orifices, with diameters of 0.0432 cm (0.017 in.), were also found using the Zeiss machine. The surface finish was measured with a profilometer as 1.016×10^{-4} mm (4.0×10^{-6} in.) root mean square.

Prior to installation in the tunnel, the model was "cryocycled" three times from ambient to cryogenic temperatures and back at a rate similar to actual operating conditions in the 0.3-m TCT. The thermocouple located midspan at the leading edge was used to determine model temperature equilibrium during the test. The "cryocycling" did not alter the shape of the model and indicated that the model was acceptable for cryogenic testing.

TEST APPARATUS AND PROCEDURES

Test Instrumentation and Apparatus

A detailed discussion of the instrumentation and procedures selected for the calibration and control of the 0.3-m TCT can be found in reference 28. For two-dimensional airfoil tests, the 0.3-m TCT is equipped to measure static pressures on the airfoil model surface, total pressures in the model wake, and static pressures on the test-section sidewalls, floor, and ceiling. The pressures are measured with individual transducers, except for the tunnel floor and ceiling pressures, which are measured with a scanning valve system. Because of the large changes in the pressure of the tunnel over its operational range, commercially available, high-precision, variable-capacitance pressure transducers are used instead of conventional strain-gauge pressure transducers. For airfoil model tests, the data are derived from (1) the pressure distributions around the airfoil model, (2) the definition of the wake defect, and (3) the corresponding angle of attack.

Airfoil model pressures.- The pressures on the airfoil model are measured by individual transducers connected to tubing from each orifice on the model. The pressure transducers are located adjacent to the test section in order to reduce response time. To provide increased accuracy, the transducers are mounted on thermostatically controlled heater bases to maintain a constant temperature and on "shock" mounts to reduce possible vibration effects. The electrical outputs from the transducers are connected to individual signal conditioners located in the tunnel control

room. The signal conditioners have autoranging capability and have seven ranges available. As a result of the autoranging capability, the analog electrical output to the data acquisition system is kept at a high level, even though the pressure transducer may be operating at the low end of its range. The maximum range of these differential transducers is about ±689 kPa (±6.8 atm) with an accuracy of ±0.25 percent of the reading from -25 percent to 100 percent full scale.

Wake pressures.- A vertically traversing survey mechanism is located on the left sidewall of the two-dimensional test section downstream of the turntables. The primary purpose of this mechanism is to move a total-pressure probe rake through the airfoil wake to survey the total pressures within the wake. Details of this survey rake are shown in figure 6. The survey mechanism has a maximum traversing range of 25.4 cm (10 in.), 17.78 cm (7.0 in.) above the tunnel centerline and 7.62 cm (3.0 in.) below the centerline. The rake support can be located with the measurement plane of the rake either at tunnel station 21.0 cm (8.3 in.) or at 26.0 cm (10.2 in.). For this test, the wake survey measurements were made at the 26.0-cm (10.2-in.) station, which placed the measurement plane about 1.2 chord lengths downstream of the airfoil trailing edge. The survey mechanism is driven by an electric stepper motor and is designed to operate at speeds from about 0.25 cm/sec (0.1 in./sec) to about 15 cm/sec (6 in./sec). The stroke (that portion of the total traversing range used in a given survey) and speed of the survey mechanism can be controlled from the operator's panel in the control room to suit the research requirements. The vertical position of the rake is recorded using the output from a digital shaft encoder geared to the survey mechanism. The active total-pressure probes are located on the survey rake at five spanwise stations: $y(b/2) = 0.0$, -0.125, -0.375, -0.500, and -0.750. Nine tunnel sidewall static-pressure taps are also provided in the measurement plane of the rake. Data from the static taps are used in the determination of the momentum loss, which is used to calculate airfoil drag coefficient, based on the method outlined in reference 34. More sensitive individual differential pressure transducers, with a maximum range of ±137.8 kPa (±1.36 atm) (of the variable capacitance type described previously), are used on each tube on the survey rake and for each of the sidewall taps.

Angle of attack.- The angle-of-attack mechanism has a traversing range of ±20°, which can be offset from 0° in either direction at model installation. The mechanism is driven by an electric stepper motor, which is connected through a yoke to the perimeter of both turntables. This arrangement drives both ends of the model through the angle-of-attack range to eliminate possible model twisting. The angular position of the turntables and, therefore, the angle of attack of the model are recorded using the output from a digital shaft encoder geared to one of the turntables.

Sidewall-boundary-layer removal.- A passive boundary-layer removal system (see figs. 1, 2, and 7) was operated with the discharge from each sidewall exhausted directly to the atmosphere. In the passive mode of operation, the test-section static pressure must be at least 15 percent higher than the ambient pressure, and the maximum rate of mass that can be removed is limited to the rate of liquid nitrogen that is being injected into the tunnel in order to maintain a steady operating condition. The perforated plates (figs. 2(a) and 7) that are used to remove the sidewall boundary layer are fitted flush on both sidewalls and are located upstream of the model. The plates currently in use have a nominal porosity of about 10 percent. The holes are electron-beam drilled and have a nominal diameter of 0.275 mm (0.011 in.) and spacing of 0.75 mm (0.030 in.). The surfaces of the perforated plates are etched and polished to obtain a smooth surface. This surface preparation and fabrication technique ensured that there was no appreciable thickening of the boundary layer over the perforated plate compared with boundary-layer growth over

the more frequently used solid plates. Precise control of the rate of sidewall-boundary-layer removal by the passive system (see figs. 1, 2, and 7) is possible with the two digital valves and their associated controls. Each of the two digital valves (fig. 7(b)) consists of a number of different sized calibrated binary sonic nozzles operating in either an open or closed mode. The sonic nozzles are used in appropriate combinations to give the required flow rate. The 11-bit digital valves have a resolution of 0.05 percent and are microprocessor controlled. The microprocessor maintains a constant mass removal through the perforated plates at a level specified by command set points. Each of the digital valves can be driven to a command set point by a feedback control loop which sets the mass flow in terms of either actual rate of flow or percent of the test-section mass flow. The tunnel total pressure, static pressure, and total temperature are put into the microprocessor to determine the test-section mass-flow rate. The mass-flow rate through the digital valves is determined by the microprocessor from an input of the inlet total pressure and temperature from each of the two digital valves. The pressure at the junction of the two discharge lines from the digital valves is also input to the microprocessor to make sure that there is an adequate pressure drop (at least 15 percent) across the digital valve to have sonic flow through the nozzle element.

Test Program

The nominal test conditions used in this investigation are summarized in table 3 in terms of Mach number, Reynolds number, percent sidewall-boundary-layer removal, and free or fixed transition. The Mach number and Reynolds number for these tests were selected from a limited Mach number, Reynolds number calibration at various levels of sidewall-boundary-layer removal. The calibration procedure with sidewall-boundary-layer removal is described in reference 16. The level of the sidewall removal for this investigation was selected at either 1.0 percent of the test-section mass-flow rate or at the maximum mass-flow rate available for the given test condition. The extent of the effort to establish the effects of Mach number, Reynolds number, sidewall-boundary-layer removal, and transition (fixed and free) can be seen from table 3.

Test Procedures

Pressure data.- For the results reported herein, airfoil static-pressure data were taken in 1 second while the drag rake was in its first position. During the 1 second, pressures from individual transducers for each orifice on the model were sampled 20 times and averaged to obtain the airfoil pressures. Also, 20 samples of total-pressure (wake-rake) data were taken and averaged at the first rake position. For each succeeding rake position (vertical), the procedure for the rake data was repeated. When the wake rake was stepped to a new position, a 0.5-second delay was followed by the 1-second averaging period. Typically, for each angle of attack at each test condition, the rake was stepped in 75 increments through the wake. To provide an optimum definition of the model wake, the vertical stroke of the rake (the distance traversed to define the wake) and number of steps within the stroke can be changed for each test condition, such as angle of attack or Mach number. For this test, the number of steps within the stroke was held constant at 75. However, the stroke was changed as required to survey the entire wake.

Transition.- Transition strips were attached to the upper and lower surfaces during the final portion of the test program to evaluate their effect on the aerodynamic characteristics of the model. The transition strips were sized for a chord

Reynolds number of 6×10^6 but were small enough to be used for a Reynolds number of 15×10^6. The strips consisted of 0.041-mm (0.0016-in.) diameter glass microbeads placed in a 3.175-mm (0.125-in.) wide strip located along the 5-percent chord line. Bonding of the glass beads to the model surface was accomplished with a clear acrylic spray adhesive, which was applied before and after the placement of the beads.

DATA REDUCTION AND QUALITY

0.3-m TCT Data Acquisition System

For the present study, data were recorded on magnetic tape with a computer-controlled high-speed digital data acquisition system located in the control room of the 0.3-m TCT. This system has a total of 192 analog channels with five selectable ranges from 8.191 mV to 131 mV and a resolution of 1 part in 8191. All analog data were filtered with a 10-Hz low-pass filter. An operating and acquisition program is used by the computer to scan the data acquisition hardware and to write the raw data on tape.

Through the use of a separate "real-time" program, visual displays of Mach number, Reynolds number, stagnation pressure, and other flow and tunnel parameters are provided on LED readouts on the tunnel control panel and on a color CRT. This real-time program provides many on-line data reduction functions, such as correcting Mach number for real-gas effects and tunnel calibration and calculating the local pressure ratios and pressure coefficients, which are then integrated around the airfoil to determine values of c_n and c_m. Values of c_d are computed on-line by integrating the total head loss through the model wake. Local pressure coefficients, local pressure ratios, local Mach numbers, total head loss through the model wake, and model aerodynamic coefficients (c_n, c_d, and c_m) can be displayed graphically on an intelligent graphics terminal interfaced with the computer. This information can then be sent to a plotter/printer which produces hard copies.

Data Reduction

As mentioned in the preceding section, Mach number is corrected for real-gas effects and tunnel calibration. Real-gas effects are included in the data reduction process using the thermodynamic properties of nitrogen gas calculated from the Beattie-Bridgeman equation of state. This equation of state has been shown in reference 35 to give essentially the same thermodynamic properties and flow calculation results, in the temperature-pressure regime of the 0.3-m TCT, as are given by the more complicated Jacobsen equation of state. Detailed discussions of real-gas effects when testing in cryogenic nitrogen are contained in references 36 and 37. The test Mach number is based on the average longitudinal Mach number distributions measured as a function of Reynolds number during the calibration of the "empty" test section.

Normal-force and pitching-moment coefficients are calculated from numerical integrations of the pressures around the surface of the model. Drag coefficient is obtained from the wake survey pressures by computing an incremental or point drag coefficient using the method of reference 34. These point drag coefficients are then integrated across the model wake to obtain the drag coefficient. A typical survey plot of the wake-rake measurements displays the incremental drag as a function of survey width. (See fig. 3 in ref. 38.) Generally, the base levels of these curves do not coincide with the zero axis; therefore, a correction method is used to

account for this zero shift. This method generates corrected drag coefficients referred to as CDCOR1 to CDCOR5 in reference 38. The corrected drag coefficients are used in the discussions of spanwise drag data in this report. For a given test condition, the corrected drag coefficient obtained from the tunnel centerline tube ($y/(b/2) = 0$) is assumed to be the drag coefficient for the airfoil at that condition. The results from the data reduction process are presented in table 4.

Data Quality

Mach number fluctuations.- In transonic wind-tunnel testing, the ability to maintain a constant Mach number as well as constant tunnel stagnation conditions has direct bearing on the quality of the final aerodynamic data. With individual pressure transducers on each of the model pressure orifices, and with all the model data being recorded in 1 second at the first rake step, Mach number fluctuations in the model data are virtually nonexistent. However, the possibility of some Mach number fluctuations during the time required for the 75 steps of the wake survey does exist. The Mach numbers and Reynolds numbers presented in table 4 are tabulated with increasing Reynolds number and increasing Mach number. All values of Mach number and Reynolds number were averaged from the 75 steps through the wake survey. To statistically determine the variation of Mach number, the mean, standard deviation, and maximum deviation of the Mach number are presented in table 4 for each polar (i.e., angle-of-attack sweep at a constant nominal Mach number, Reynolds number, and sidewall removal condition). The nominal test conditions are given in table 3. In general, the mean value of Mach number (for a polar) was within ±0.002 or less of the nominal Mach number, and the standard deviation of Mach number for a given polar was about 0.002. In only a few instances did the maximum deviation go as high as ±0.005; it was generally on the order of ±0.002.

Repeatability of data.- Two examples illustrating the ability to repeat the Mach number, normal-force, pitching-moment, and axial-force coefficients at a nominal Mach number of 0.730 and Reynolds number of 15×10^6 are shown in figures 8 and 9. In general, the repeatability of data is good for c_n and c_m for all angles of attack. For these conditions, the repeatability of c_d is good up to a c_n of about 0.7; however, above this value of c_n, the c_d is not as repeatable. The repeatability of the Mach number is as expected, based on typical tabular data of Mach number from previous tests. (See ref. 5.)

PRESENTATION OF RESULTS

The experimental data are presented with no corrections for wall interference effects due to the top and bottom slotted walls or to the sidewalls. A correction procedure that can be used to account for wall interference is described in reference 23 and includes some typical corrected results from other tests in the 0.3-m TCT. An outline of the plotted aerodynamic coefficient data presented herein is given below, along with the applicable figure references. The variation of Mach number is also presented in the figures that show the effect of free and fixed transition, Reynolds number, and sidewall-boundary-layer removal and is included to aid in assessing these effects on the basic aerodynamic characteristics of the airfoil. Caution should be used in placing much significance on the results at a high normal-force coefficient, where separation may be present on the model at the shock wave and possibly near the trailing edge. This separation may result in a deterioration of the two-dimensionality of the flow. In addition, at these conditions, the effects of tunnel sidewall-boundary-layer separation may be present.

Figure

Repeatability of data:
M ≈ 0.730; R ≈ 15.0 × 10^6; $\dot{m}_{bl}$ = 0; fixed transition 8
M ≈ 0.730; R ≈ 15.0 × 10^6; $\dot{m}_{bl}$ = 0; free transition 9

Spanwise drag (with free transition) for several Mach numbers:
R ≈ 6.0 × 10^6; $\dot{m}_{bl}$ = 0 10
R ≈ 15.0 × 10^6; $\dot{m}_{bl}$ = 0 11
R ≈ 30.0 × 10^6; $\dot{m}_{bl}$ = 0 12

Spanwise drag (with free transition) for several Reynolds numbers:
M ≈ 0.500; $\dot{m}_{bl}$ = 0 13
M ≈ 0.600; $\dot{m}_{bl}$ = 0 14
M ≈ 0.700; $\dot{m}_{bl}$ = 0 15
M ≈ 0.730; $\dot{m}_{bl}$ = 0 16
M ≈ 0.750; $\dot{m}_{bl}$ = 0 17
M ≈ 0.765; $\dot{m}_{bl}$ = 0 18
M ≈ 0.780; $\dot{m}_{bl}$ = 0 19

Effect of sidewall-boundary-layer removal on spanwise drag (with free transition) for several Mach numbers:
R ≈ 15.0 × 10^6 20
R ≈ 30.0 × 10^6 21

Spanwise drag for free and fixed transition for several Mach numbers:
R ≈ 6.0 × 10^6; $\dot{m}_{bl}$ = 0 22
R ≈ 15.0 × 10^6; $\dot{m}_{bl}$ = 0 23

Effect of fixing transition on aerodynamic characteristics of airfoil:
M ≈ 0.600; R ≈ 6.0 × 10^6; $\dot{m}_{bl}$ = 0 24
M ≈ 0.700; R ≈ 6.0 × 10^6; $\dot{m}_{bl}$ = 0 25
M ≈ 0.730; R ≈ 6.0 × 10^6; $\dot{m}_{bl}$ = 0 26
M ≈ 0.750; R ≈ 6.0 × 10^6; $\dot{m}_{bl}$ = 0 27
M ≈ 0.765; R ≈ 6.0 × 10^6; $\dot{m}_{bl}$ = 0 28
M ≈ 0.780; R ≈ 6.0 × 10^6; $\dot{m}_{bl}$ = 0 29
M ≈ 0.730; R ≈ 15.0 × 10^6; $\dot{m}_{bl}$ = 0 30
M ≈ 0.765; R ≈ 15.0 × 10^6; $\dot{m}_{bl}$ = 0 31

Effect of Reynolds number on aerodynamic characteristics of airfoil with free transition:
M ≈ 0.500; $\dot{m}_{bl}$ = 0 32
M ≈ 0.600; $\dot{m}_{bl}$ = 0 33
M ≈ 0.700; $\dot{m}_{bl}$ = 0 34
M ≈ 0.730; $\dot{m}_{bl}$ = 0 35
M ≈ 0.750; $\dot{m}_{bl}$ = 0 36
M ≈ 0.765; $\dot{m}_{bl}$ = 0 37
M ≈ 0.780; $\dot{m}_{bl}$ = 0 38
M ≈ 0.600; $\dot{m}_{bl}$ = 1.0 39
M ≈ 0.700; $\dot{m}_{bl}$ = 1.0 40
M ≈ 0.730; $\dot{m}_{bl}$ = 1.0 41
M ≈ 0.750; $\dot{m}_{bl}$ = 1.0 42
M ≈ 0.765; $\dot{m}_{bl}$ = 1.0 43
M ≈ 0.780; $\dot{m}_{bl}$ = 1.0 44

Figure

Effect of Reynolds number on aerodynamic characteristics of airfoil with fixed transition:
$M \approx 0.730$; $\dot{m}_{bl} = 0$ 45
$M \approx 0.765$; $\dot{m}_{bl} = 0$ 46

Effect of Mach number on aerodynamic characteristics of airfoil with free transition:
$R \approx 6.0 \times 10^6$; $\dot{m}_{bl} = 0$ 47
$R \approx 15.0 \times 10^6$; $\dot{m}_{bl} = 0$ 48
$R \approx 30.0 \times 10^6$; $\dot{m}_{bl} = 0$ 49
$R \approx 15.0 \times 10^6$; $\dot{m}_{bl} = 1.0$ 50
$R \approx 15.0 \times 10^6$; $1.1 \leq \dot{m}_{bl} \leq 1.8$ 51
$R \approx 30.0 \times 10^6$; $\dot{m}_{bl} = 1.0$ 52

Effect of Mach number on aerodynamic characteristics of airfoil with fixed transition:
$R \approx 6.0 \times 10^6$; $\dot{m}_{bl} = 0$ 53
$R \approx 6.0 \times 10^6$; $\dot{m}_{bl} = 1.0$ 54
$R \approx 6.0 \times 10^6$; $\dot{m}_{bl} = 2.0$ 55
$R \approx 15.0 \times 10^6$; $\dot{m}_{bl} = 0$ 56

Effect of sidewall-boundary-layer removal on aerodynamic characteristics of airfoil with free transition:
$M \approx 0.600$; $R \approx 15.0 \times 10^6$ 57
$M \approx 0.700$; $R \approx 15.0 \times 10^6$ 58
$M \approx 0.730$; $R \approx 15.0 \times 10^6$ 59
$M \approx 0.750$; $R \approx 15.0 \times 10^6$ 60
$M \approx 0.765$; $R \approx 15.0 \times 10^6$ 61
$M \approx 0.780$; $R \approx 15.0 \times 10^6$ 62
$M \approx 0.600$; $R \approx 30.0 \times 10^6$ 63
$M \approx 0.700$; $R \approx 30.0 \times 10^6$ 64
$M \approx 0.730$; $R \approx 30.0 \times 10^6$ 65
$M \approx 0.750$; $R \approx 30.0 \times 10^6$ 66
$M \approx 0.765$; $R \approx 30.0 \times 10^6$ 67
$M \approx 0.780$; $R \approx 30.0 \times 10^6$ 68

Effect of sidewall-boundary-layer removal on aerodynamic characteristics of airfoil with fixed transition:
$M \approx 0.730$; $R \approx 6.0 \times 10^6$ 69
$M \approx 0.765$; $R \approx 6.0 \times 10^6$ 70

Effect of Reynolds number on variation of section drag coefficient with Mach number 71

Effect of sidewall-boundary-layer removal on variation of section drag coefficient with Mach number 72

DISCUSSION

Assessment of Two-Dimensionality of Flow

The wake survey rake shown in figure 6 is equipped with several spanwise total-pressure probes which enable an assessment of the airfoil model drag levels across the tunnel and provide an indication of the two-dimensionality of the flow over the model. All these data are shown in figures 10 through 23. In these figures, the zero value for $y/(b/2)$ is the centerline of the test section. The plots have been arranged to illustrate the effects of Mach number, Reynolds number, sidewall-boundary-layer removal, and transition (free or fixed) on the spanwise drag levels for various normal-force coefficients. Figures 10 through 12 show the effects of Mach number on the drag levels at three Reynolds numbers, all with no sidewall-boundary-layer removal and free transition. Figure 10 ($R \approx 6.0 \times 10^6$) indicates a nonuniform distribution for all levels of normal-force coefficient for Mach numbers greater than 0.6. At Reynolds number of 15.0×10^6 and 30.0×10^6 (figs. 11 and 12), the flow retains a two-dimensional character longer as the normal force and Mach number increase.

Figures 13 through 19 show the effects of Reynolds number on the spanwise drag levels for Mach numbers from 0.50 to 0.78 with no sidewall-boundary-layer removal. For the Mach numbers tested, the effects on the spanwise drag levels due to an increase in Reynolds number from 15.0×10^6 to 30.0×10^6 are not significant. However, there is noticeable improvement of the drag levels and trends when the Reynolds number increased from 6.0×10^6 to 15.0×10^6, especially at the lower values of normal-force coefficient.

Figures 20 and 21 show the effects of sidewall-boundary-layer removal on the drag levels for Reynolds numbers of 15.0×10^6 and 30.0×10^6, respectively, with free transition. In general, the boundary-layer removal did not affect the spanwise drag levels or trends except at the highest normal-force coefficients.

Figures 22 and 23 show the effects of fixing transition (free and fixed) on the drag levels with no sidewall-boundary-layer removal. In general, figure 22 ($R \approx 6.0 \times 10^6$) shows that fixing the transition resulted in a more uniform spanwise drag distribution for normal-force coefficients below about 0.80. Figure 23 ($R \approx 15.0 \times 10^6$) shows that fixing the transition had no effect on the two-dimensionality of the data except at the highest normal-force coefficient.

Effect of Fixing Transition

The effect of fixing transition with no sidewall-boundary-layer removal was examined over a Mach number range from 0.600 to 0.780 at a Reynolds number of 6.0×10^6 (figs. 24 through 29) and at Mach numbers of 0.730 and 0.765 at a Reynolds number of 15.0×10^6 (figs. 30 and 31). At a Mach number of 0.600 and $R \approx 6.0 \times 10^6$ (fig. 24), there is very little difference between the fixed- and free-transition normal force and pitching moment; however, the drag is somewhat higher for the free transition. These differences become more pronounced at the lower angle of attack as Mach number increases (figs. 25 through 29). In addition, there is an increase in the normal force and nose-down pitching moment for the free-transition data at all angles of attack. The reason for this behavior is not obvious from the data presented in the report. At a Reynolds number of 15.0×10^6, there is very little difference in drag. This slight difference indicates that the boundary layer is turbulent close to the leading edge of the airfoil.

Effect of Reynolds Number, Mach Number, and Sidewall-Boundary-Layer Removal on Basic Aerodynamic Characteristics

Figures 32 through 46 show the effects of Reynolds number (for each test Mach number and sidewall removal rate) on the basic aerodynamic characteristics of the airfoil. These results for free transition (figs. 32 through 44) exhibit a slight increase in both the normal force and nose-down pitching moment with increasing Reynolds number. The results for fixed transition (figs. 45 and 46) indicate a somewhat larger increase in normal force and nose-down pitching moment than was observed for the free-transition data for an increase in Reynolds number from 6.0×10^6 to 15.0×10^6. The longitudinal stability parameter (dc_m/dc_n) appears to be relatively insensitive to changes in Reynolds number. Increasing Reynolds number generally reduced the level of drag with the exception of some of the data at high lift conditions at higher Mach numbers.

In figures 47 through 56, the data have been plotted to show the effect of Mach number (at a given Reynolds number and sidewall removal rate) on the basic aerodynamic characteristic of the model. The data presented are representative of the trends seen in the normal force and pitching moment at all Reynolds numbers. The data indicate the usual increase in normal-force slope and nose-down pitching moment with increasing Mach number. In addition, it can be seen that stall occurs at progressively lower angles of attack for the two highest Mach numbers. For Mach numbers above 0.700, the slopes of the normal-force and pitching-moment curves become somewhat nonlinear above normal-force coefficients between 0.5 and 0.7. As the Mach number increases, there is a progressive increase in drag, and the greatest increase occurs at the higher Mach numbers associated with expected drag-rise effects. A comparison of figures 47 and 53 indicates that the increase in normal-force slope and nose-down pitching moment with increasing Mach number ($R \approx 6.0 \times 10^6$) is less with fixed transition than with free transition.

Figures 57 through 70 are representative of the effects of sidewall-boundary-layer removal (at a given Mach number and Reynolds number) seen on the aerodynamic data. The sidewall boundary layer was removed at a minimum level of 1.0 percent of the test-section mass flow. The higher levels of removal that were used for some conditions were the maximum sidewall removal that could be obtained at the particular Mach number and Reynolds number using the passive mode of removal. At a Mach number of 0.60, the normal force, pitching moment, and drag indicated virtually no effect of sidewall removal. At Mach numbers above 0.60, the effect of sidewall removal was to slightly decrease the normal force and slightly decrease the nose-down pitching moment above a normal-force coefficient of about 0.60. For Mach numbers above 0.730, the sidewall removal, in general, increases the drag level.

Figure 71 summarizes effects of Reynolds number and transition fixing on the variation of drag with Mach number for normal-force coefficients of 0.60, 0.70, and 0.80. In general, the results show the expected decrease in drag coefficient with increasing Reynolds number and the characteristic drag rise at the highest Mach number, particularly at normal-force coefficients of 0.70 and 0.80. The increase in drag coefficient which occurs between low Mach numbers and the drag rise is referred to as "drag creep." The drag creep is a complex phenomenon which is highly dependent on the boundary layer and its impact on the resulting aerodynamic shape of the airfoil. (See ref. 39.) The data for the two highest normal forces in figure 71 show an increased drag creep with decreasing Reynolds number above a Mach number of 0.70. An examination of pressure distributions indicates that this increase in drag at the low Reynolds numbers is a result of the reduced aft loading, which results in a stronger shock required for a fixed normal force. In addition, as the normal force

increases, the drag creep also increases and extends to higher Mach numbers. There is no discernible trend or effect of fixing transition at a Reynolds number of 15.0×10^6, where the flow is turbulent very close to the leading edge. However, at a Reynolds number of 6.0×10^6, fixing transition results in an increase in the rate of drag creep prior to drag divergence. This increase in drag creep could be the result of the elimination of aft-moving transition location with increasing Mach number. Without a means for determining the location of transition on the upper and lower surfaces of the airfoil, a precise cause for the increase in drag creep cannot be established.

A summary of the effects of sidewall-boundary-layer removal on the variation of drag with Mach number for three normal-force coefficients are illustrated in figure 72. The results in figure 72(a) at a Reynolds number of 6.0×10^6 are inconclusive. However, at Reynolds numbers of 15.0×10^6 and 30.0×10^6 (figs. 72(b) and 72(c)), particularly at the lower normal-force coefficient where sidewall-boundary-layer separation is not a factor, the drag level (above the drag-rise Mach number) obtained without sidewall removal is more favorable than those obtained with removal. This is an indication of the increase in the effective (i.e., uncorrected) Mach number when sidewall-boundary-layer removal is not used. This trend is not as clear at the higher normal-force coefficients because of possible sidewall-boundary-layer separation coincident with separation at the shock on the model (based on model pressure data) and perhaps even near the airfoil trailing edge.

Model Assessment

Model accuracies and surface finish are major considerations for the high Reynolds number conditions available in the cryogenic pressure wind tunnel. Therefore, a thorough assessment of the accuracy of the model contours and a quantitative definition of the model surface finish, both before and after the tests, are considered to be essential parts of the research program. The model performed well throughout the test, and no structural problems were encountered with the load-carrying components of the model. A post-test examination of the model indicated no change in the local hand-finished surface of the Hysol-carbon mixture used to fill each of the numerous lower-surface bolt and pin holes. A post-test Zeiss coordinate inspection of the model planform and contour revealed no deviations in shape as a result of repeated cryogenic cycling. The densely oriented static-pressure orifices and surface thermocouples worked without failure throughout the test, except for those orifices which were identified as being questionable prior to the beginning of the test. The glass-bead transition strip also performed adequately during the last phase of testing (i.e., fixed transition), although a post-test inspection revealed that portions of the strip had worn off. In general, the design and fabrication techniques used for this model were more than adequate for models being tested in a cryogenic environment.

CONCLUDING REMARKS

A wind-tunnel investigation, which represents the final NASA/U.S. industry two-dimensional airfoil study in the Advanced Technology Airfoil Tests (ATAT) program, has been conducted in the Langley 0.3-Meter Transonic Cyrogenic Tunnel. Integrated forces and moments are presented; however, pressure distributions are not presented. This investigation was designed to test a Douglas advanced-technology airfoil.

Douglas objectives in the program were somewhat different from other ATAT participants, since they had experience in testing transonic airfoils at cryogenic conditions in the pilot cryogenic wind tunnel at Douglas. In addition, they already had a high Reynolds number data base on this airfoil from extensive testing with sidewall boundary layer at the National Aeronautical Establishment (NAE) in Canada. Therefore, the Douglas ATAT program focused on evaluating sidewall-boundary-layer effects on the airfoil performance characteristics by systematically varying Mach number, Reynolds number, and sidewall-boundary-layer removal.

All the objectives of this cooperative test were met. Limited analysis of the data indicated the following general conclusions:

1. Increasing Reynolds number generally increased normal force and nose-down pitching moment and, in general, decreased drag force. Drag creep, for Mach numbers greater than 0.7 at the two highest normal forces, increased as the Reynolds number decreased.

2. Increasing Mach number indicated the expected results, such as increased normal-force slope, increased nose-down pitching moment, and increased drag force.

3. The boundary-layer transition strips appeared to adequately trip the flow at a Reynolds number of 6.0×10^6. However, for the lower normal forces, the drag force for free transition was greater than for fixed transition. At a Reynolds number of 15.0×10^6 the free- and fixed-transition drag levels were virtually the same.

4. The spanwise measurement of drag in the wake of the airfoil indicated that two-dimensional flow was obtained at the higher Reynolds numbers. For the high-angle-of-attack postseparation conditions, the spanwise distributions become less two-dimensional.

5. A limited amount of data (at $M \approx 0.730$ and $R \approx 15.0 \times 10^6$) indicated that the repeatability of these data is good except for the drag above a normal force of about 0.70.

6. The sidewall-boundary-layer removal resulted in a slight decrease in the normal force and nose-down pitching moment. The drag-rise characteristics obtained without sidewall-boundary-layer removal are more favorable than those with removal, indicating an increase in the effective (i.e., uncorrected) Mach number when no sidewall boundary layer is used.

7. In general, the design and fabrication techniques used for this model were more than adequate for models being tested in a cryogenic environment. The model was structurally sound and remained dimensionally stable through repeated cryogenic cycling.

NASA Langley Research Center
Hampton, VA 23665-5225
February 13, 1986

REFERENCES

1. Ladson, Charles L.; and Ray, Edward J.: Status of Advanced Airfoil Tests in the Langley 0.3-Meter Transonic Cryogenic Tunnel. Advanced Aerodynamics - Selected NASA Research, NASA CP-2208, 1981, pp. 37-53.

2. Reaser, J. S.: Design of an Advanced Technology Airfoil for High Reynolds Number Testing. LR 29678, Lockheed-California Co., Jan. 31, 1981.

3. Murthy, A. V.; Johnson, C. B.; Ray, E. J.; and Lawing, P. L.: Recent Sidewall Boundary-Layer Investigations With Suction in the Langley 0.3-m Transonic Cryogenic Tunnel. AIAA-82-0234, Jan. 1982.

4. Reaser, J. S.: Transonic Testing in a Cryogenic 2-D Wind Tunnel of an Advanced Technology Airfoil. LR 30047, Lockheed-California Co., Jan. 1982.

5. Johnson, William G., Jr.; Hill, Acquilla S.; Ray, Edward J.; Rozendaal, Roger A.; and Butler, Thomas W.: High Reynolds Number Tests of a Boeing BAC I Airfoil in the Langley 0.3-Meter Transonic Cryogenic Tunnel. NASA TM-81922, 1982.

6. Ray, Edward J.: A Review of Reynolds Number Studies Conducted in the Langley 0.3-m Transonic Cryogenic Tunnel. AIAA-82-0941, June 1982.

7. Hall, Robert M.; Dotson, Edward H.; and Vennemann, Dietrich H.: Homogeneous and Heterogeneous Condensation of Nitrogen in Transonic Flow. NASA paper presented at 13th International Symposium on Rarefied Gas Dynamics (Novosibirsk, USSR), July 1982.

8. Schächterle, G.; Ludewig, K.-H.; Stanewsky, E.; and Ray, E. J.: Design and Construction of Two Transonic Airfoil Models for Tests in the NASA Langley 0.3-M TCT. Paper presented at the ETW Cryogenic Technology Review Meeting (Amsterdam), Sept. 15-17, 1982. (Available as NASA TM-85325.)

9. Murthy, A. V.; Johnson, C. B.; Ray, E. J.; Lawing, P. L.; and Thibodeaux, J. J.: Investigation of the Effects of Upstream Sidewall Boundary-Layer Removal on a Supercritical Airfoil. AIAA-83-0386, Jan. 1983.

10. Reaser, J. S.: Testing of an Advanced Technology Transonic Airfoil in a 2-D Cryogenic Wind Tunnel. LR 30418, Lockheed-California Co., Feb. 1983.

11. Murthy, A. V.; Johnson, Charles B.; Ray, Edward J.; Lawing, Pierce L.; and Thibodeaux, Jerry J.: Studies of Sidewall Boundary Layer in the Langley 0.3-Meter Transonic Cryogenic Tunnel With and Without Suction. NASA TP-2096, 1983.

12. Dress, David A.; Johnson, Charles B.; McGuire, Peggy D.; Stanewsky, Egon; and Ray, Edward J.: High Reynolds Number Tests of the CAST 10-2/DOA 2 Airfoil in the Langley 0.3-Meter Transonic Cryogenic Tunnel - Phase I. NASA TM-84620, 1983.

13. Reaser, J. S.; Hallissy, J. B.; and Campbell, R. L.: Design and True Reynolds Number 2-D Testing of an Advanced Technology Airfoil. AIAA-83-1792, July 1983.

14. Stanewsky, E.; Demurie, F.; Ray, E. J.; and Johnson, C. B.: High Reynolds Number Tests of the CAST 10-2/DOA2 Transonic Airfoil at Ambient and Cryogenic Temperature Conditions. Wind Tunnels and Testing Techniques, AGARD-CP-348, Feb. 1984, pp. 10-1 - 10-13.

15. Plentovich, E. B.; Ladson, Charles L.; and Hill, Acquilla S.: Tests of a NACA 65_1-213 Airfoil in the NASA Langley 0.3-Meter Transonic Cryogenic Tunnel. NASA TM-85732, 1984.

16. Murthy, A. V.; Johnson, C. B.; Ray, E. J.; and Stanewsky, E.: Investigation of Sidewall Boundary Layer Removal Effects on Two Different Chord Airfoil Models in the Langley 0.3-Meter Transonic Cryogenic Tunnel. AIAA-84-0598, Mar. 1984.

17. Jenkins, Renaldo V.; Johnson, William G., Jr.; Hill, Acquilla S.; Mueller, Rudolf; and Redeker, Günter: Data From Tests of a R4 Airfoil in the Langley 0.3-Meter Transonic Cryogenic Tunnel. NASA TM-85739, 1984.

18. Ray, E. J.; and Ladson, C. L.: Review of the Advanced Technology Airfoil Test Program in the 0.3-Meter Transonic Cryogenic Tunnel. Wind Tunnel Wall Interference Assessment/Correction - 1983, Perry A. Newman and Richard W. Barnwell, eds., NASA CP-2319, 1984, pp. 361-373.

19. Jenkins, Renaldo V.: Some Experience With Barnwell-Sewall Type Correction to Two-Dimensional Airfoil Data. Wind Tunnel Wall Interference Assessment/Correction - 1983, Perry A. Newman and Richard W. Barnwell, eds., NASA CP-2319, 1984, pp. 375-392.

20. Gumbert, Clyde R.; Newman, Perry A.; Kemp, William B., Jr.; and Adcock, Jerry B.: Adaptation of a Four-Wall Interference Assessment/Correction Procedure for Airfoil Tests in the 0.3-m TCT. Wind Tunnel Wall Interference Assessment/Correction - 1983, Perry A. Newman and Richard W. Barnwell, eds., NASA CP-2319, 1984, pp. 393-411.

21. Johnson, C. B.; Murthy, A. V.; Ray, E. J.; Lawing, P. L.; and Thibodeaux, J. J.: Effect of Upstream Sidewall Boundary Layer Removal on an Airfoil Test. Wind Tunnel Wall Interference Assessment/Correction - 1983, Perry A. Newman and Richard W. Barnwell, eds., NASA CP-2319, 1984, pp. 143-163.

22. Dress, David A.; Stanewsky, Egon; McGuire, Peggy D.; and Ray, Edward J.: High Reynolds Number Tests of the CAST 10-2/DOA 2 Airfoil in the Langley 0.3-Meter Transonic Cryogenic Tunnel - Phase II. NASA TM-86273, 1984.

23. Gumbert, Clyde R.; and Newman, Perry A.: Validation of a Wall-Interference Assessment/Correction Procedure for Airfoil Tests in the Langley 0.3-Meter Transonic Cryogenic Tunnel. AIAA-84-2151, Aug. 1984.

24. Hall, Robert W.: Studies of Condensation Effects on Airfoil Testing in a Transonic Cryogenic Tunnel. AIAA-85-0229, Jan. 1985.

25. Johnson, William G., Jr.; Hill, Acquilla S.; and Eichmann, Otto: High Reynolds Number Tests of a NASA SC(3)-0712(B) Airfoil in the Langley 0.3-Meter Transonic Cryogenic Tunnel. NASA TM-86371, 1985.

26. Johnson, William G., Jr.; Hill, Acquilla S.; and Eichmann, Otto: Pressure Distributions From High Reynolds Number Tests of a NASA SC(3)-0712(B) Airfoil in the Langley 0.3-Meter Transonic Cryogenic Tunnel. NASA TM-86370, 1985.

27. Johnson, William G., Jr.; and Hill, Acquilla S.: Pressure Distributions From High Reynolds Number Tests of a Boeing BAC I Airfoil in the Langley 0.3-Meter Transonic Cryogenic Tunnel. NASA TM-87600, 1985.

28. Ray, Edward J.; Ladson, Charles L.; Adcock, Jerry B.; Lawing, Pierce L.; and Hall, Robert M.: Review of Design and Operational Characteristics of the 0.3-Meter Transonic Cryogenic Tunnel. NASA TM-80123, 1979.

29. Lynch, F. T.; Fancher, M. F.; Patel, D. R.; and Inger, G. R.: Nonadiabatic Model Wall Effects on Transonic Airfoil Performance in a Cryogenic Wind Tunnel. Wind Tunnels and Testing Techniques, AGARD-CP-348, Feb. 1984, pp. 14-1 - 14-11.

30. Ohman, L. H.; and Brown, D.: The NAE High Reynolds Number 15" × 60" Two-Dimensional Test Facility: Description, Operating Experiences and Some Representative Results. AIAA Paper No. 71-293, Mar. 1971.

31. Kilgore. Robert A.; Adcock, Jerry B.; and Ray, Edward J.: The Cryogenic Transonic Wind Tunnel for High Reynolds Number Research. Windtunnel Design and Testing Techniques, AGARD-CP-174, 1976, pp. 1-1 - 1-20.

32. Kilgore, Robert A.: Design Features and Operational Characteristics of the Langley 0.3-Meter Transonic Cryogenic Tunnel. NASA TN D-8304, 1976.

33. Ladson, Charles L.; and Kilgore, Robert A.: Instrumentation for Calibration and Control of a Continuous-Flow Cryogenic Tunnel. NASA TM-81825, 1980.

34. Baals, Donald D.; and Mourhess, Mary J.: Numerical Evaluation of the Wake-Survey Equations for Subsonic Flow Including the Effect of Energy Addition. NACA WR L-5, 1945. (Formerly NACA ARR L5H27.)

35. Hall, Robert M.; and Adcock, Jerry B.: Simulation of Ideal-Gas Flow by Nitrogen and Other Selected Gases at Cryogenic Temperatures. NASA TP-1901, 1981.

36. Adcock, Jerry B.: Real-Gas Effects Associated With One-Dimensional Transonic Flow of Cryogenic Nitrogen. NASA TN D-8274, 1976.

37. Adcock, Jerry B.; and Johnson, Charles B.: A Theoretical Analysis of Simulated Transonic Boundary Layers in Cryogenic-Nitrogen Wind Tunnels. NASA TP-1631, 1980.

38. Jenkins, Renaldo V.: Tabulation of Data From Tests of an NPL 9510 Airfoil in the Langley 0.3-Meter Transonic Cryogenic Tunnel. NASA TM-84579, 1983.

39. Harris, Charles D.: Transonic Aerodynamic Characteristics of the 10-Percent-Thick NASA Supercritical Airfoil 31. NASA TM X-3203, 1975.

TABLE 1.- MODEL ORIFICE LOCATIONS

Upper surface

Orifice	x/c	y/(b/2)
1	0.000	0.000
2	.002	−.063
3	.005	−.031
4	.010	.063
5	.020	−.063
6	.030	0.000
7	.050	.063
8	.075	−.063
9	.100	0.000
10	.125	.063
11	.150	−.063
12	.180	0.000
13	.210	.063
14	.240	−.063
15	.270	0.000
16	.300	.063
17	.320	−.063
18	.340	0.000
19	.360	.063
20	.380	−.063
21	.390	0.000
22	.400	.063
23	.410	−.063
24	.420	0.000
25	.430	.063
26	.440	−.063
27	.460	.063
28	.470	−.063
29	.480	0.000
30	.490	.063
31	.510	0.000
32	.520	.063
33	.540	−.063
34	.560	0.000
35	.580	.063
36	.610	−.063
37	.640	0.000
38	.670	.063
39	.700	−.063
40	.730	0.000
41	.76	.063
42	.790	−.063
43	.820	0.000
44	.850	.063
45	.880	−.063
46	.910	−.021
47	.940	.042
48	.970	−.042
49	1.000	0.000

Upper surface

Additional spanwise orifices		
Orifice	x/c	y/(b/2)
1	.060	−.750
2	↓	−.500
3	↓	.500
4	↓	.750
5	.300	−.750
6	↓	−.500
7	↓	−.225
8	↓	.500
9	↓	.750
10	.610	−.750
11	↓	−.500
12	↓	−.250
13	↓	.250
14	↓	.500
15	↓	.750

Lower surface

Orifice	x/c	y/(b/2)
1	0.000	0.000
2	.005	−.063
3	.010	0.000
4	.025	.063
5	.050	−.063
6	.075	0.000
7	.100	.063
8	.150	−.063
9	.200	0.000
10	.250	.063
11	.300	−.063
12	.350	0.000
13	.400	.063
14	.450	−.063
15	.500	0.000
16	.550	.063
17	.600	−.063
18	.650	0.000
19	.700	.063
20	.750	−.063
21	.800	0.000
22	.850	.063
23	.880	−.063
24	.910	.021
25	.940	.083
26	.970	−.083
27	1.000	0.000

TABLE 2.- MODEL THERMOCOUPLE LOCATIONS

Upper surface

Thermocouple	x/c	y/(b/2)
1	0.00	−.824
2	↓	.031
3		.375
4		.824
5	.10	−.040
6	.20	0.000
7	.40	−.824
8	↓	−.375
9		0.000
10		.375
11		.824
12	.60	0.000
13	.80	−.824
14	↓	.040
15		.824

Lower surface

Thermocouple	x/c	y/(b/2)
1	.10	0.000
2	.20	−.040
3	.40	0.000
4	.60	0.000

TABLE 3.- TEST CONDITIONS

Run	M	R x 10^{-6}	$\dot{m}_{bl}$	Transition
10	.50	6	0	Free
25	↓	15	↓	↓
1	↓	30	↓	↓
11	.60	6	0	Free
23	↓	15	↓	↓
2	↓	30	↓	↓
24	↓	15	1	↓
3	↓	30	↓	↓
26	↓	15	1.1	↓
50	↓	6	0	Fixed
27	.70	6	0	Free
20	↓	15	↓	↓
4,5	↓	30	↓	↓
21	↓	15	1	↓
6	↓	30	↓	↓
22	↓	15	1.5	↓
51	↓	6	0	Fixed
28	.73	6	0	Free
32	↓	15	↓	↓
7	↓	30	↓	↓
33	↓	15	1	↓
8	↓	30	↓	↓
34	↓	15	1.5	↓
52	↓	6	0	Fixed
48	↓	15	↓	↓
53	↓	6	1	↓
54	↓	6	2	↓

Run	M	R x 10^{-6}	$\dot{m}_{bl}$	Transition
29	.75	6	0	Free
35,36	↓	15	↓	↓
9	↓	30	↓	↓
37,38	↓	15	1	↓
12,13	↓	30	↓	↓
39	↓	15	1.5	↓
58	↓	6	0	Fixed
30	.765	6	0	Free
40	↓	15	↓	↓
14,15	↓	30	↓	↓
41	↓	15	1	↓
16	↓	30	↓	↓
42	↓	15	1.6	↓
57	↓	6	0	Fixed
49	↓	15	↓	↓
56	↓	6	1	↓
55	↓	6	2	↓
31	.78	6	0	Free
43	↓	15	↓	↓
17	↓	30	↓	↓
44	↓	15	1	↓
18,19	↓	30	↓	↓
45	↓	15	1.6	↓
59	↓	6	0	Fixed

TABLE 4.- TEST RESULTS

(a) Free transition

Point	M	R x 10^{-6}	$\dot{m}_{bl}$	α	c_n	c_m	c_d
Run 10 $\bar{M}$ = .500 σ = .001 σ_m = .002							
93	.499	5.996	0.00	-2.00	.128	-.122	.00886
94	.501	6.033	0.00	.00	.352	-.126	.00867
95	.500	6.016	0.00	1.00	.462	-.127	.00863
96	.500	6.029	0.00	2.01	.576	-.128	.00864
97	.500	6.027	0.00	2.51	.631	-.128	.00880
98	.499	6.021	0.00	3.02	.687	-.128	.00892
99	.501	6.039	0.00	3.51	.744	-.129	.00901
100	.502	6.056	0.00	3.99	.799	-.129	.00918
101	.500	5.994	0.00	5.00	.907	-.126	.00961
103	.501	5.990	0.00	6.02	1.001	-.120	.01141
Run 11 $\bar{M}$ = .600 σ = .000 σ_m = -.001							
104	.600	5.959	0.00	-1.98	.128	-.130	.00955
105	.601	5.968	0.00	.01	.369	-.133	.00923
106	.601	5.968	0.00	1.02	.492	-.135	.00903
107	.600	5.968	0.00	2.02	.610	-.135	.00907
108	.601	5.971	0.00	2.51	.668	-.135	.00919
109	.600	5.967	0.00	3.02	.733	-.135	.00952
110	.601	5.976	0.00	3.51	.793	-.133	.00961
111	.600	5.971	0.00	4.01	.840	-.130	.01018
112	.600	5.971	0.00	5.02	.956	-.124	.01356
113	.600	5.973	0.00	6.03	1.091	-.119	.02175
Run 27 $\bar{M}$ = .701 σ = .001 σ_m = .002							
252	.701	5.986	0.00	-.99	.265	-.143	.01041
253	.700	5.972	0.00	.00	.393	-.145	.01037
254	.702	5.985	0.00	.52	.464	-.146	.01042
255	.702	5.999	0.00	1.01	.528	-.146	.00998
256	.703	6.000	0.00	1.51	.593	-.145	.00973
257	.702	6.002	0.00	2.02	.668	-.145	.00964
258	.699	5.991	0.00	2.53	.739	-.143	.01032
259	.701	5.997	0.00	3.02	.818	-.141	.01233
260	.700	5.994	0.00	4.02	1.003	-.142	.02310
261	.700	5.985	0.00	5.01	1.159	-.149	.04266

TABLE 4.- Continued

(a) Continued

Point	M	R x 10^{-6}	$\dot{m}_{bl}$	α	c_n	c_m	c_d
Run 28 $\bar{M}$ = .731 σ = .001 σ_m = .002							
262	.731	6.028	0.00	-.99	.263	-.148	.01091
263	.731	6.036	0.00	-.51	.335	-.150	.01051
264	.732	6.039	0.00	.00	.406	-.152	.01019
265	.730	6.032	0.00	.50	.474	-.151	.00994
266	.732	6.036	0.00	1.00	.544	-.151	.00976
267	.733	6.030	0.00	1.51	.625	-.151	.00980
268	.730	6.014	0.00	2.02	.703	-.150	.01047
269	.731	6.014	0.00	2.51	.789	-.149	.01315
270	.732	6.016	0.00	3.03	.908	-.157	.01782
271	.731	6.017	0.00	3.52	.996	-.163	.02459
Run 29 $\bar{M}$ = .750 σ = .001 σ_m = .002							
273	.751	5.983	0.00	-2.00	.107	-.146	.01279
274	.752	5.980	0.00	-.99	.260	-.149	.01140
275	.750	5.972	0.00	.01	.410	-.152	.01045
276	.750	5.969	0.00	.51	.488	-.154	.01011
277	.751	5.970	0.00	1.02	.572	-.156	.01004
278	.749	5.964	0.00	1.51	.651	-.155	.01050
279	.749	5.966	0.00	2.02	.751	-.158	.01146
280	.749	5.957	0.00	2.02	.750	-.158	.01139
281	.751	5.978	0.00	2.52	.860	-.169	.01445
282	.750	5.968	0.00	3.03	.947	-.180	.01954
283	.750	5.971	0.00	3.52	1.015	-.184	.02907
Run 30 $\bar{M}$ = .765 σ = .001 σ_m = .002							
284	.766	6.001	0.00	-1.99	.103	-.148	.01337
285	.765	6.000	0.00	-.98	.267	-.153	.01187
286	.766	6.008	0.00	.01	.423	-.157	.01084
287	.766	6.009	0.00	.52	.508	-.160	.01064
288	.765	6.006	0.00	1.01	.591	-.160	.01060
289	.765	6.002	0.00	1.52	.686	-.163	.01111
290	.765	6.006	0.00	2.02	.788	-.174	.01441
291	.763	6.001	0.00	2.53	.877	-.185	.01925
292	.764	6.005	0.00	3.02	.937	-.190	.02830
293	.766	6.011	0.00	3.48	.938	-.185	.04337
294	.765	6.010	0.00	3.51	.947	-.188	.04426

TABLE 4.- Continued

(a) Continued

Point	M	R x 10^{-6}	$\dot{m}_{bl}$	α	c_n	c_m	c_d
Run 31 $\bar{M}$ = .781 σ = .001 σ_m = .003							
295	.781	6.007	0.00	-2.00	.099	-.153	.01398
296	.782	6.015	0.00	-.98	.272	-.159	.01273
297	.781	6.010	0.00	.01	.439	-.164	.01161
298	.781	6.020	0.00	.51	.527	-.167	.01134
299	.780	6.012	0.00	1.01	.620	-.174	.01244
300	.782	6.023	0.00	1.50	.701	-.182	.01733
301	.784	6.031	0.00	2.02	.759	-.186	.02676
302	.782	6.020	0.00	2.54	.812	-.186	.03564
303	.781	6.018	0.00	2.99	.848	-.185	.04228
304	.781	6.016	0.00	3.51	.850	-.179	.05696
Run 25 $\bar{M}$ = .500 σ = .001 σ_m = -.002							
228	.500	15.051	0.00	-2.03	.135	-.125	.00822
229	.500	15.025	0.00	-1.99	.144	-.126	.00835
230	.499	14.960	0.00	.01	.369	-.128	.00796
231	.501	14.966	0.00	1.01	.482	-.130	.00787
232	.502	15.002	0.00	2.01	.592	-.130	.00803
234	.502	14.944	0.00	2.53	.650	-.130	.00816
235	.502	14.956	0.00	3.01	.702	-.131	.00822
236	.498	14.870	0.00	3.51	.756	-.131	.00837
237	.499	14.893	0.00	4.01	.813	-.131	.00852
238	.500	14.932	0.00	4.99	.923	-.129	.00903
239	.500	14.915	0.00	6.04	1.022	-.121	.01093
Run 23 $\bar{M}$ = .601 σ = .001 σ_m = .001							
204	.602	14.928	0.00	-2.01	.137	-.133	.00835
205	.601	14.924	0.00	.01	.376	-.136	.00818
206	.601	14.919	0.00	1.01	.497	-.137	.00817
207	.600	14.879	0.00	2.03	.622	-.138	.00828
208	.601	14.913	0.00	2.53	.686	-.138	.00842
209	.602	14.927	0.00	3.02	.746	-.138	.00853
210	.601	14.909	0.00	3.53	.810	-.137	.00878
211	.601	14.912	0.00	4.02	.858	-.134	.00946
212	.600	14.884	0.00	5.01	.980	-.128	.01316
214	.600	14.895	0.00	6.03	1.104	-.120	.02167

TABLE 4.- Continued

(a) Continued

Point	M	R x 10^{-6}	$\dot{m}_{bl}$	α	c_n	c_m	c_d
Run 24 $\bar{M}$ = .599 σ = .001 σ_m = −.003							
217	.598	14.794	1.00	-1.98	.144	-.133	.00834
218	.601	14.845	1.00	.00	.382	-.136	.00831
219	.600	14.827	1.00	1.01	.507	-.138	.00827
220	.600	14.822	1.00	2.02	.628	-.138	.00834
221	.601	14.842	1.00	2.53	.689	-.138	.00841
222	.600	14.834	1.00	3.02	.747	-.136	.00855
223	.600	14.824	1.00	3.51	.811	-.137	.00879
224	.599	14.806	1.00	4.02	.861	-.134	.00948
225	.597	14.750	1.00	4.99	.970	-.128	.01275
226	.599	14.798	1.00	6.02	1.104	-.122	.02126
Run 26 $\bar{M}$ = .601 σ = .001 σ_m = −.002							
242	.600	14.816	1.10	-2.00	.141	-.132	.00817
243	.600	14.826	1.10	.02	.394	-.136	.00807
244	.601	14.846	1.10	1.02	.519	-.138	.00808
245	.601	14.839	1.10	2.02	.635	-.138	.00821
246	.602	14.866	1.10	2.53	.696	-.138	.00835
247	.602	14.867	1.10	3.02	.755	-.136	.00853
248	.602	14.857	1.10	3.53	.817	-.134	.00879
249	.601	14.855	1.10	4.01	.866	-.134	.00959
250	.601	14.852	1.10	5.01	.981	-.126	.01329
251	.599	14.827	1.10	6.04	1.098	-.120	.02142
Run 20 $\bar{M}$ = .700 σ = .001 σ_m = .002							
171	.701	14.937	0.00	-1.01	.264	-.144	.00861
172	.700	14.911	0.00	-.01	.400	-.146	.00850
173	.700	14.912	0.00	.51	.470	-.148	.00855
174	.699	14.897	0.00	1.01	.539	-.148	.00860
175	.700	14.909	0.00	1.52	.607	-.148	.00866
176	.701	14.923	0.00	2.03	.684	-.148	.00884
177	.700	14.925	0.00	2.50	.759	-.146	.00971
178	.701	14.918	0.00	3.05	.840	-.144	.01222
179	.701	14.919	0.00	3.05	.839	-.143	.01213
180	.700	14.905	0.00	4.03	1.011	-.144	.02269
181	.702	14.948	0.00	5.04	1.177	-.155	.04432

TABLE 4.- Continued

(a) Continued

Point	M	R x 10^{-6}	$\dot{m}_{bl}$	α	c_n	c_m	c_d
Run 21 $\bar{M}$ = .701 σ = .001 σ_m = −.001							
183	.700	14.813	1.00	-1.00	.269	-.146	.00879
184	.702	14.858	1.00	-.01	.414	-.149	.00869
185	.701	14.845	1.00	.49	.477	-.148	.00866
186	.701	14.847	1.00	1.01	.543	-.149	.00873
187	.700	14.827	1.00	1.52	.611	-.148	.00877
188	.702	14.860	1.00	2.03	.683	-.148	.00902
189	.700	14.830	1.00	2.53	.754	-.145	.00968
190	.699	14.826	1.00	3.01	.827	-.143	.01117
191	.700	14.847	1.00	4.00	1.001	-.144	.02036
192	.701	14.849	1.00	5.01	1.160	-.151	.03892
Run 22 $\bar{M}$ = .700 σ = .001 σ_m = −.002							
194	.699	14.816	1.50	-.99	.267	-.145	.00863
195	.702	14.890	1.50	.01	.406	-.148	.00861
196	.701	14.834	1.50	.52	.475	-.148	.00860
197	.700	14.816	1.50	1.01	.540	-.148	.00866
198	.700	14.831	1.50	1.50	.609	-.148	.00868
199	.701	14.843	1.50	2.02	.679	-.147	.00889
200	.701	14.845	1.50	2.51	.750	-.146	.00955
201	.699	14.815	1.50	3.02	.824	-.142	.01120
202	.698	14.801	1.50	4.03	.995	-.142	.01910
203	.699	14.814	1.50	5.03	1.160	-.149	.03567
Run 32 $\bar{M}$ = .730 σ = .002 σ_m = .002							
305	.733	14.997	0.00	-.94	.260	-.149	.00895
306	.732	14.967	0.00	-.51	.327	-.148	.00890
307	.730	14.922	0.00	.01	.405	-.151	.00883
308	.731	14.912	0.00	.54	.484	-.152	.00881
309	.730	14.860	0.00	1.04	.557	-.152	.00892
310	.728	14.835	0.00	1.52	.632	-.152	.00908
311	.730	14.888	0.00	2.04	.718	-.151	.00991
313	.732	14.913	0.00	2.52	.810	-.153	.01227
314	.729	14.883	0.00	3.03	.900	-.155	.01650
315	.728	14.875	0.00	3.53	.995	-.163	.02293
Run 46 $\bar{M}$ = .732 σ = .001 σ_m = −.001							
445	.732	14.924	0.00	.01	.410	-.151	.00887
446	.730	14.930	0.00	1.02	.555	-.152	.00887
447	.733	14.971	0.00	2.96	.895	-.157	.01586

TABLE 4.- Continued

(a) Continued

Point	M	R x 10^{-6}	$\dot{m}_{bl}$	α	c_n	c_m	c_d
Run 33 $\bar{M}$ = .729 σ = .001 σ_m = .002							
316	.728	14.892	1.00	-1.00	.266	-.146	.00885
317	.730	14.919	1.00	-.51	.336	-.148	.00878
318	.730	14.908	1.00	.01	.408	-.149	.00877
319	.730	14.911	1.00	.52	.484	-.150	.00879
320	.730	14.911	1.00	1.01	.551	-.150	.00885
321	.729	14.886	1.00	1.51	.617	-.149	.00889
322	.728	14.891	1.00	2.02	.694	-.148	.00922
323	.728	14.890	1.00	2.51	.772	-.146	.01056
324	.731	14.931	1.00	3.01	.865	-.149	.01429
325	.731	14.940	1.00	3.53	.960	-.154	.01969
Run 34 $\bar{M}$ = 730 σ = .002 σ_m = −.005							
327	.731	14.840	1.50	-1.01	.266	-.149	.00920
328	.730	14.837	1.50	-.48	.345	-.151	.00903
329	.731	14.841	1.50	.02	.415	-.152	.00903
330	.730	14.829	1.50	.52	.483	-.152	.00901
331	.732	14.860	1.50	1.01	.559	-.153	.00908
332	.731	14.842	1.50	1.50	.631	-.152	.00911
333	.730	14.836	1.50	2.02	.709	-.151	.00940
334	.728	14.820	1.50	2.53	.790	-.150	.01095
335	.731	14.860	1.50	3.02	.883	-.154	.01360
336	.724	14.736	1.50	3.51	.964	-.155	.01954
Run 35 and Run 36 $\bar{M}$ = .751 σ = .001 σ_m = −.001							
337	.752	15.014	0.00	-2.00	.112	-.146	.00948
338	.751	15.009	0.00	-.99	.264	-.150	.00919
339	.751	15.012	0.00	.02	.416	-.154	.00904
340	.751	15.016	0.00	.52	.492	-.155	.00908
341	.751	15.015	0.00	1.01	.574	-.157	.00913
342	.751	15.020	0.00	1.51	.661	-.158	.00949
343	.750	14.998	0.00	2.00	.755	-.160	.01064
344	.751	15.004	0.00	2.54	.861	-.169	.01438
345	.752	15.005	0.00	3.02	.947	-.181	.01972
348	.750	14.930	0.00	3.52	1.014	-.184	.02880

TABLE 4.- Continued

(a) Continued

Point	M	R x 10^{-6}	$\dot{m}_{bl}$	α	c_n	c_m	c_d
Run 37 and Run 38 $\bar{M}$ = .750 σ = .002 σ_m = .005							
349	.749	14.761	1.00	-2.00	.101	-.147	.00977
351	.750	14.767	1.00	-.98	.267	-.152	.00946
354	.751	14.783	1.00	.01	.417	-.156	.00936
356	.752	14.787	1.00	.53	.497	-.157	.00936
357	.752	14.785	1.00	1.02	.570	-.157	.00934
358	.751	14.792	1.00	1.51	.654	-.157	.00960
359	.748	14.747	1.00	2.00	.735	-.158	.01024
360	.747	14.745	1.00	2.53	.832	-.162	.01255
361	.749	14.774	1.00	3.03	.928	-.173	.01777
362	.755	14.839	1.00	3.53	.962	-.184	.02821
Run 39 $\bar{M}$ = .750 σ = .001 σ_m = .002							
365	.750	14.775	1.50	-1.99	.103	-.146	.00973
366	.749	14.752	1.50	-1.00	.257	-.151	.00938
367	.750	14.762	1.50	.01	.413	-.155	.00922
368	.750	14.772	1.50	.50	.489	-.156	.00916
369	.751	14.779	1.50	1.00	.566	-.156	.00930
370	.751	14.779	1.50	1.52	.652	-.157	.00952
371	.750	14.765	1.50	2.01	.733	-.158	.01028
373	.749	14.768	1.50	2.51	.833	-.164	.01278
374	.750	14.779	1.50	3.00	.913	-.170	.01701
375	.752	14.802	1.50	3.53	.978	-.181	.02474
Run 40 $\bar{M}$ = .766 σ = .001 σ_m = .002							
376	.764	14.949	0.00	-2.01	.100	-.148	.00982
378	.768	14.990	0.00	-.98	.262	-.153	.00947
379	.765	14.963	0.00	.02	.424	-.158	.00927
380	.764	14.945	0.00	.51	.500	-.159	.00929
381	.765	14.961	0.00	1.00	.587	-.161	.00951
382	.767	14.985	0.00	1.50	.703	-.171	.01094
383	.767	14.998	0.00	2.03	.783	-.178	.01490
384	.768	14.998	0.00	2.52	.857	-.184	.02086
385	.765	14.968	0.00	3.03	.922	-.187	.02739
386	.767	14.987	0.00	3.52	.915	-.180	.03768

TABLE 4.- Continued

(a) Continued

Point	M	R x 10^{-6}	$\dot{m}_{bl}$	α	c_n	c_m	c_d
Run 41 $\bar{M}$ = .765 σ = .002 σ_m = −.003							
387	.762	14.786	1.00	-2.00	.095	-.149	.00995
388	.766	14.831	1.00	-.98	.262	-.155	.00961
389	.766	14.836	1.00	.01	.421	-.159	.00952
390	.768	14.860	1.00	.53	.505	-.161	.00957
391	.765	14.834	1.00	1.03	.586	-.161	.00961
392	.763	14.805	1.00	1.50	.672	-.165	.01006
393	.765	14.844	1.00	2.03	.769	-.175	.01280
394	.765	14.852	1.00	2.53	.832	-.182	.01790
395	.763	14.829	1.00	3.03	.912	-.184	.02354
396	.767	14.869	1.00	3.51	.931	-.182	.03441
Run 42 $\bar{M}$ = .764 σ = .002 σ_m = .005							
397	.763	14.746	1.60	-2.00	.095	-.148	.00984
398	.769	14.813	1.60	-.98	.257	-.154	.00965
399	.762	14.731	1.60	.01	.416	-.157	.00932
401	.762	14.757	1.60	.01	.423	-.157	.00935
402	.764	14.764	1.60	.52	.500	-.160	.00939
403	.765	14.788	1.60	1.03	.583	-.161	.00946
404	.763	14.759	1.60	1.52	.665	-.162	.00986
405	.761	14.744	1.60	2.01	.751	-.167	.01157
406	.763	14.760	1.60	2.53	.836	-.176	.01582
408	.767	14.798	1.60	3.01	.909	-.182	.02258
409	.766	14.798	1.60	3.53	.881	-.175	.02983
Run 43 $\bar{M}$ = .781 σ = .001 σ_m = .002							
410	.781	14.943	0.00	-2.00	.093	-.151	.01065
411	.781	14.941	0.00	-.98	.266	-.157	.00994
412	.780	14.938	0.00	.03	.433	-.163	.00967
413	.780	14.944	0.00	.53	.525	-.167	.00997
414	.781	14.967	0.00	1.03	.621	-.175	.01194
415	.780	14.937	0.00	1.52	.697	-.182	.01575
416	.782	14.958	0.00	2.00	.763	-.186	.02273
417	.782	14.955	0.00	2.54	.801	-.184	.02958
418	.783	14.970	0.00	3.01	.834	-.183	.03497
419	.783	14.963	0.00	3.51	.833	-.174	.04805

TABLE 4.- Continued

(a) Continued

Point	M	R x 10^{-6}	$\dot{m}_{bl}$	α	c_n	c_m	c_d
Run 44 $\bar{M}$ = .780 σ = .002 σ_m = −.004							
421	.776	14.897	1.00	-2.00	.082	-.150	.01082
422	.778	14.911	1.00	-.97	.260	-.158	.01005
423	.779	14.905	1.00	.01	.427	-.163	.00986
426	.779	14.843	1.00	.50	.510	-.167	.00993
427	.780	14.808	1.00	1.01	.593	-.170	.01181
428	.780	14.812	1.00	1.52	.681	-.177	.01502
429	.780	14.816	1.00	2.02	.745	-.183	.01965
430	.781	14.836	1.00	2.53	.806	-.185	.02716
431	.783	14.855	1.00	3.01	.804	-.178	.03274
432	.782	14.848	1.00	3.53	.826	-.173	.04299
Run 45 $\bar{M}$ = .781 σ = .002 σ_m = .004							
433	.779	14.803	1.60	-2.00	.078	-.150	.01170
434	.780	14.808	1.60	-.98	.254	-.158	.01032
435	.782	14.810	1.60	.02	.425	-.166	.01032
436	.781	14.801	1.60	.52	.512	-.170	.01067
437	.780	14.792	1.60	1.00	.596	-.173	.01243
438	.780	14.789	1.60	1.51	.679	-.177	.01531
440	.781	14.795	1.60	2.02	.750	-.184	.01985
441	.782	14.703	1.60	2.53	.753	-.180	.02552
442	.784	14.733	1.60	3.00	.813	-.179	.03149
443	.785	14.740	1.60	3.52	.841	-.175	.04259
Run 1 $\bar{M}$ = .500 σ = .001 σ_m = .002							
1	.501	29.944	0.00	-1.99	.143	-.128	.00741
2	.500	29.882	0.00	.03	.372	-.131	.00737
3	.502	30.003	0.00	1.01	.489	-.132	.00731
4	.502	29.952	0.00	2.03	.603	-.133	.00742
5	.499	29.910	0.00	2.53	.655	-.133	.00749
6	.500	29.970	0.00	3.02	.712	-.134	.00764
7	.500	29.990	0.00	3.51	.765	-.133	.00776
8	.500	30.015	0.00	4.03	.824	-.133	.00802
9	.501	30.023	0.00	4.99	.931	-.131	.00848
10	.500	29.908	0.00	6.02	1.028	-.124	.01062

TABLE 4.- Continued

(a) Continued

Point	M	R x 10^{-6}	$\dot{m}_{bl}$	α	c_n	c_m	c_d
Run 2 $\bar{M}$ = .600 σ = .001 σ_m = −.002							
11	.600	29.839	0.00	-1.99	.155	-.137	.00728
12	.601	29.857	0.00	.02	.394	-.139	.00733
13	.601	29.891	0.00	.99	.513	-.141	.00740
14	.601	29.858	0.00	2.02	.635	-.141	.00753
16	.601	29.848	0.00	2.51	.699	-.141	.00766
17	.599	29.723	0.00	3.02	.754	-.140	.00775
18	.599	29.818	0.00	3.49	.818	-.139	.00801
19	.601	29.915	0.00	4.01	.876	-.137	.00883
20	.601	29.916	0.00	5.04	.993	-.130	.01294
21	.601	29.935	0.00	6.00	1.116	-.123	.02150
Run 3 $\bar{M}$ = .596 σ = .000 σ_m = −.001							
23	.596	29.713	.90	-1.98	.151	-.136	.00749
24	.597	29.729	.90	.02	.400	-.139	.00735
25	.597	29.720	.90	1.01	.521	-.140	.00747
26	.596	29.691	.90	2.00	.638	-.140	.00760
27	.597	29.712	.90	2.51	.698	-.140	.00770
28	.596	29.703	.90	3.03	.761	-.140	.00783
29	.596	29.712	.90	3.51	.819	-.139	.00813
30	.596	29.708	.90	4.01	.866	-.136	.00876
31	.597	29.708	.90	5.02	.989	-.129	.01240
32	.597	29.720	.90	6.00	1.104	-.122	.02021
Run 4 and Run 5 $\bar{M}$ = .701 σ = .000 σ_m = .000							
33	.701	29.973	0.00	-.99	.288	-.150	.00758
34	.701	29.972	0.00	.02	.419	-.152	.00741
35	.701	29.944	0.00	.52	.484	-.152	.00744
36	.701	29.976	0.00	1.02	.550	-.152	.00778
37	.701	29.983	0.00	1.54	.630	-.153	.00788
38	.701	29.996	0.00	2.00	.691	-.152	.00810
39	.701	29.912	0.00	2.52	.768	-.149	.00925
40	.701	29.908	0.00	3.10	.864	-.148	.01166
41	.701	29.914	0.00	3.99	1.026	-.149	.02234
42	.701	29.911	0.00	4.98	1.187	-.156	.04165

TABLE 4.- Continued

(a) Continued

Point	M	R x 10^{-6}	$\dot{m}_{bl}$	α	c_n	c_m	c_d
Run 6 $\bar{M}$ = .700 σ = .001 σ_m = −.004							
44	.701	29.646	1.00	-.98	.294	-.152	.00772
45	.700	29.638	1.00	.01	.425	-.154	.00777
46	.701	29.641	1.00	.54	.498	-.154	.00755
47	.701	29.668	1.00	1.01	.561	-.154	.00771
48	.701	29.665	1.00	1.50	.632	-.154	.00793
49	.701	29.661	1.00	2.00	.705	-.153	.00818
50	.701	29.671	1.00	2.52	.769	-.150	.00887
51	.700	29.666	1.00	3.03	.844	-.148	.01071
52	.702	29.582	1.00	4.01	1.022	-.149	.02075
54	.697	29.438	1.00	5.01	1.183	-.155	.03695
Run 7 $\bar{M}$ = .730 σ = .001 σ_m = −.002							
55	.730	30.092	0.00	-.99	.296	-.156	.00793
56	.731	30.109	0.00	-.49	.358	-.156	.00776
57	.732	30.032	0.00	.01	.428	-.157	.00791
58	.731	30.023	0.00	.50	.494	-.157	.00774
60	.732	30.008	0.00	1.00	.572	-.158	.00792
61	.729	29.954	0.00	1.50	.646	-.157	.00817
63	.730	29.956	0.00	2.02	.733	-.157	.00858
64	.732	30.003	0.00	2.51	.825	-.158	.01100
66	.728	29.891	0.00	3.02	.918	-.161	.01457
67	.730	29.840	0.00	3.49	1.022	-.175	.02155
68	.702	29.856	0.00	4.99	1.196	-.159	.04339
Run 8 $\bar{M}$ = .730 σ = .001 σ_m = .002							
69	.729	29.534	1.00	-1.00	.297	-.157	.00821
70	.729	29.526	1.00	-.48	.356	-.157	.00830
71	.731	29.612	1.00	.01	.437	-.160	.00807
72	.729	29.542	1.00	.51	.504	-.159	.00798
73	.731	29.586	1.00	1.00	.576	-.159	.00809
74	.730	29.562	1.00	1.51	.650	-.158	.00829
75	.729	29.554	1.00	2.01	.726	-.157	.00854
76	.728	29.540	1.00	2.51	.815	-.157	.01011
77	.729	29.568	1.00	3.01	.908	-.161	.01282
78	.731	29.450	1.00	3.51	.998	-.169	.01822

TABLE 4.- Continued

(a) Continued

Point	M	R x 10^{-6}	$\dot{m}_{bl}$	α	c_n	c_m	c_d
Run 9 $\bar{M}$ = .752 σ = .001 σ_m = .002							
80	.751	29.976	0.00	-2.00	.140	-.155	.00846
81	.753	30.013	0.00	-1.01	.284	-.159	.00818
82	.752	30.016	0.00	.03	.437	-.162	.00811
84	.754	29.877	0.00	.51	.513	-.163	.00820
85	.754	29.852	0.00	.51	.513	-.162	.00801
86	.751	29.803	0.00	1.00	.590	-.163	.00833
87	.750	29.793	0.00	1.50	.676	-.163	.00856
88	.750	29.774	0.00	1.99	.775	-.168	.01003
89	.752	29.817	0.00	2.53	.871	-.176	.01429
90	.752	29.856	0.00	3.01	.957	-.188	.02063
91	.752	29.857	0.00	3.50	1.022	-.192	.02879
Run 12 and Run 13 $\bar{M}$ = .749 σ = .002 σ_m = -.003							
115	.749	29.727	1.00	-1.99	.123	-.155	.00843
116	.746	29.650	1.00	-1.01	.287	-.159	.00843
118	.750	29.690	1.00	.00	.444	-.163	.00815
119	.750	29.702	1.00	.50	.516	-.163	.00823
120	.748	29.655	1.00	1.00	.587	-.162	.00823
121	.748	29.604	1.00	1.52	.667	-.162	.00848
122	.749	29.626	1.00	2.03	.753	-.164	.00970
123	.751	29.805	1.00	2.51	.851	-.172	.01272
124	.747	29.695	1.00	3.02	.924	-.173	.01670
125	.750	29.720	1.00	3.52	1.002	-.187	.02476
Run 14 and Run 15 $\bar{M}$ = .762 σ = .002 σ_m = -.004							
126	.763	29.818	0.00	-1.99	.150	-.159	.00869
127	.762	29.784	0.00	-.99	.292	-.161	.00836
128	.762	29.798	0.00	.02	.440	-.163	.00840
129	.762	30.067	0.00	.52	.523	-.165	.00850
130	.763	30.084	0.00	1.01	.602	-.166	.00872
132	.761	29.973	0.00	1.50	.701	-.171	.00953
133	.761	29.987	0.00	2.01	.799	-.181	.01292
134	.761	29.982	0.00	2.52	.872	-.188	.01889
135	.763	30.047	0.00	3.00	.921	-.194	.02718
136	.758	29.922	0.00	3.49	.970	-.190	.03274

TABLE 4.- Continued

(a) Concluded

Point	M	R x 10^{-6}	$\dot{m}_{bl}$	α	c_n	c_m	c_d
Run 16 $\bar{M}$ = .763 σ = .002 σ_m = −.003							
137	.763	29.651	1.00	-1.99	.136	-.161	.00883
138	.764	29.697	1.00	-.98	.289	-.164	.00855
140	.765	29.699	1.00	.02	.453	-.168	.00861
141	.763	29.614	1.00	.51	.525	-.168	.00851
142	.762	29.589	1.00	1.01	.608	-.168	.00876
143	.760	29.552	1.00	1.49	.686	-.169	.00931
144	.764	29.576	1.00	2.02	.772	-.181	.01351
145	.765	29.638	1.00	2.52	.851	-.189	.01919
146	.764	29.557	1.00	3.01	.917	-.193	.02460
147	.765	29.510	1.00	3.50	.939	-.187	.03289
Run 17 $\bar{M}$ = .780 σ = .001 σ_m = .002							
148	.781	29.918	0.00	-1.98	.134	-.162	.00933
149	.783	29.965	0.00	-1.01	.282	-.166	.00918
150	.780	29.899	0.00	-.01	.455	-.171	.00908
151	.779	29.854	0.00	.50	.541	-.174	.00926
152	.779	29.894	0.00	1.02	.634	-.181	.01173
153	.780	29.920	0.00	1.49	.713	-.189	.01549
155	.782	29.964	0.00	2.01	.767	-.193	.02328
156	.779	29.930	0.00	2.51	.819	-.193	.02903
157	.781	29.970	0.00	3.02	.833	-.188	.03464
158	.781	29.940	0.00	3.51	.862	-.183	.04391
Run 18 and Run 19 $\bar{M}$ = .780 σ = .002 σ_m = −.004							
159	.776	29.569	1.00	-2.00	.123	-.162	.00954
161	.778	29.628	1.00	-1.00	.288	-.169	.00927
163	.779	29.632	1.00	.00	.450	-.175	.00954
164	.781	29.657	1.00	.50	.541	-.178	.01037
165	.779	29.666	1.00	1.01	.616	-.181	.01215
166	.779	29.664	1.00	1.53	.702	-.187	.01565
167	.782	29.727	1.00	2.03	.768	-.190	.02207
168	.778	29.624	1.00	2.51	.807	-.190	.02677
169	.782	29.721	1.00	3.08	.821	-.184	.03588
170	.781	29.706	1.00	3.53	.874	-.184	.04100

TABLE 4.- Continued

(b) Fixed transition

Point	M	R x 10^{-6}	$\dot{m}_{bl}$	α	c_n	c_m	c_d
Run 50 $\bar{M}$ = .601 σ = .001 σ_m = .002							
479	.602	6.032	0.00	-2.00	.111	-.124	.00894
480	.602	6.003	0.00	.02	.359	-.129	.00848
481	.602	6.008	0.00	1.03	.484	-.131	.00838
482	.600	5.995	0.00	2.02	.603	-.131	.00851
484	.600	5.989	0.00	2.50	.664	-.131	.00885
485	.601	5.996	0.00	3.02	.725	-.131	.00893
486	.601	6.000	0.00	3.53	.783	-.128	.00927
487	.604	6.018	0.00	4.02	.845	-.127	.00995
488	.603	6.012	0.00	5.01	.960	-.122	.01331
489	.599	5.989	0.00	6.03	1.074	-.115	.02013
Run 51 $\bar{M}$ = .701 σ = .001 σ_m = −.001							
491	.701	5.965	0.00	-.98	.229	-.134	.00961
492	.701	5.965	0.00	.02	.369	-.136	.00928
493	.700	5.964	0.00	.52	.436	-.137	.00918
494	.701	5.972	0.00	1.02	.506	-.138	.00935
495	.702	5.973	0.00	1.52	.575	-.138	.00941
496	.702	5.979	0.00	2.03	.652	-.139	.00951
497	.702	5.978	0.00	2.52	.727	-.137	.01007
498	.702	5.980	0.00	3.02	.804	-.136	.01177
499	.700	5.971	0.00	4.00	.973	-.137	.02059
500	.700	5.967	0.00	5.00	1.131	-.143	.03755
Run 52 $\bar{M}$ = .730 σ = .001 σ_m = −.002							
504	.729	5.967	0.00	-1.01	.224	-.134	.01006
505	.731	5.980	0.00	-.48	.300	-.137	.00989
506	.731	5.980	0.00	.03	.373	-.139	.00979
507	.730	5.978	0.00	.53	.446	-.140	.00974
508	.730	5.982	0.00	1.01	.518	-.141	.00972
509	.731	5.986	0.00	1.52	.596	-.140	.00983
510	.730	5.996	0.00	2.03	.679	-.141	.01033
511	.730	5.993	0.00	2.53	.764	-.141	.01219
512	.728	5.987	0.00	3.03	.861	-.144	.01547
513	.731	6.000	0.00	3.53	.954	-.151	.02176

TABLE 4.- Continued

(b) Continued

Point	M	R x 10^{-6}	$\dot{m}_{bl}$	α	c_n	c_m	c_d
Run 53 $\bar{M}$ = .730 σ = .001 σ_m = .002							
514	.731	5.973	1.00	-1.00	.219	-.134	.01006
515	.730	5.966	1.00	-.49	.293	-.136	.01035
516	.729	5.952	1.00	.02	.368	-.138	.01018
517	.730	5.949	1.00	.51	.439	-.139	.01017
518	.730	5.945	1.00	1.03	.510	-.140	.01014
519	.730	5.949	1.00	1.53	.584	-.140	.01017
521	.729	5.942	1.00	2.02	.657	-.138	.01063
522	.729	5.940	1.00	2.53	.745	-.139	.01227
523	.731	5.952	1.00	3.04	.840	-.142	.01580
524	.732	5.957	1.00	3.52	.934	-.148	.02116
Run 54 $\bar{M}$ = .730 σ = .001 σ_m = .003							
526	.733	5.868	2.00	-1.00	.212	-.133	.01023
527	.730	5.848	2.00	-.48	.287	-.135	.01009
528	.731	5.864	2.00	.02	.364	-.138	.01006
529	.732	5.867	2.00	.52	.435	-.139	.00999
530	.730	5.863	2.00	1.02	.508	-.140	.01007
531	.730	5.870	2.00	1.52	.581	-.140	.01006
532	.730	5.872	2.00	2.02	.657	-.139	.01041
533	.729	5.876	2.00	2.52	.738	-.138	.01179
535	.729	5.871	2.00	3.02	.832	-.141	.01457
536	.729	5.877	2.00	3.54	.922	-.145	.01947
Run 58 $\bar{M}$ = .752 σ = .001 σ_m = .002							
570	.752	5.984	0.00	-2.00	.059	-.131	.01027
571	.754	5.993	0.00	-.99	.214	-.136	.01004
572	.752	5.988	0.00	.02	.367	-.139	.00984
573	.750	5.975	0.00	.50	437	-.140	.00995
574	.751	5.986	0.00	1.02	.524	-.143	.01005
575	.752	5.990	0.00	1.52	.604	-.143	.01047
576	.752	5.992	0.00	2.02	.703	-.147	.01145
577	.752	5.985	0.00	2.53	.795	-.151	.01432
578	.752	5.995	0.00	3.01	.892	-.165	.01924
579	.751	5.988	0.00	3.51	.968	-.171	.02671

TABLE 4.- Continued

(b) Continued

Point	M	R x 10^{-6}	$\dot{m}_{bl}$	α	c_n	c_m	c_d
Run 57 $\bar{M}$ = .767 σ = .001 σ_m = .002							
559	.766	6.014	0.00	-1.99	.048	-.131	.01056
560	.769	6.025	0.00	-1.00	.209	-.136	.01041
561	.767	6.019	0.00	.01	.368	-.142	.01029
562	.765	6.008	0.00	.51	.450	-.144	.01036
563	.767	6.016	0.00	1.01	.529	-.145	.01036
565	.766	5.990	0.00	1.49	.621	-.148	.01115
566	.766	5.994	0.00	2.02	.727	-.157	.01381
567	.766	5.975	0.00	2.51	.807	-.166	.01868
568	.766	5.977	0.00	3.03	.881	-.172	.02490
569	.768	6.033	0.00	3.53	.889	-.170	.03443
Run 56 $\bar{M}$ = .767 σ = .001 σ_m = −.002							
548	.764	5.968	1.00	-1.95	.036	-.129	.01071
549	.766	5.975	1.00	-.99	.198	-.135	.01043
550	.767	5.978	1.00	.00	.360	-.141	.01054
552	.769	5.986	1.00	.51	.444	-.144	.01048
553	.768	5.983	1.00	1.01	.525	-.145	.01053
554	.767	5.978	1.00	1.52	.611	-.146	.01081
555	.767	5.977	1.00	2.02	.707	-.153	.01262
556	.767	5.966	1.00	2.51	.789	-.160	.01670
557	.768	5.972	1.00	3.02	.862	-.167	.02336
558	.766	6.008	1.00	3.52	.913	-.169	.02957
Run 55 $\bar{M}$ = .765 σ = .002 σ_m = .003							
537	.764	5.898	2.00	-2.00	.025	-.127	.01121
538	.763	5.900	2.00	-1.01	.194	-.135	.01092
539	.764	5.904	2.00	.02	.360	-.141	.01072
540	.766	5.910	2.00	.51	.441	-.144	.01078
541	.767	5.916	2.00	1.01	.526	-.147	.01093
543	.766	5.912	2.00	1.53	.618	-.150	.01134
544	.765	5.909	2.00	2.02	.704	-.153	.01306
545	.764	5.910	2.00	2.52	.786	-.160	.01610
546	.765	5.918	2.00	3.03	.853	-.167	.02160
547	.769	5.933	2.00	3.53	.918	-.170	.02970

TABLE 4.- Continued

(b) Continued

Point	M	R x 10^{-6}	$\dot{m}_{bl}$	α	c_n	c_m	c_d
Run 59 $\bar{M}$ = .782 σ = .001 σ_m = .002							
580	.781	5.993	0.00	-2.02	.029	-.132	.01176
581	.782	5.999	0.00	-.98	.201	-.137	.01083
582	.781	5.998	0.00	.02	.371	-.144	.01087
583	.781	5.996	0.00	.52	.459	-.147	.01088
584	.781	5.997	0.00	1.01	.546	-.151	.01158
585	.781	5.998	0.00	1.51	.643	-.159	.01415
586	.782	6.002	0.00	2.03	.720	-.168	.01983
587	.783	6.006	0.00	2.51	.765	-.170	.02673
588	.781	5.998	0.00	3.03	.817	-.170	.03180
589	.784	6.008	0.00	3.53	.812	-.164	.04206
Run 60 $\bar{M}$ = .732 σ = .001 σ_m = -.002							
590	.734	15.029	0.00	-1.99	.121	-.144	.00913
591	.730	15.046	0.00	-1.00	.265	-.148	.00900
592	.732	15.012	0.00	-.48	.339	-.149	.00909
593	.730	14.997	0.00	.02	.410	-.150	.00880
594	.732	15.015	0.00	.51	.476	-.151	.00882
595	.731	15.013	0.00	1.02	.556	-.152	.00886
596	.731	14.989	0.00	1.52	.627	-.151	.00908
598	.733	15.008	0.00	2.00	.716	-.152	.00986
599	.733	15.007	0.00	2.52	.807	-.152	.01257
600	.733	14.981	0.00	3.04	.907	-.158	.01689
601	.734	15.002	0.00	3.51	.995	-.167	.02370
Run 48 $\bar{M}$ = .731 σ = .001 σ_m = .001							
458	.731	15.006	0.00	-1.00	.256	-.148	.00865
459	.732	14.966	0.00	-.49	.331	-.150	.00866
460	.730	14.941	0.00	.03	.405	-.151	.00860
461	.731	14.953	0.00	.54	.479	-.152	.00859
462	.732	14.969	0.00	1.00	.550	-.153	.00872
463	.732	14.968	0.00	1.52	.631	-.152	.00910
464	.730	14.944	0.00	2.03	.716	-.152	.01036
465	.731	14.961	0.00	2.52	.815	-.154	.01370
466	.731	14.956	0.00	3.04	.917	-.160	.01885
467	.730	14.952	0.00	3.51	.999	-.166	.02518

TABLE 4.- Concluded

(b) Concluded

Point	M	R x 10^{-6}	$\dot{m}_{bl}$	α	c_n	c_m	c_d
Run 49 $\bar{M}$ = .765 σ = .001 σ_m = .003							
468	.765	14.947	0.00	-2.00	.101	-.148	.00926
469	.765	14.954	0.00	-.99	.264	-.153	.00905
470	.766	14.969	0.00	.01	.427	-.159	.00888
471	.765	14.954	0.00	.52	.508	-.160	.00896
472	.765	14.950	0.00	1.02	.595	-.162	.00918
473	.764	14.949	0.00	1.52	.691	-.166	.01033
474	.765	14.949	0.00	2.00	.780	-.175	.01375
475	.764	14.963	0.00	2.53	.862	-.185	.02005
476	.766	14.961	0.00	3.04	.889	-.184	.02762
477	.768	15.030	0.00	3.52	.898	-.177	.04601

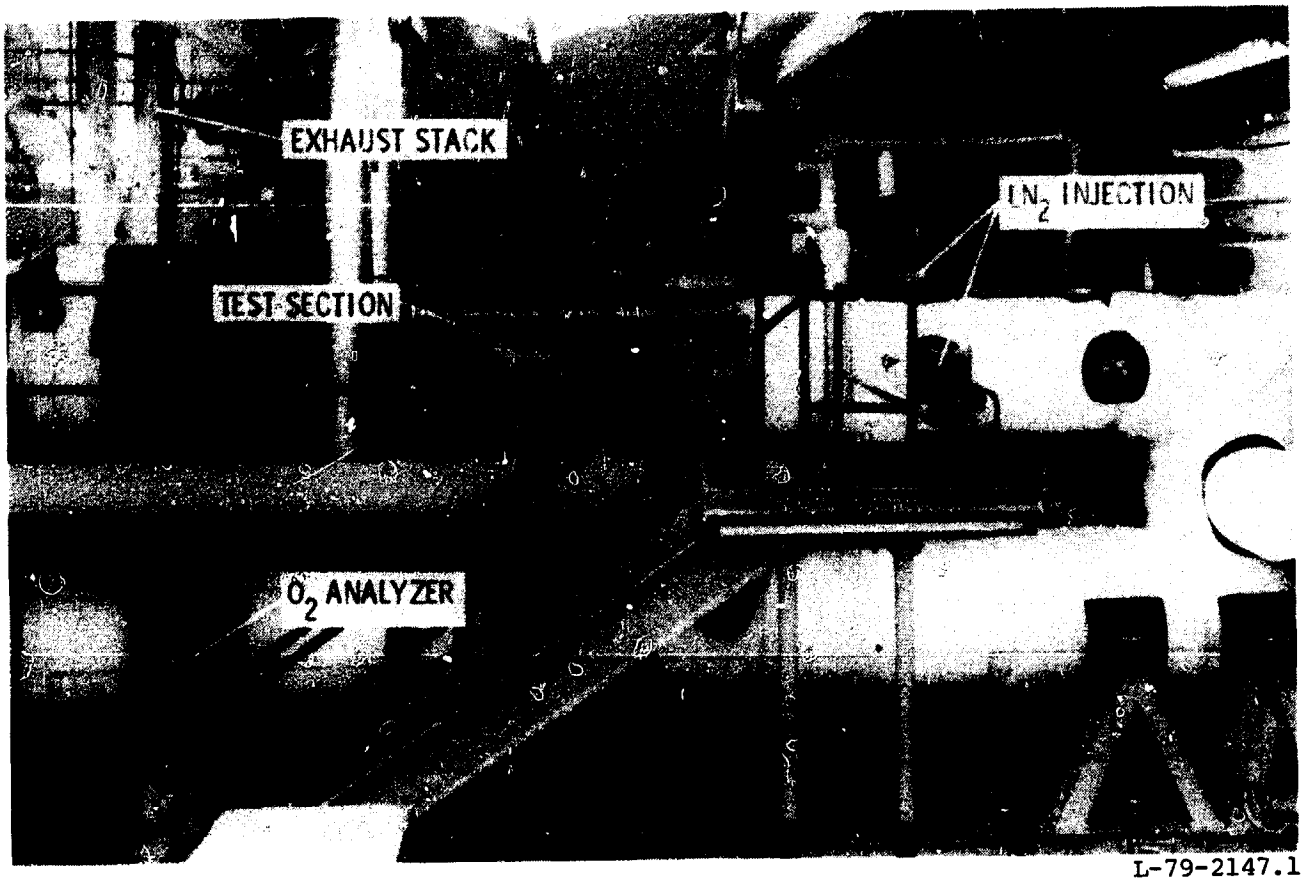

L-79-2147.1

(a) Photograph.

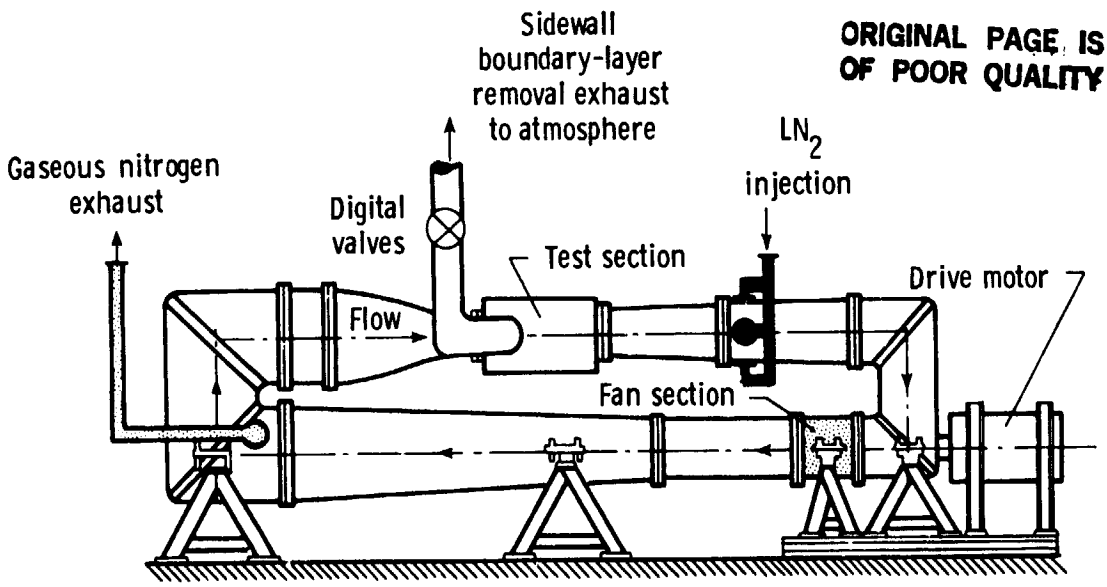

ORIGINAL PAGE IS OF POOR QUALITY

(b) Schematic.

Figure 1.- Elevation view of Langley 0.3-Meter Transonic Cryogenic Tunnel with 20- by 60-cm (8- by 24-in.) two-dimensional test section installed and with passive sidewall-boundary-layer removal system indicated.

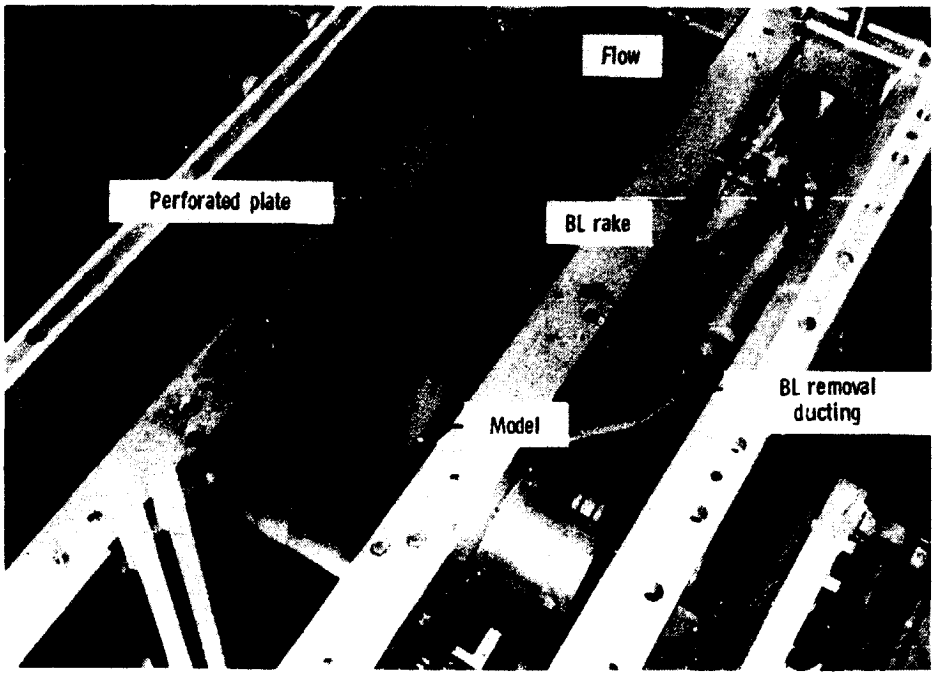

L-82-210

(a) Top-view photograph with perforated plate for boundary-layer removal.

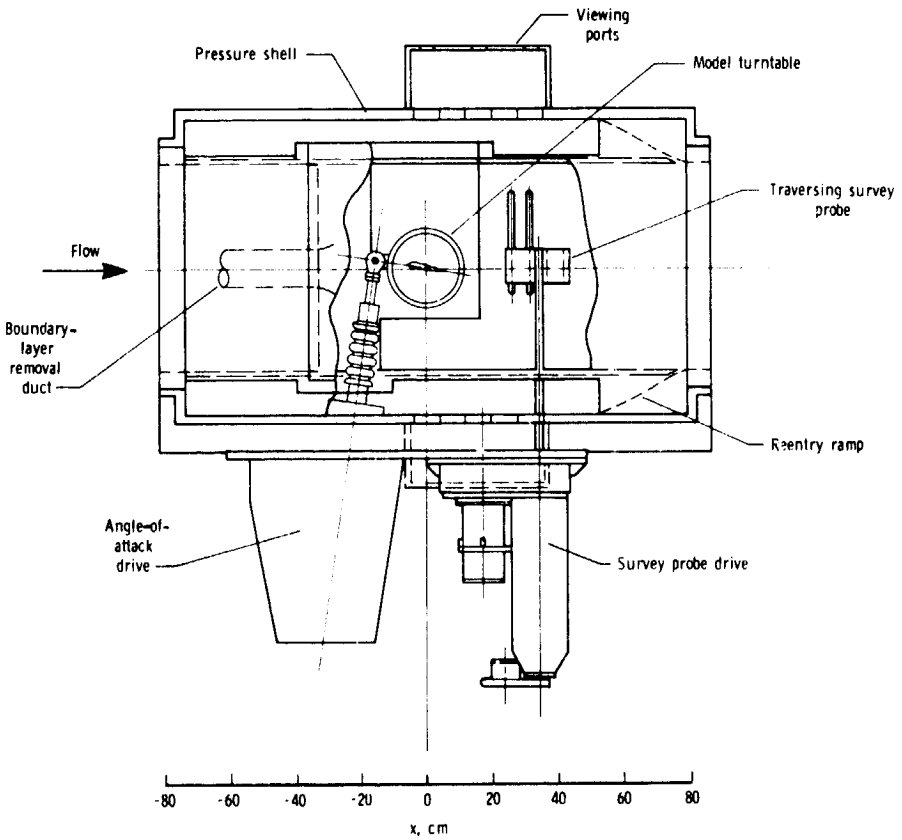

(b) Schematic showing major components.

Figure 2.- Two-dimensional test section.

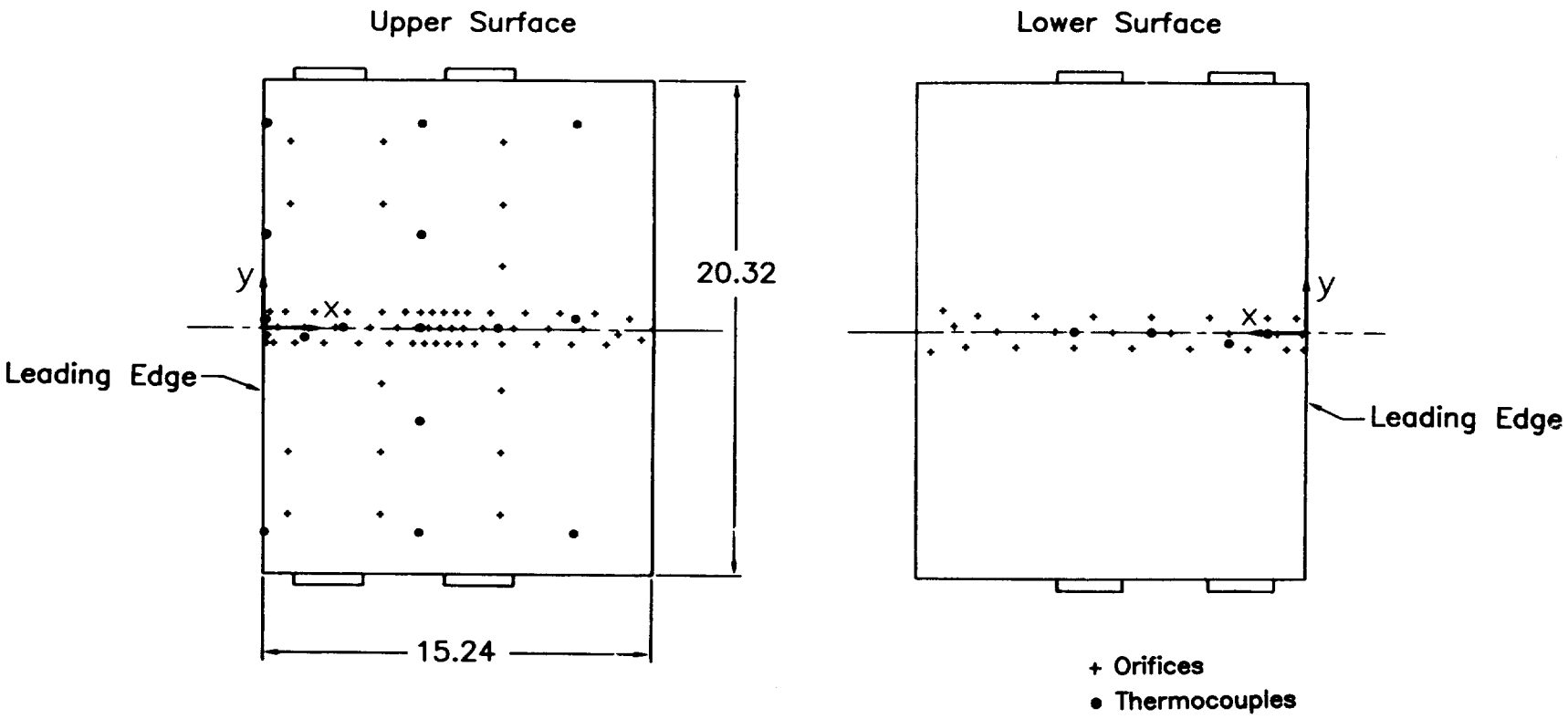

Figure 3.- Schematic of model showing orifice and thermocouple locations. Dimensions are in cm. Arrows indicate positive direction for x- and y-coordinates.

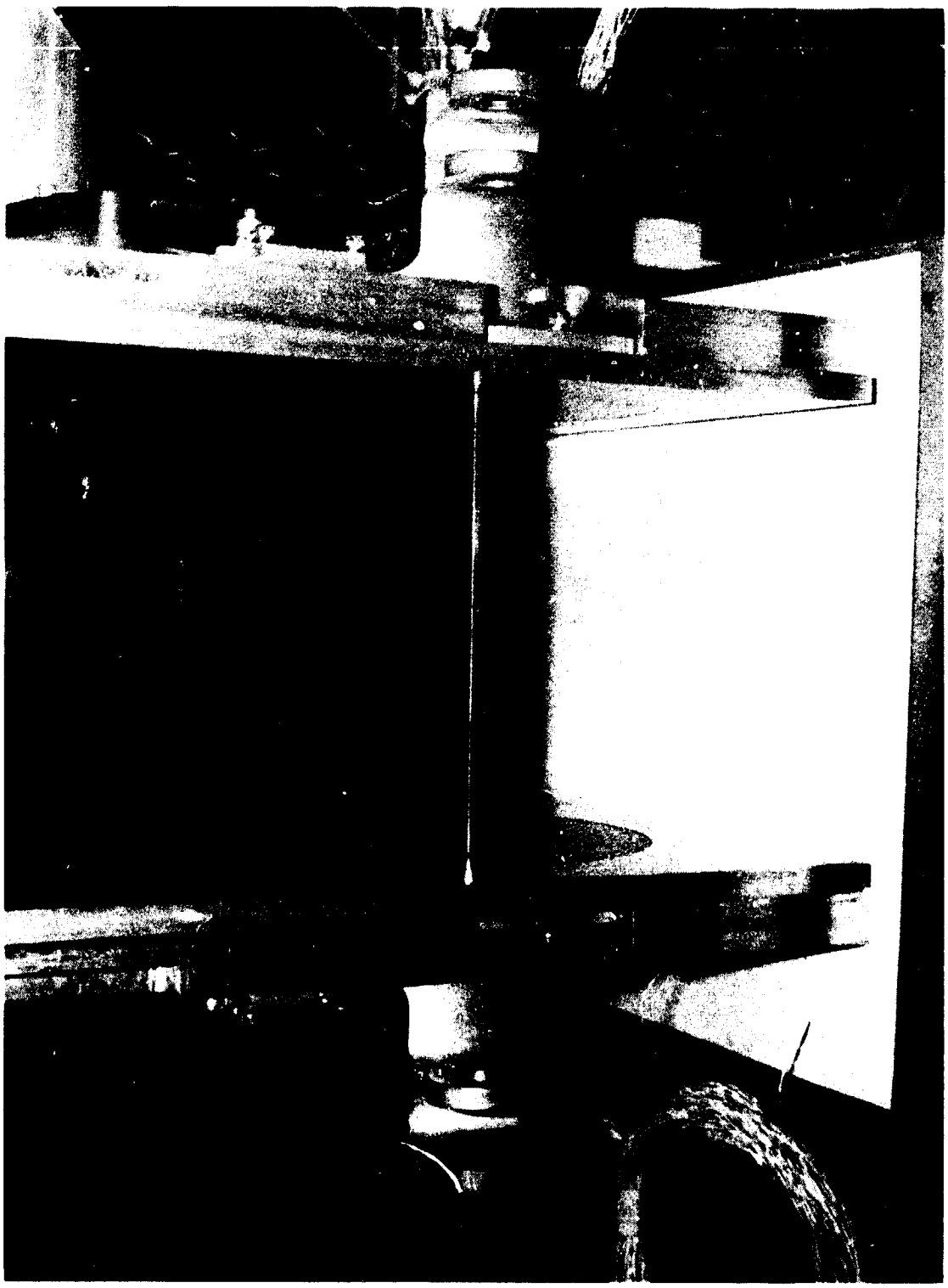

L-84-7481

Figure 4.- Photograph of DLBA 032 airfoil in turntable sidewall insert.

L-86-316

Figure 5.- Internal view of model under construction.

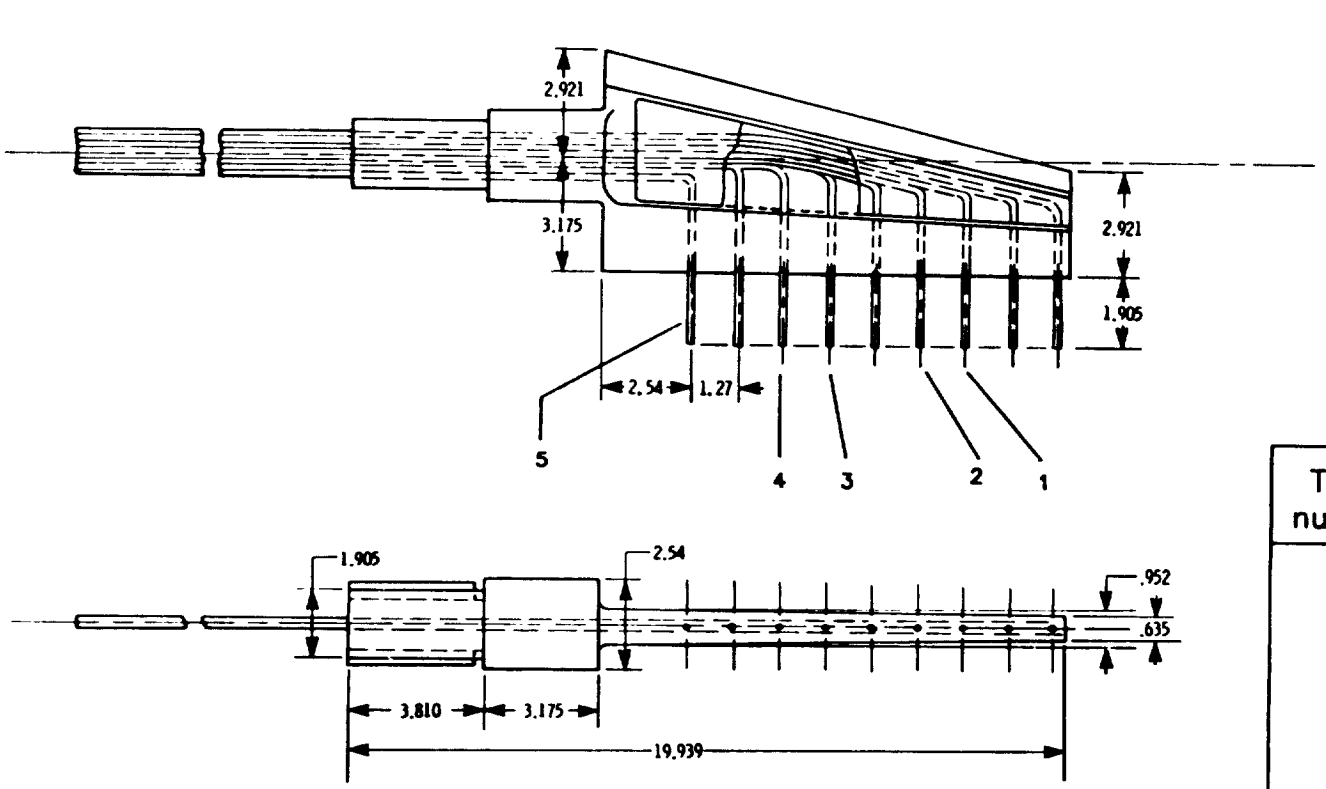

Tube number	y / b/2
1	0.000
2	−0.125
3	−0.375
4	−0.500
5	−0.750

Figure 6.- Details of wake survey probe. All dimensions are in cm.

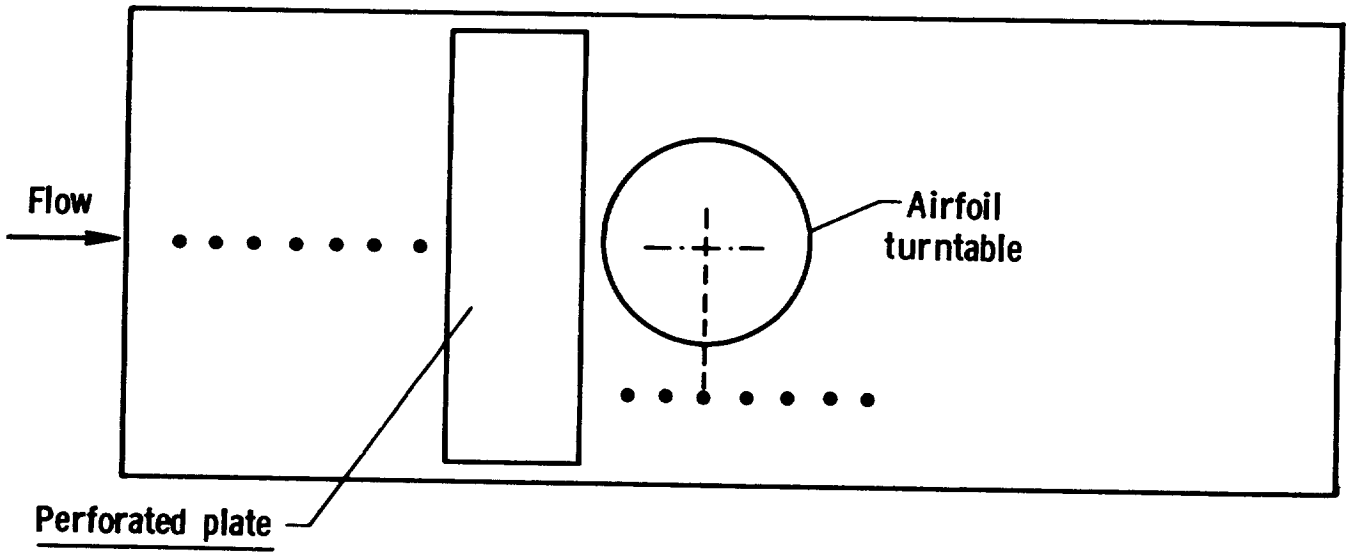

(a) Right sidewall.

Figure 7.- Sidewall-boundary-layer removal system.

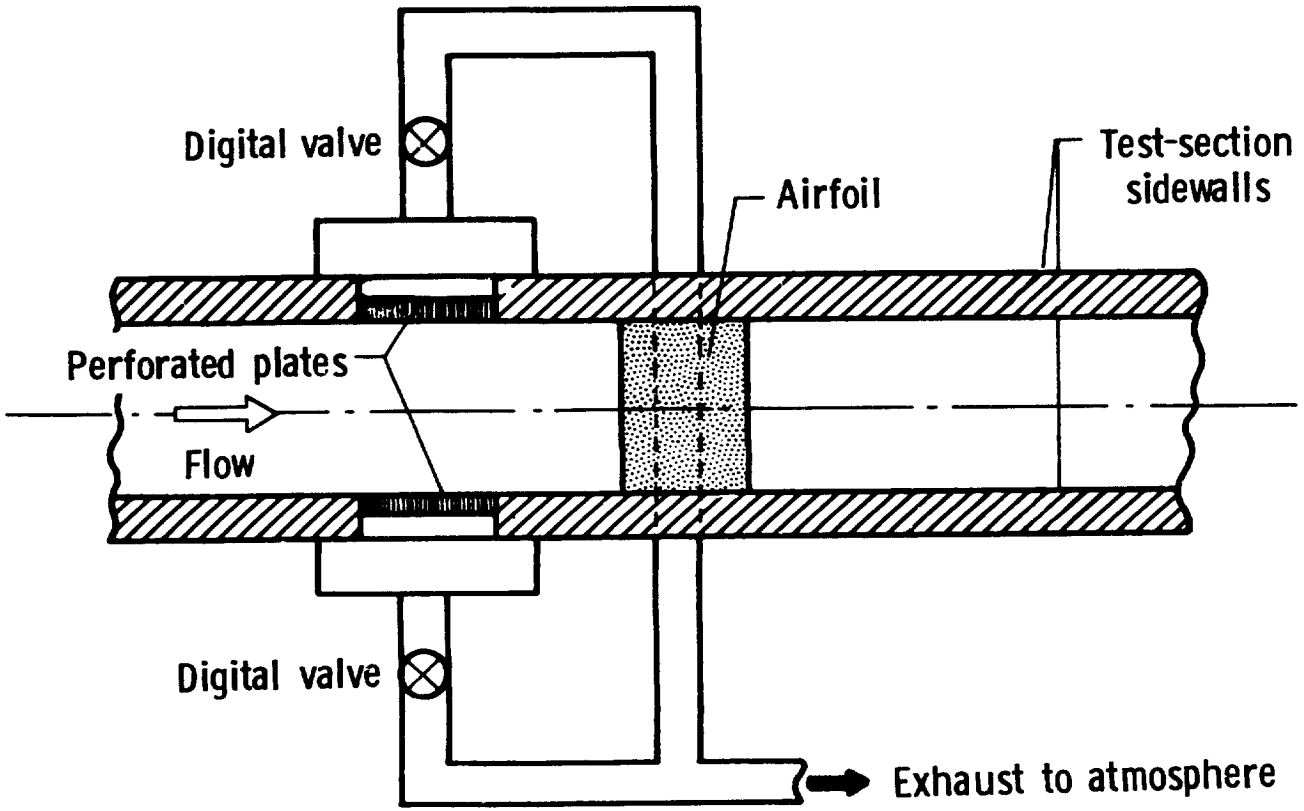

(b) Schematic of passive removal system.

Figure 7.- Concluded.

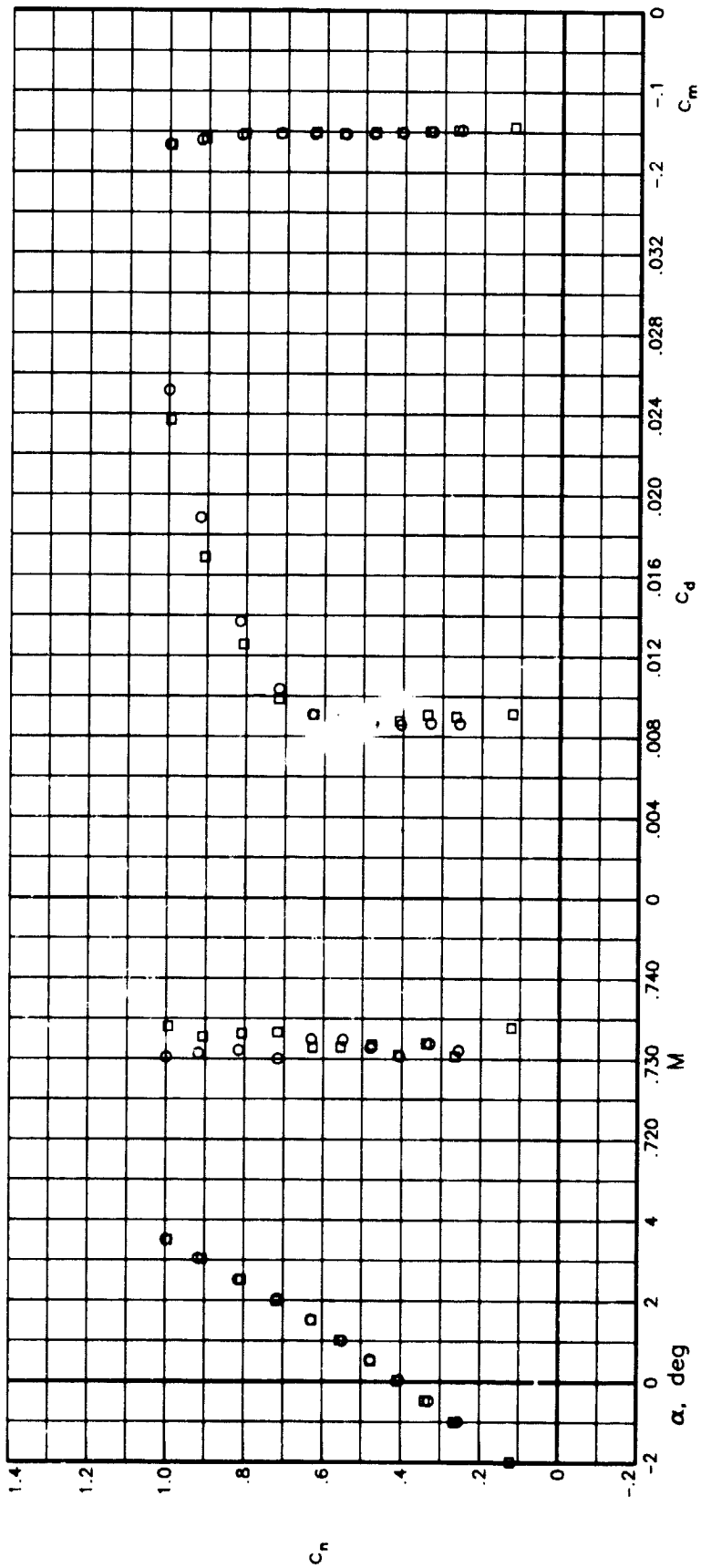

Figure 8.- Repeatability of two sets of data (O,□) with fixed transition at M = 0.730, R = 15.0 × 10^6, and $\hat{m}_{b1}$ = 0.

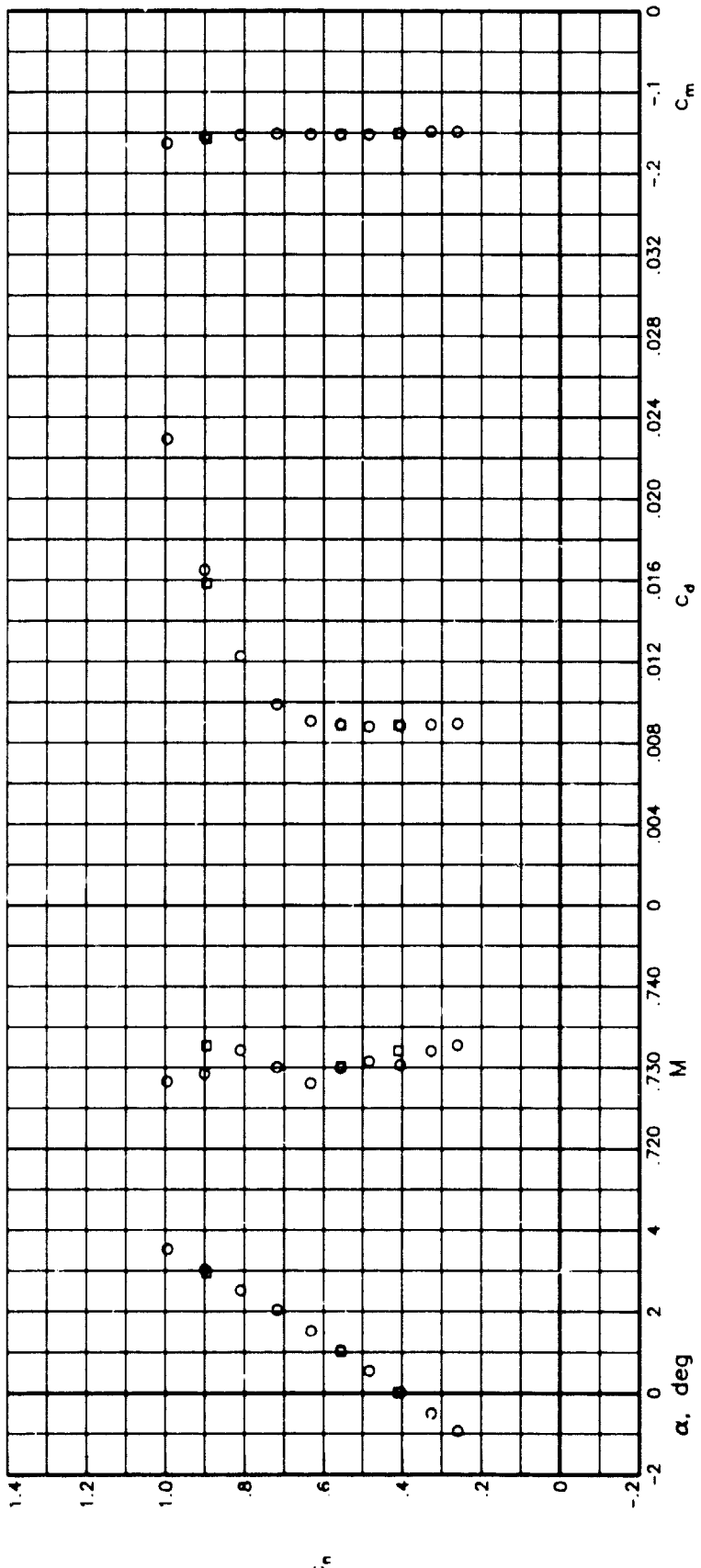

Figure 9.- Repeatability of data (○,□) with free transition at $M = 0.730$, $R = 15.0 \times 10^6$, and $\dot{m}_{bl} = 0$.

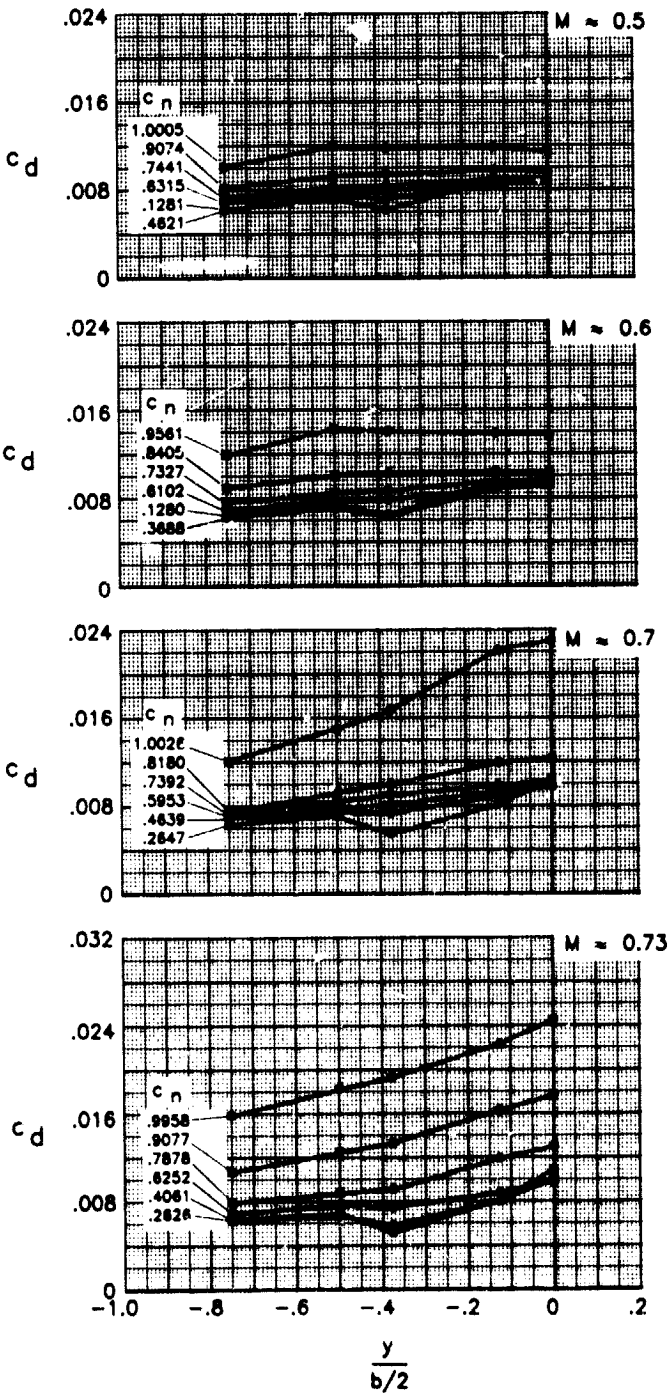

(a) $0.5 \leq M \leq 0.73$.

Figure 10.- Spanwise drag of airfoil with free transition for several Mach numbers at $R = 6.0 \times 10^6$ and $\dot{m}_{bl} = 0$.

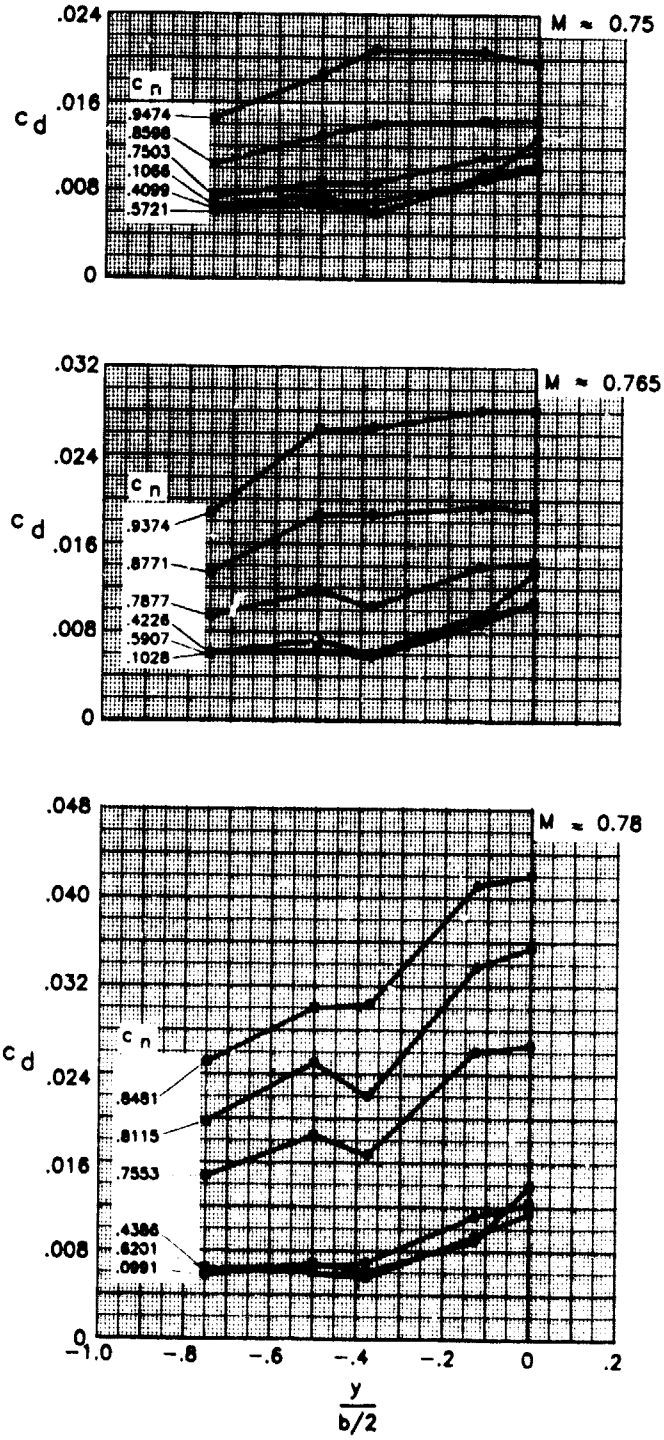

(b) $0.75 \leq M \leq 0.78$.

Figure 10.- Concluded.

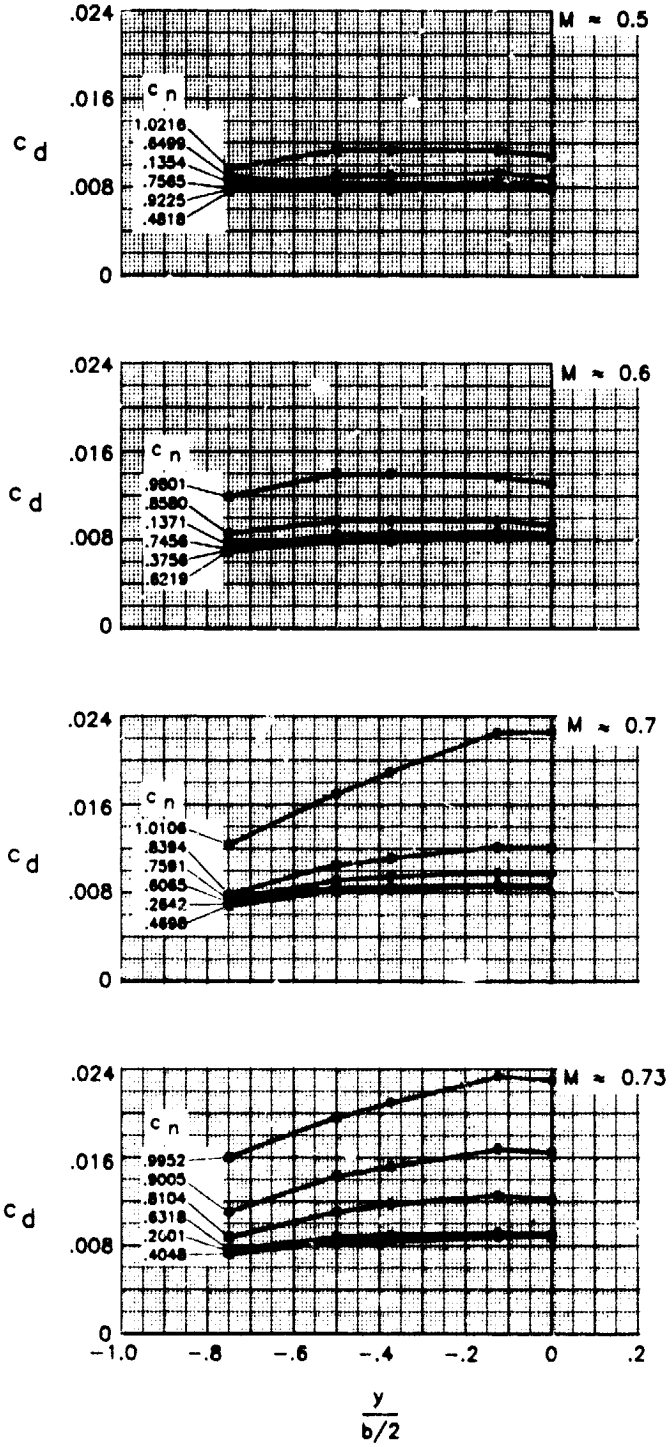

(a) $0.5 \leq M \leq 0.73$.

Figure 11.- Spanwise drag of airfoil with free transition for several Mach numbers at $R = 15.0 \times 10^6$ and $\dot{m}_{bl} = 0$.

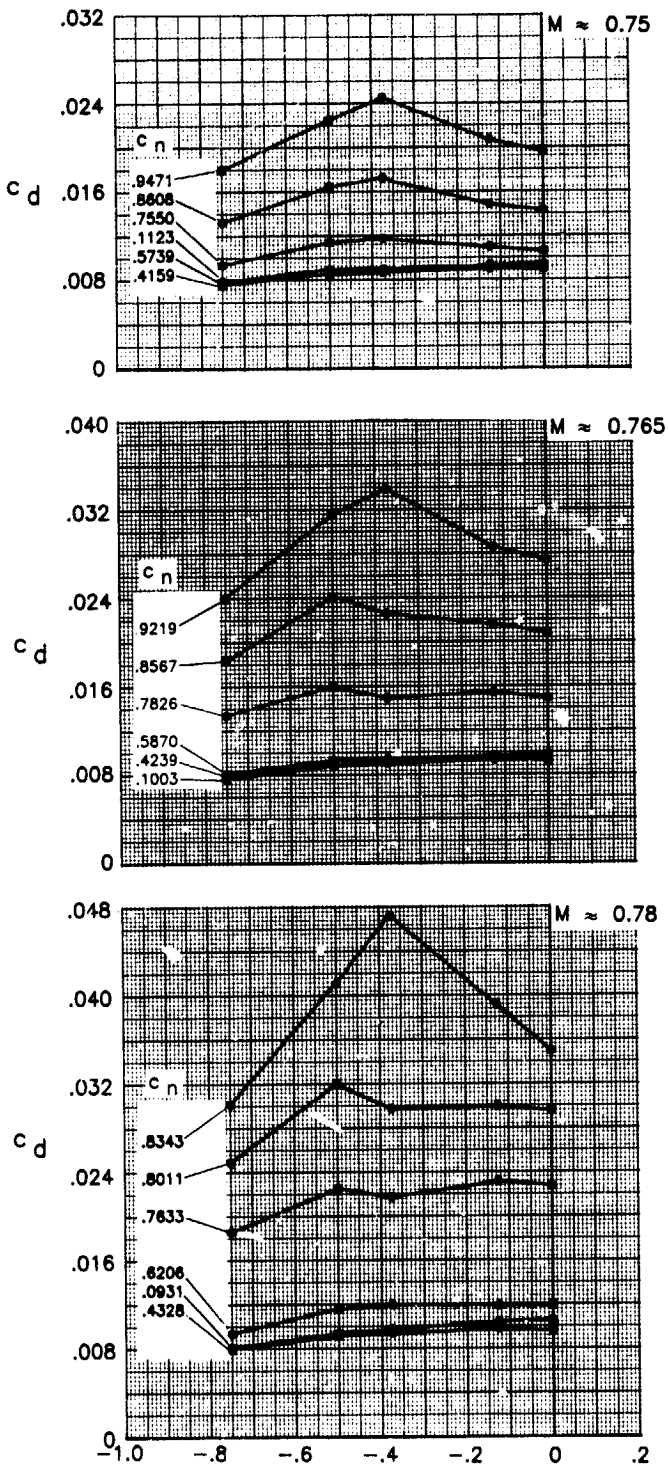

(b) $0.75 \leq M \leq 0.78$.

Figure 11.- Concluded.

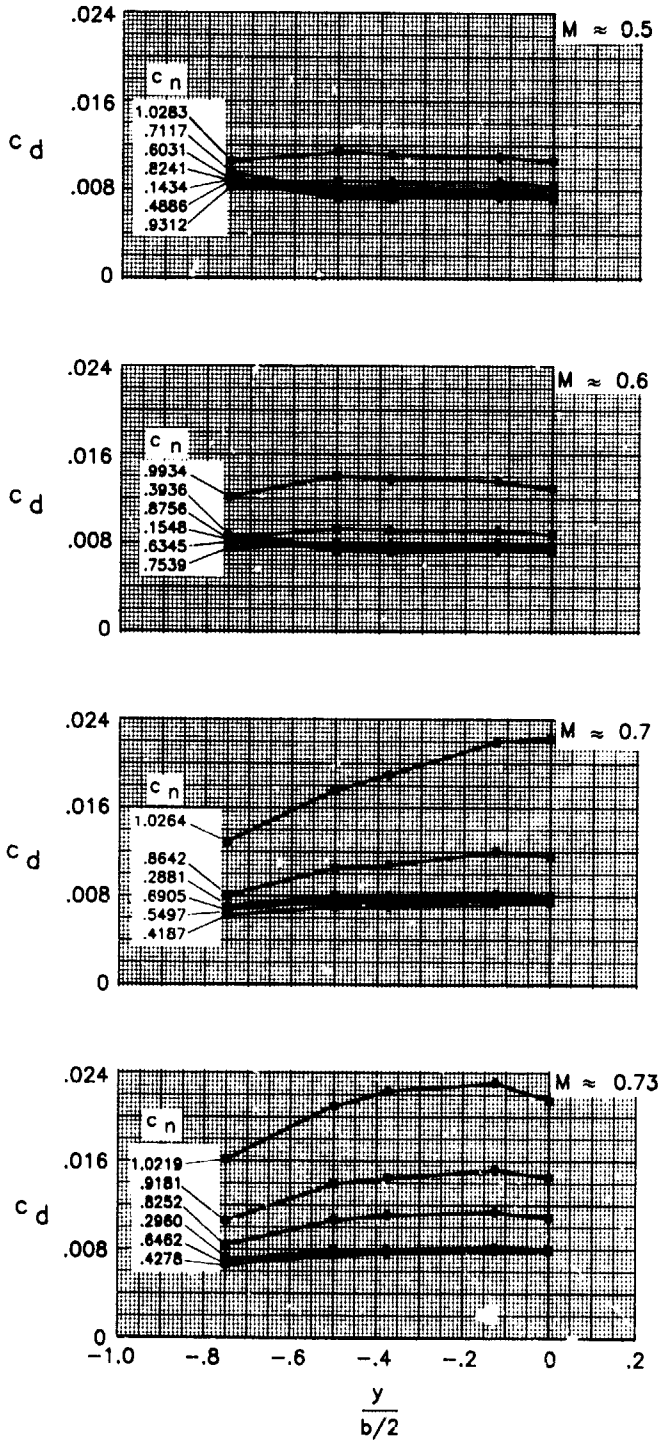

(a) $0.5 \leq M \leq 0.73$.

Figure 12.- Spanwise drag of airfoil with free transition for several Mach numbers at $R \approx 30.0 \times 10^6$ and $\dot{m}_{bl} = 0$.

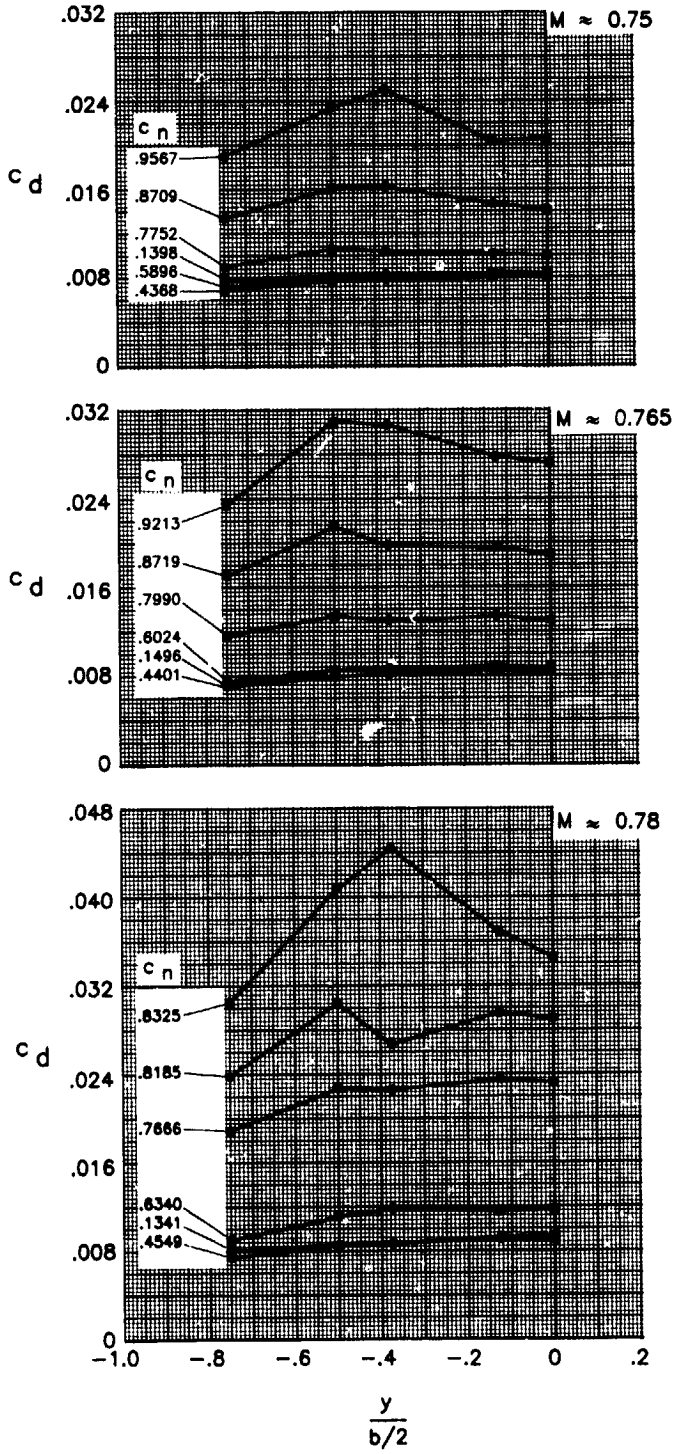

(b) $0.75 \leq M \leq 0.78$.

Figure 12.- Concluded.

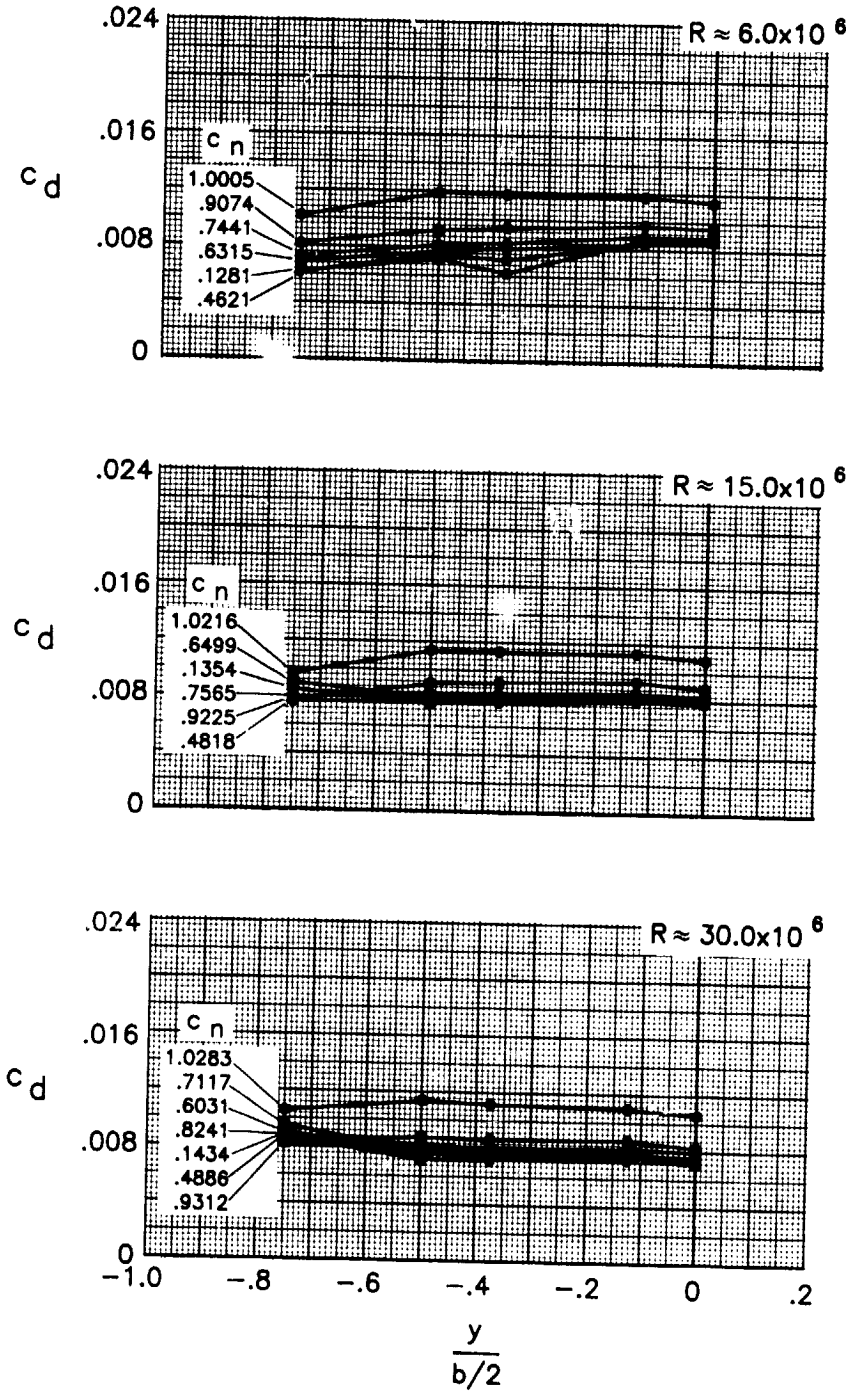

Figure 13.- Spanwise drag of airfoil with free transition for several Reynolds numbers at $M = 0.500$ and $\dot{m}_{bl} = 0$.

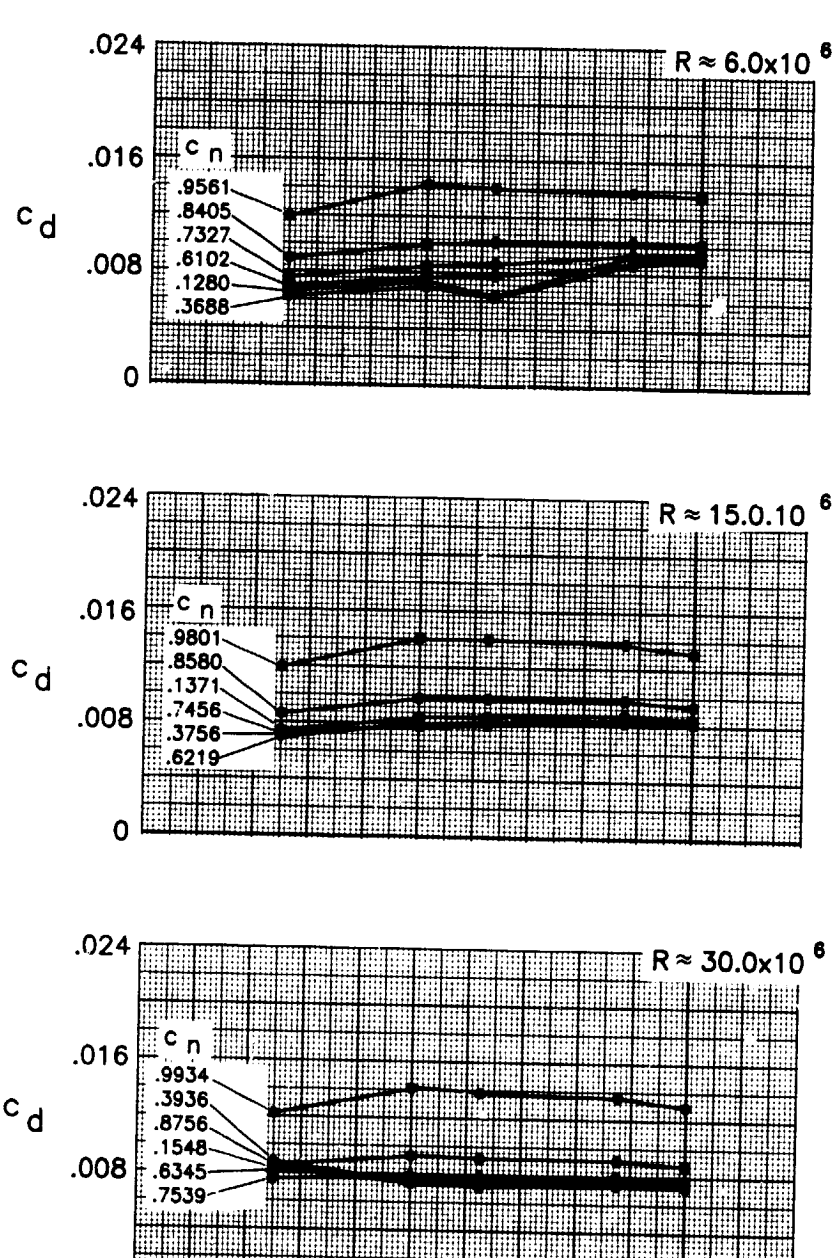

Figure 14.- Spanwise drag of airfoil with free transition for several Reynolds numbers at M ≈ 0.600 and $\dot{m}_{bl} = 0$.

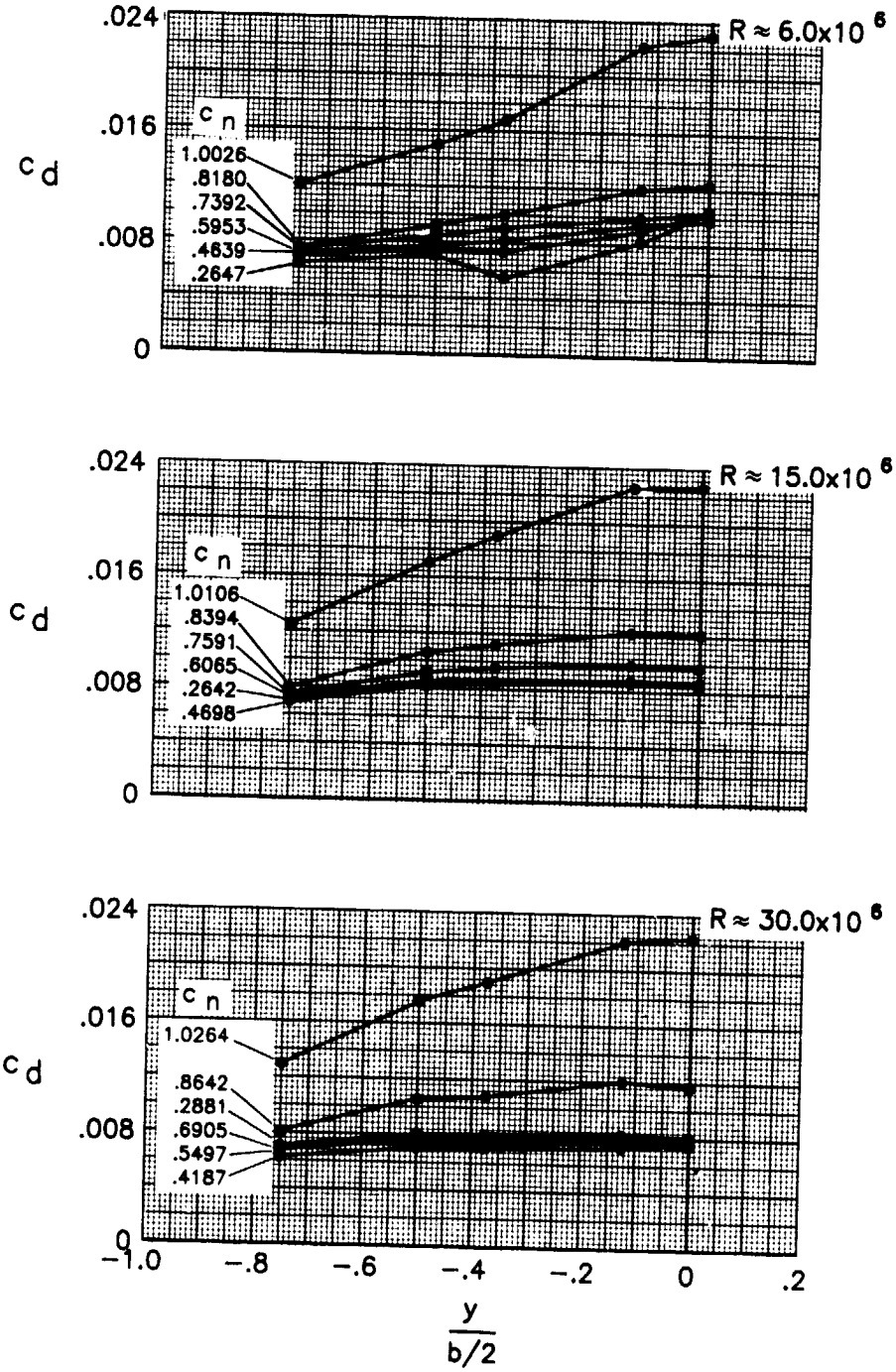

Figure 15.- Spanwise drag of airfoil with free transition for several Reynolds numbers at $M \approx 0.700$ and $\dot{m}_{bl} = 0$.

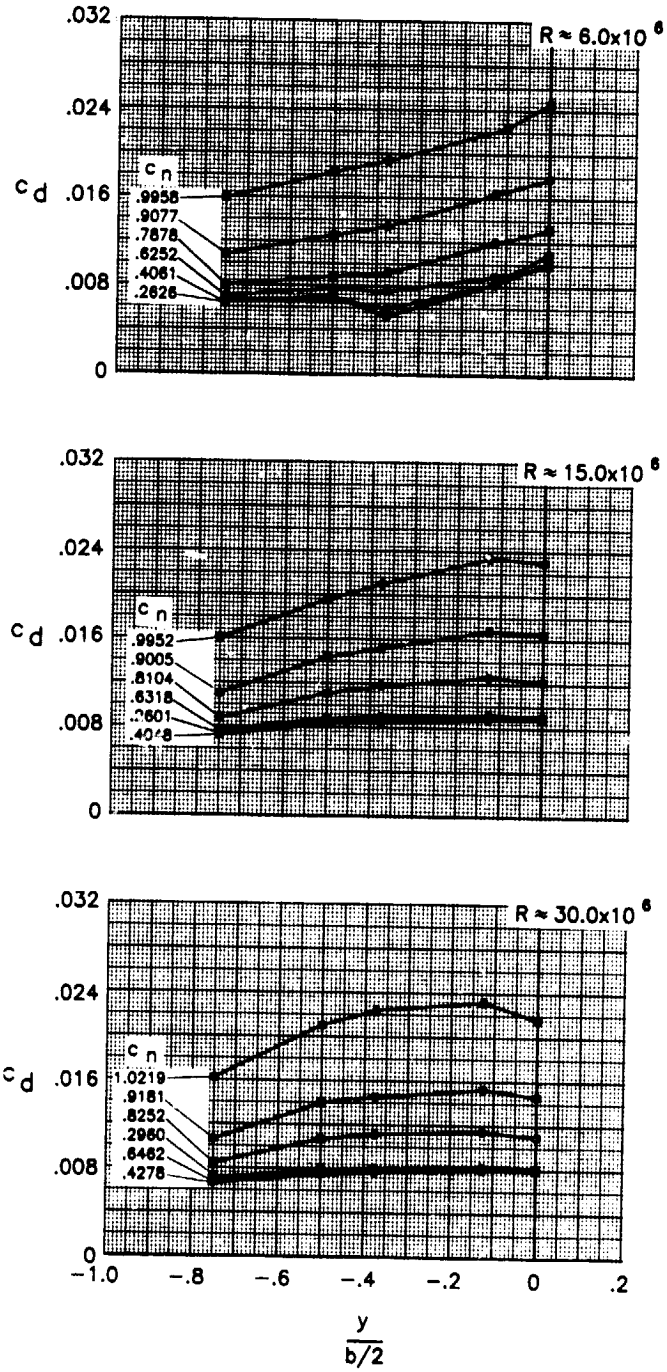

Figure 16.- Spanwise drag of airfoil with free transition for several Reynolds numbers at $M \approx 0.730$ and $\dot{m}_{bl} = 0$.

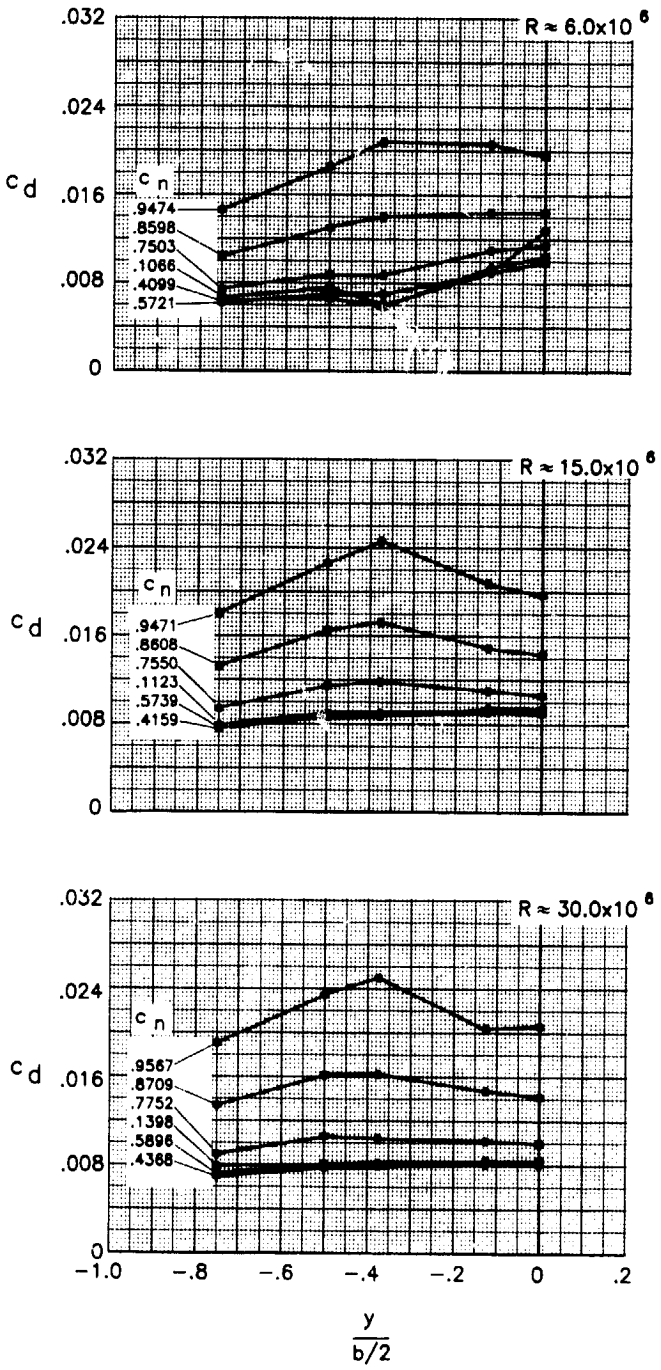

Figure 17.- Spanwise drag of airfoil with free transition for several Reynolds numbers at $M \approx 0.750$ and $\dot{m}_{bl} = 0$.

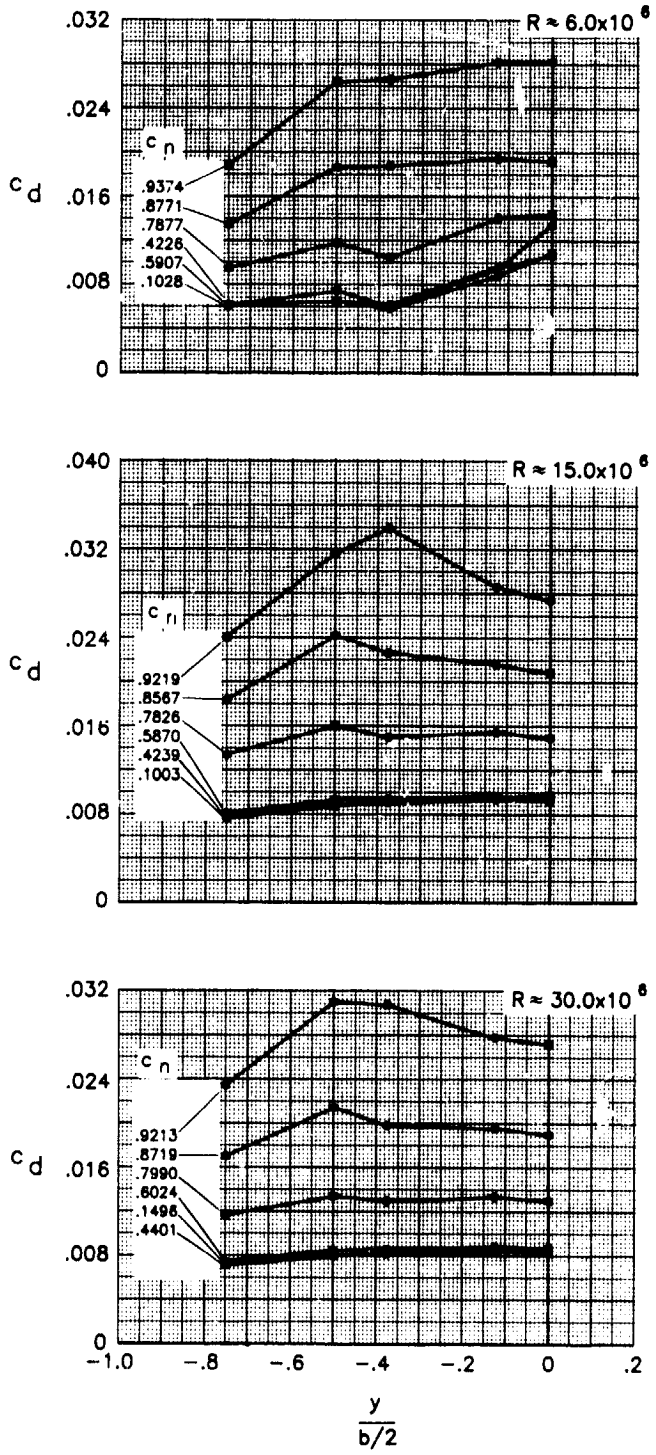

Figure 18.- Spanwise drag of airfoil with free transition for several Reynolds numbers at $M \approx 0.765$ and $\dot{m}_{bl} = 0$.

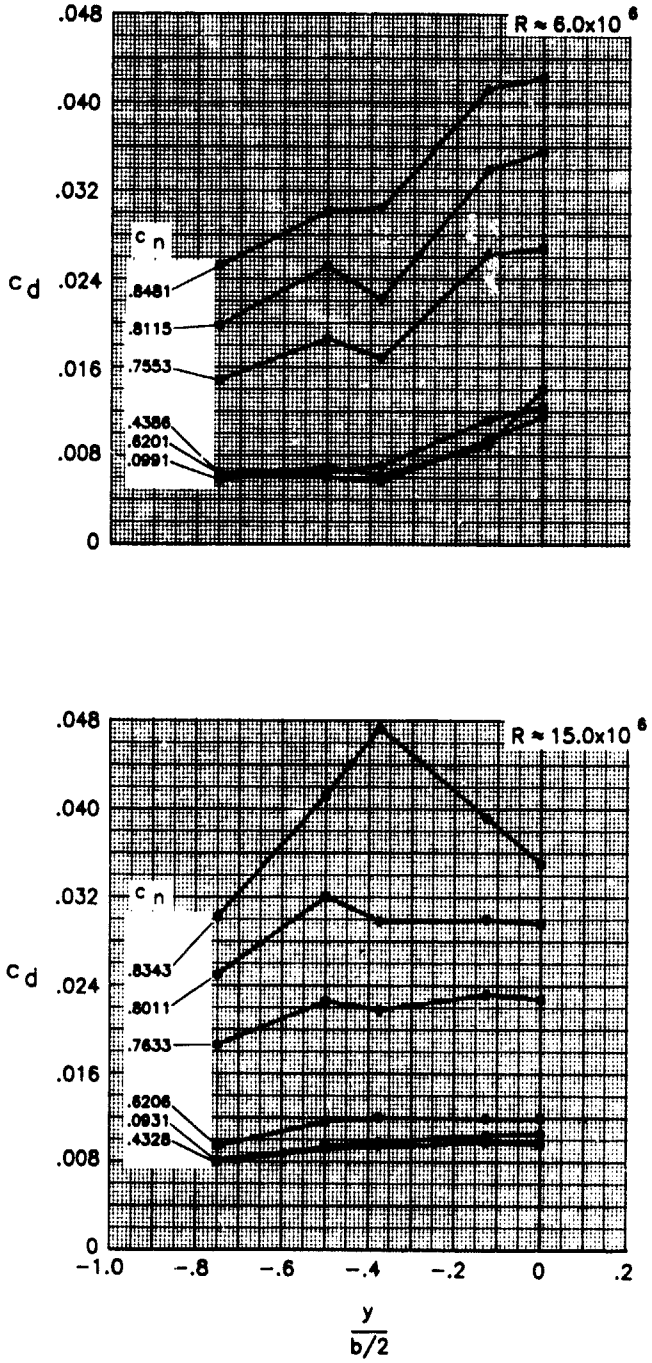

(a) $R \approx 6.0 \times 10^6$ and $R \approx 15.0 \times 10^6$.

Figure 19.- Spanwise drag of airfoil with free transition for several Reynolds numbers at $M \approx 0.780$ and $\dot{m}_{bl} = 0$.

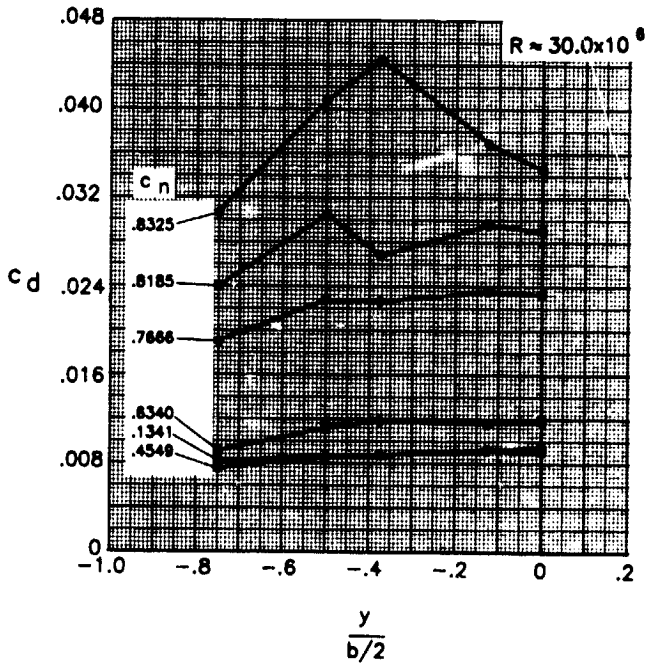

(b) $R \approx 30.0 \times 10^6$.

Figure 19.- Concluded.

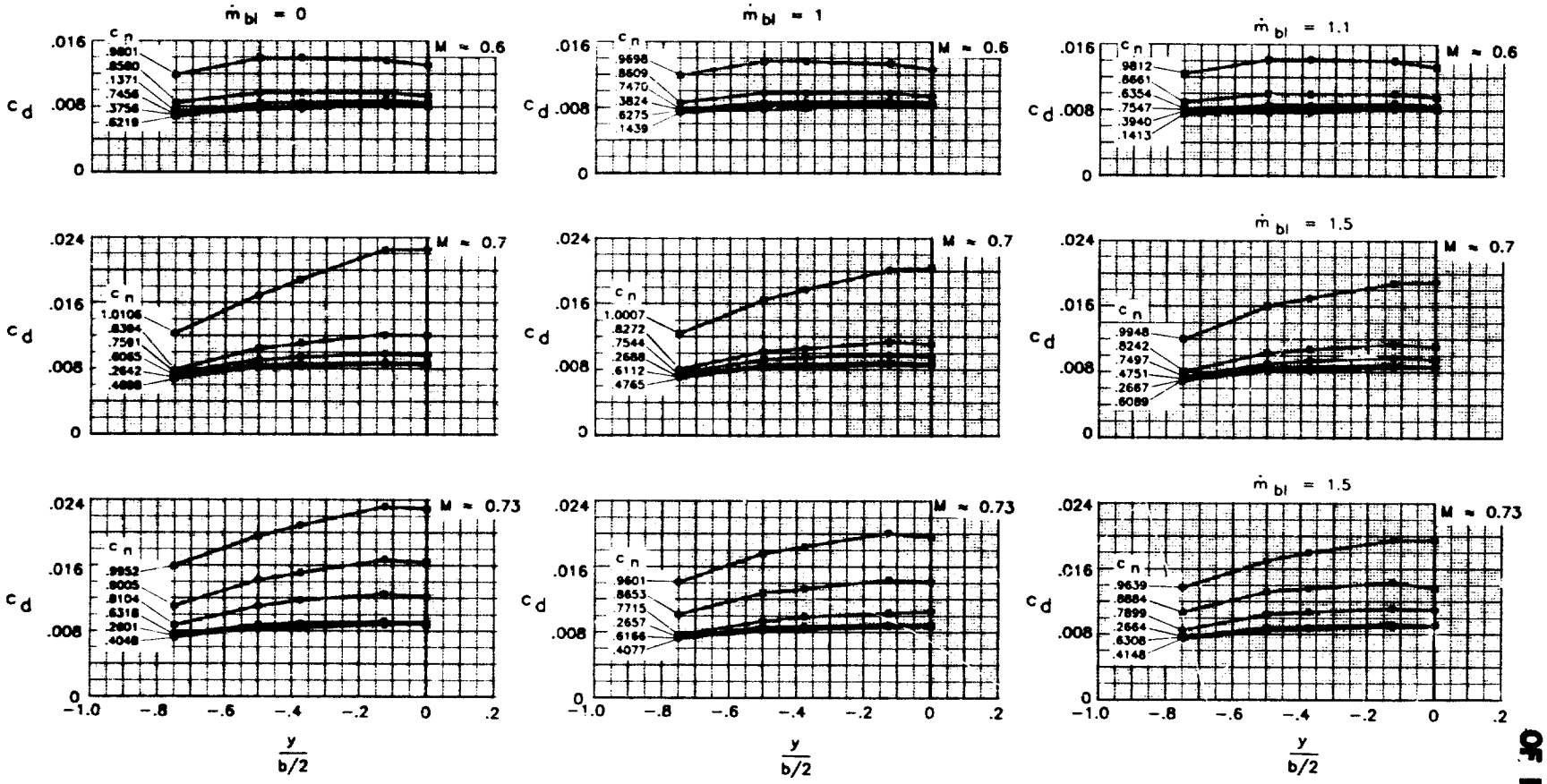

(a) $0.6 \leq M \leq 0.73$.

Figure 20.- Effect of sidewall-boundary-layer removal on spanwise drag of airfoil with free transition for several Mach numbers at $R \approx 15.0 \times 10^6$.

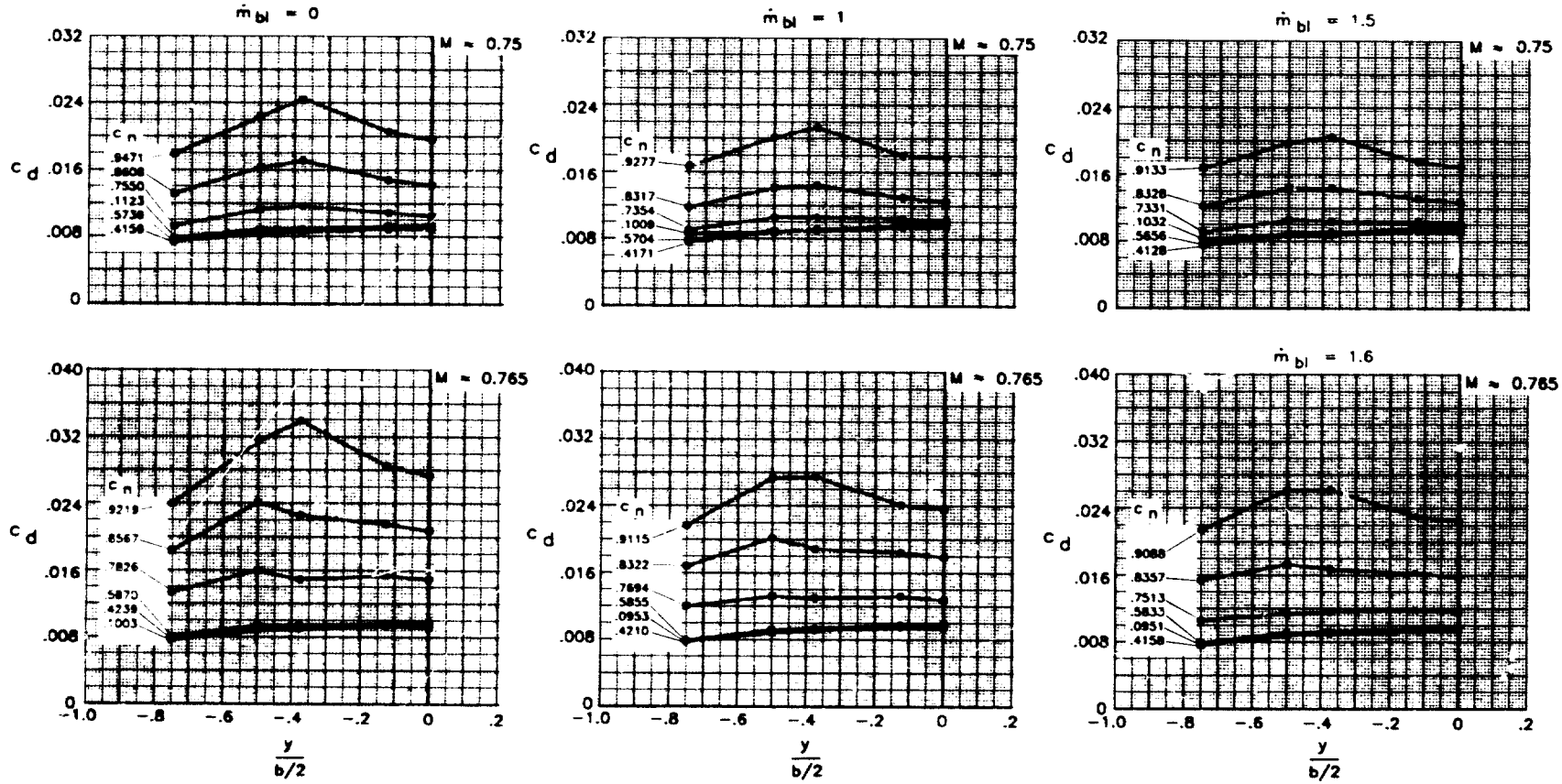

(b) $0.75 \leq M \leq 0.765$.

Figure 20.- Continued.

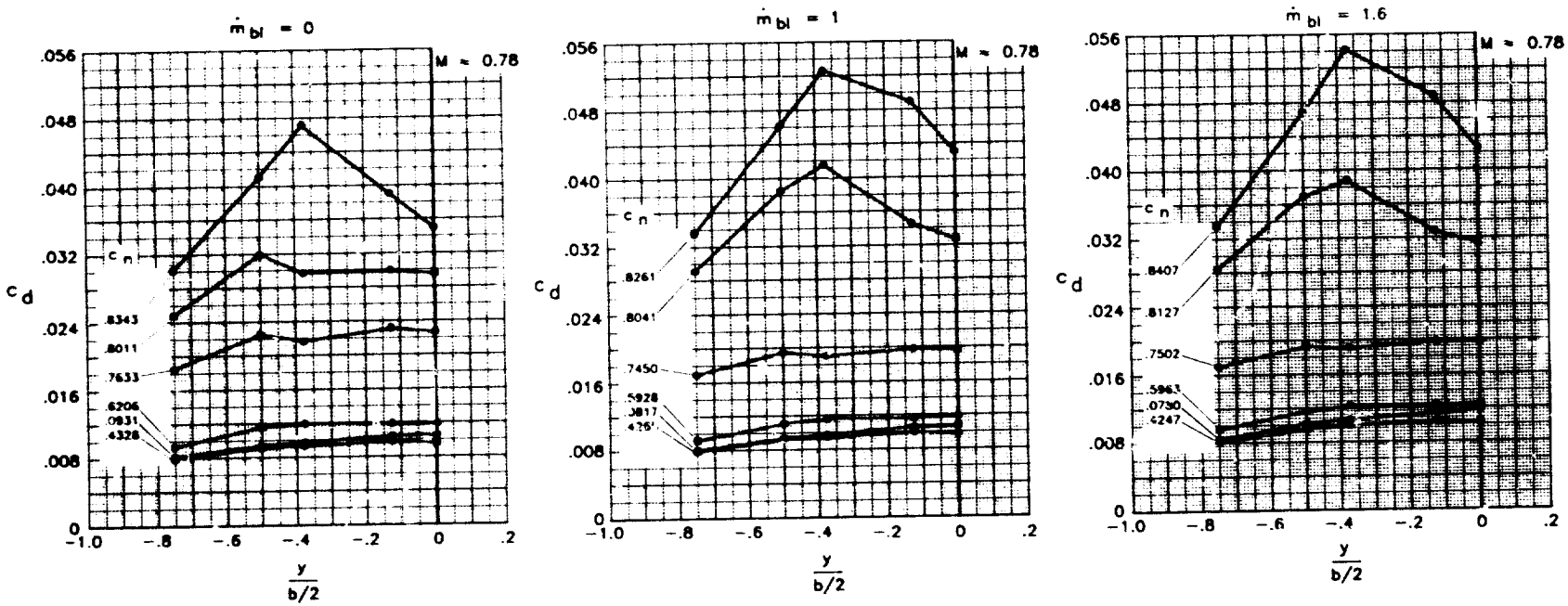

(c) M ≈ 0.78.

Figure 20.- Concluded

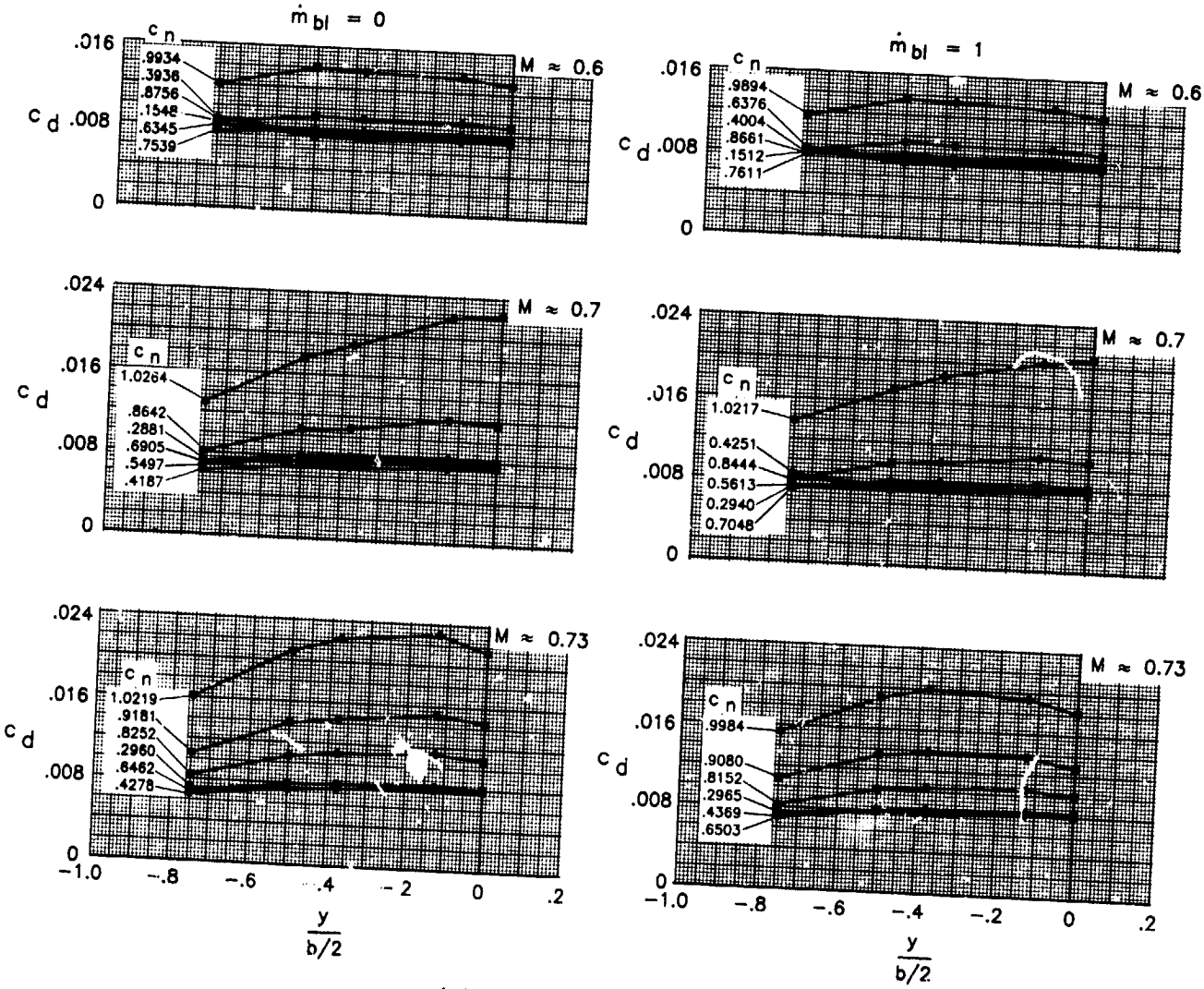

(a) $0.60 \leq M \leq 0.73$.

Figure 21.- Effect of sidewall-boundary-layer removal on spanwise drag of airfoil with free transition for several Mach numbers at $R \approx 30.0 \times 10^6$.

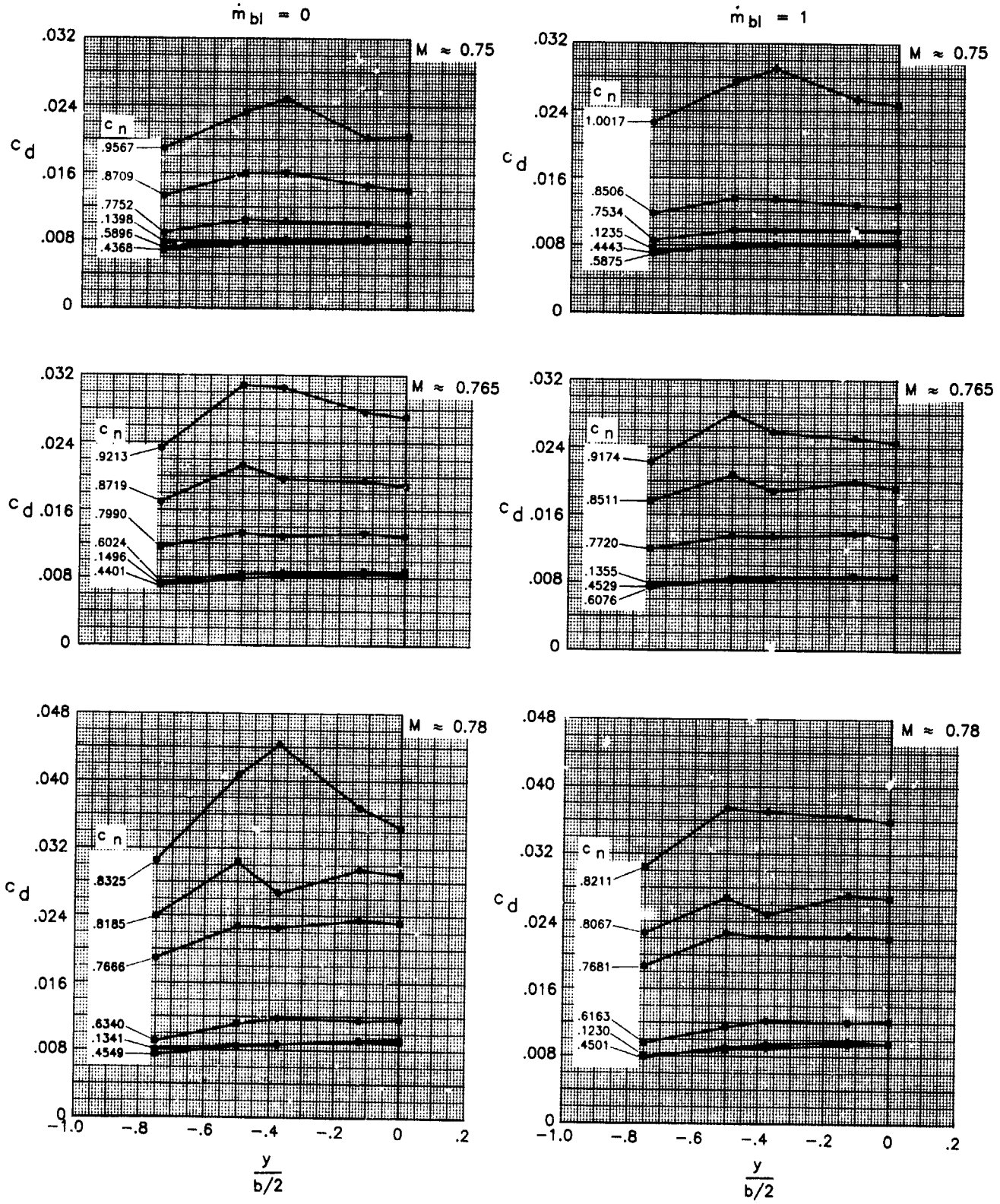

(b) $0.75 \leq M \leq 0.78$.

Figure 21.- Concluded.

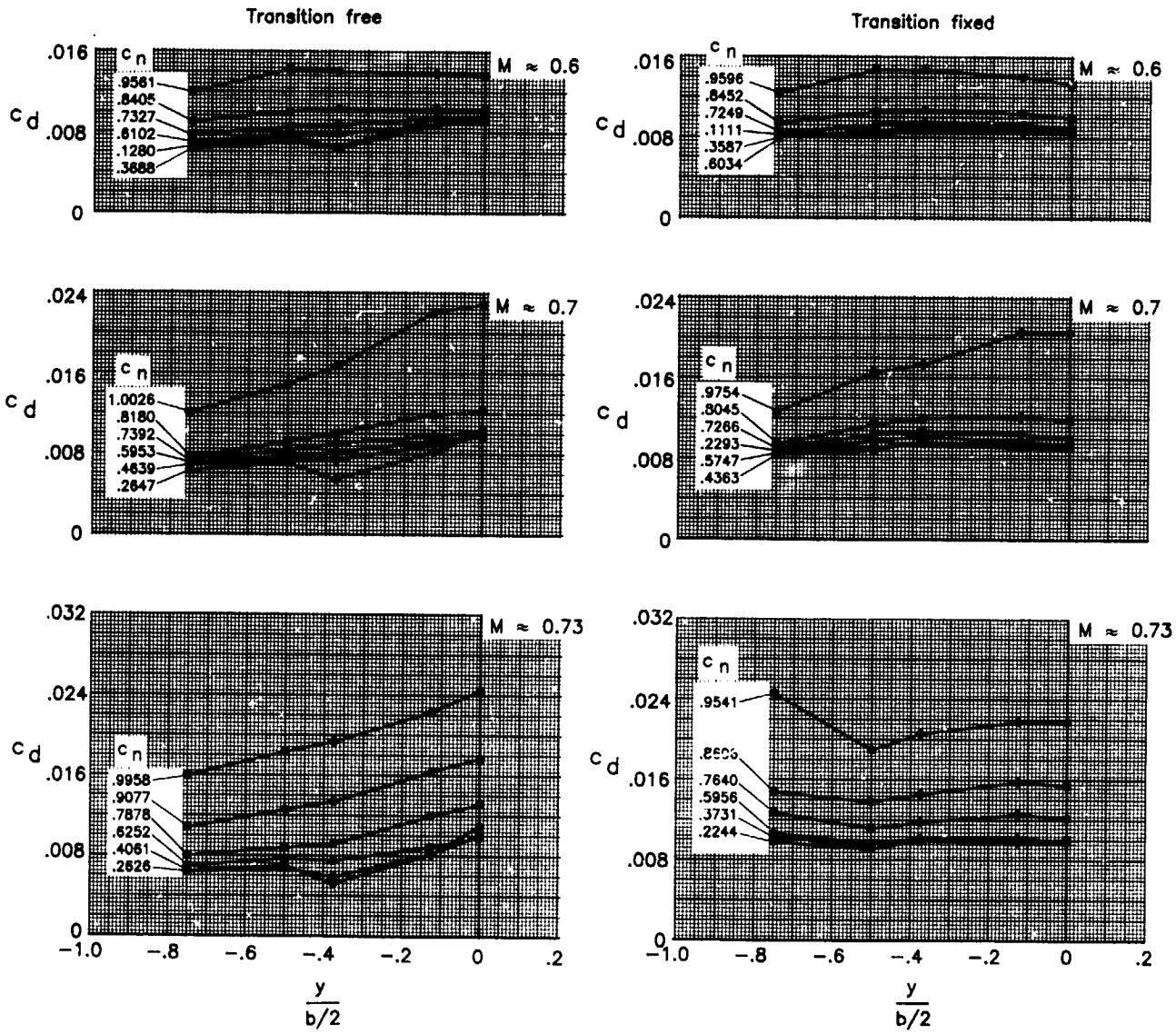

(a) $0.60 \leq M \leq 0.73$.

Figure 22.- Comparison of spanwise drag of airfoil with free and fixed transition for several Mach numbers at $R \approx 6.0 \times 10^6$ and $\dot{m}_{bl} = 0$.

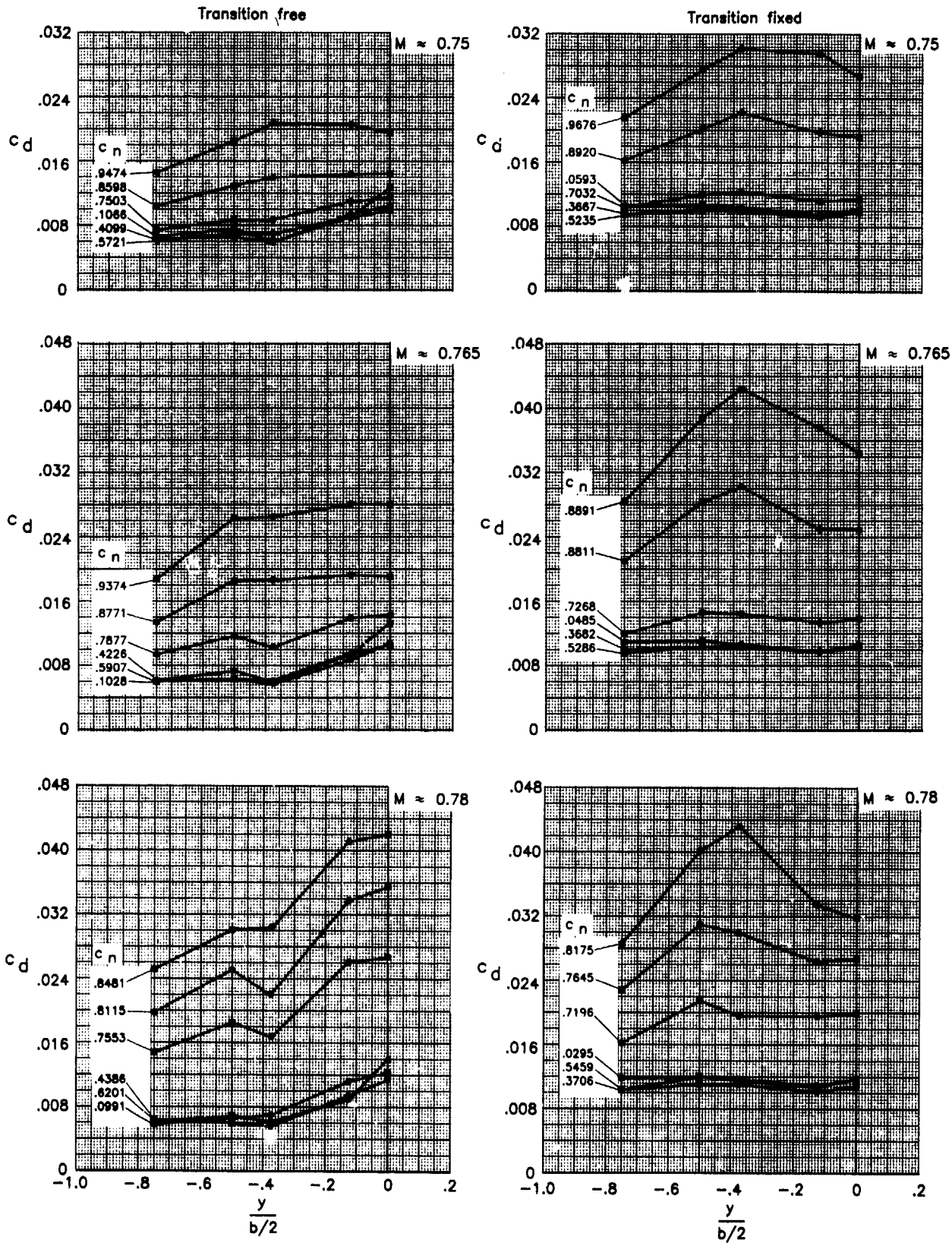

(b) $0.75 \leq M \leq 0.78$.

Figure 22.- Concluded.

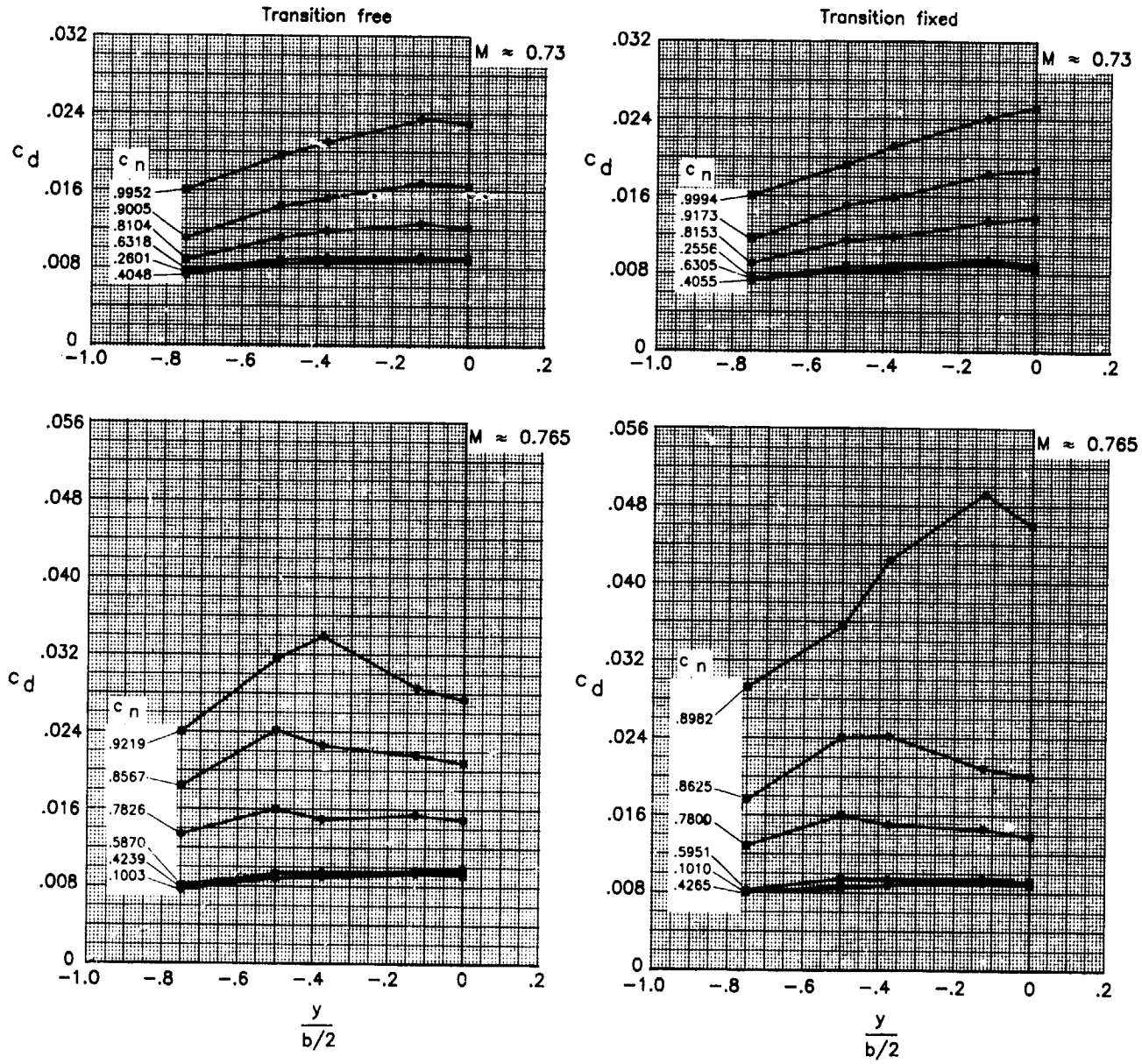

Figure 23.- Comparison of spanwise drag of airfoil with free and fixed transition for two Mach numbers at $R \approx 15.0 \times 10^6$ and $\dot{m}_{bl} = 0$.

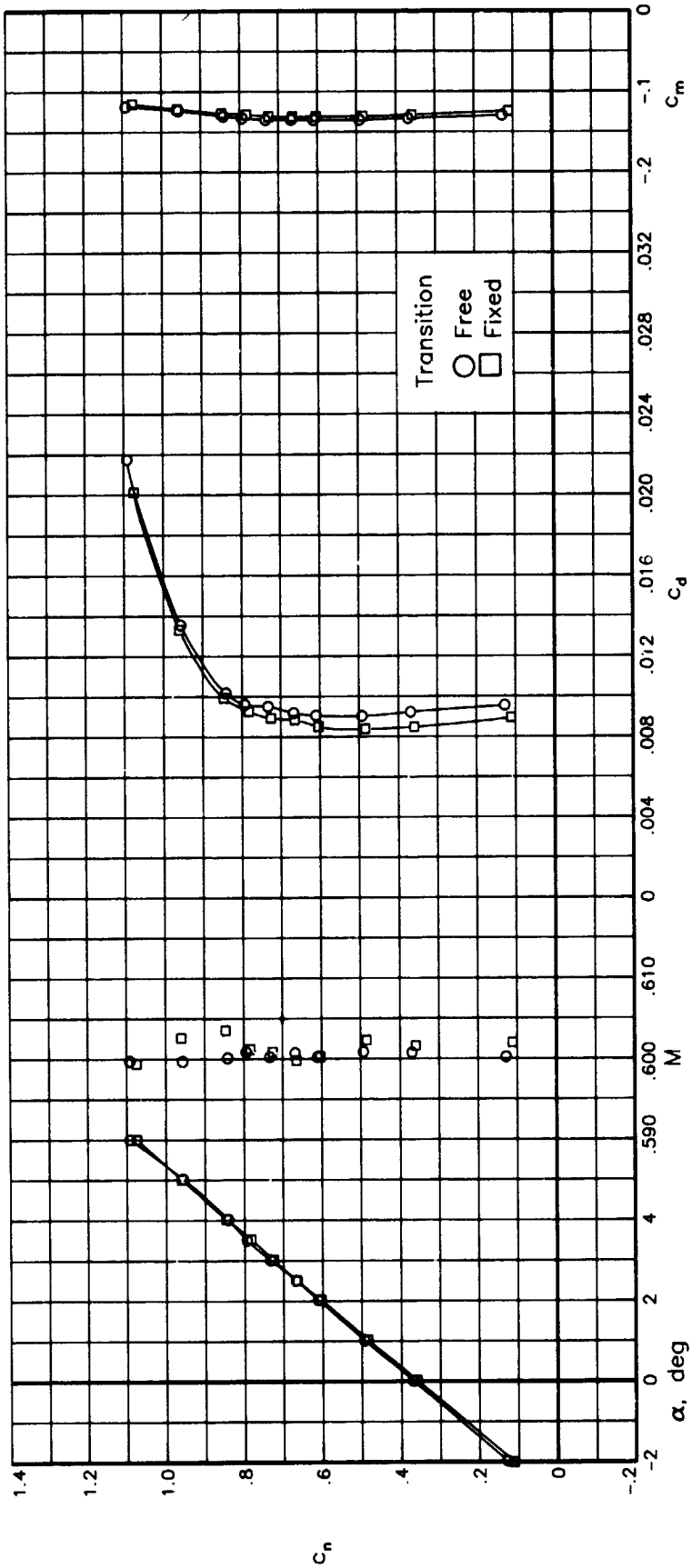

Figure 24.- Effect of fixing transition on aerodynamic characteristics of airfoil at $M \approx 0.600$, $R \approx 6.0 \times 10^6$, and $\dot{m}_{bl} = 0$.

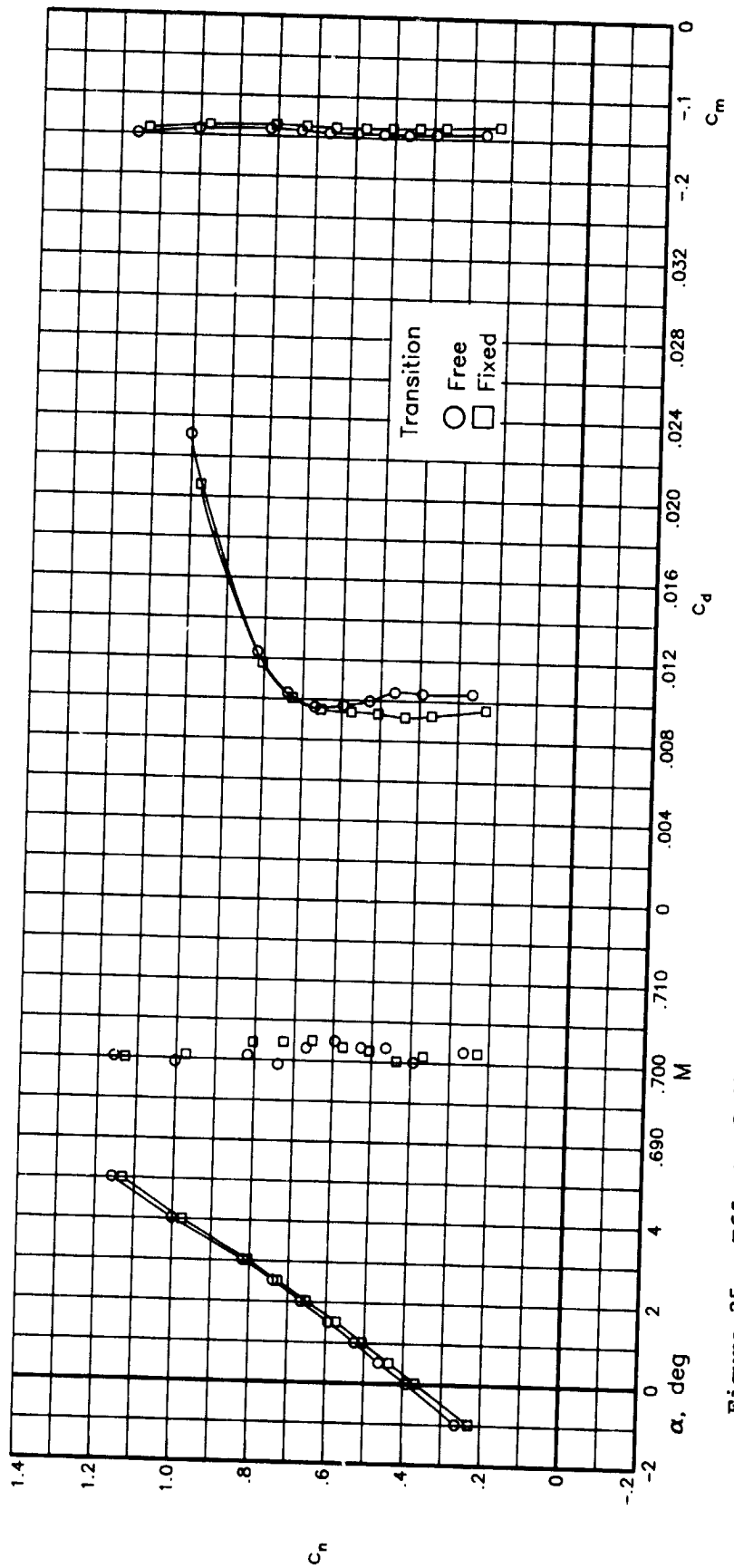

Figure 25.- Effect of fixing transition on aerodynamic characteristics of airfoil at $M \approx 0.700$, $R \approx 6.0 \times 10^6$, and $\dot{m}_{bl} = 0$.

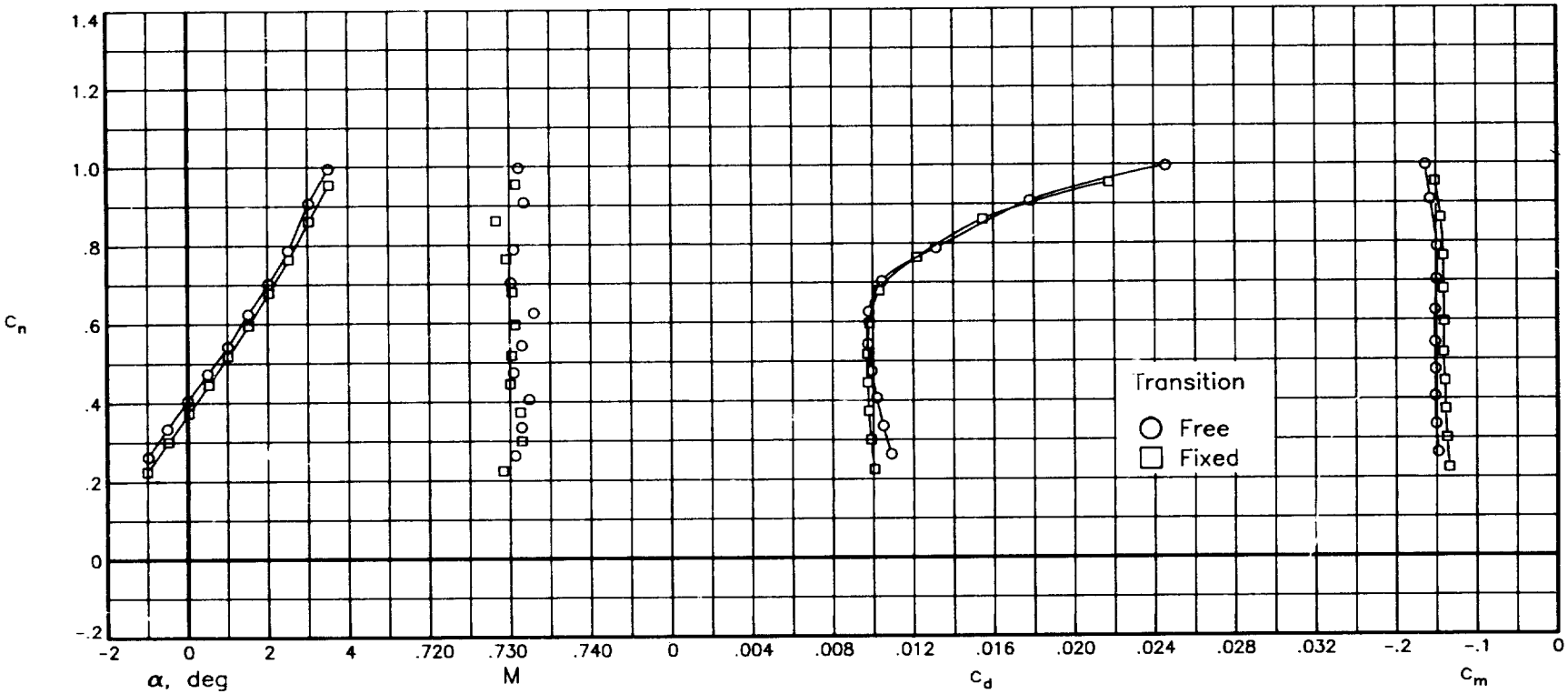

Figure 26.- Effect of fixing transition on aerodynamic characteristics of airfoil at $M \approx 0.730$, $R \approx 6.0 \times 10^6$, and $\dot{m}_{bl} = 0$.

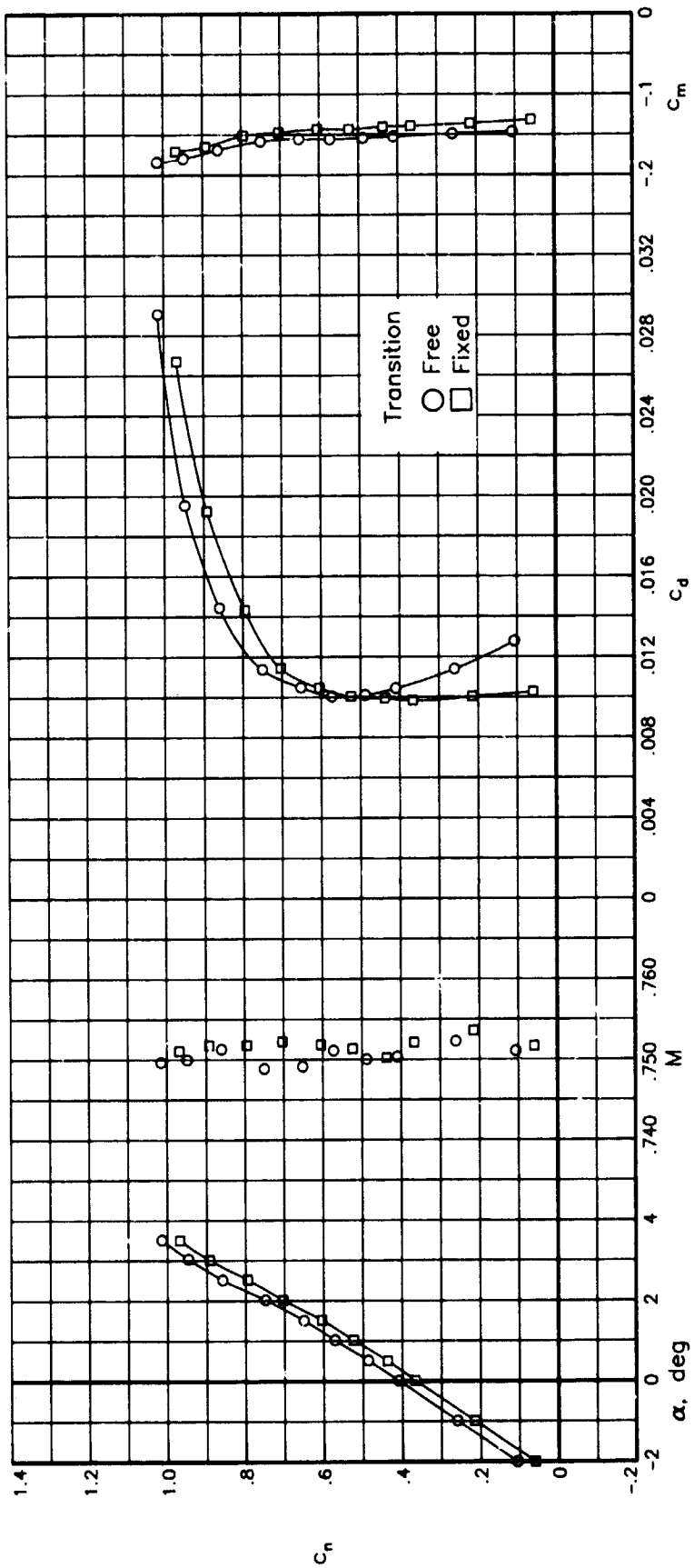

Figure 27.- Effect of fixing transition on aerodynamic characteristics of airfoil at $M = 0.750$, $R = 6.0 \times 10^6$, and $\dot{m}_{bl} = 0$.

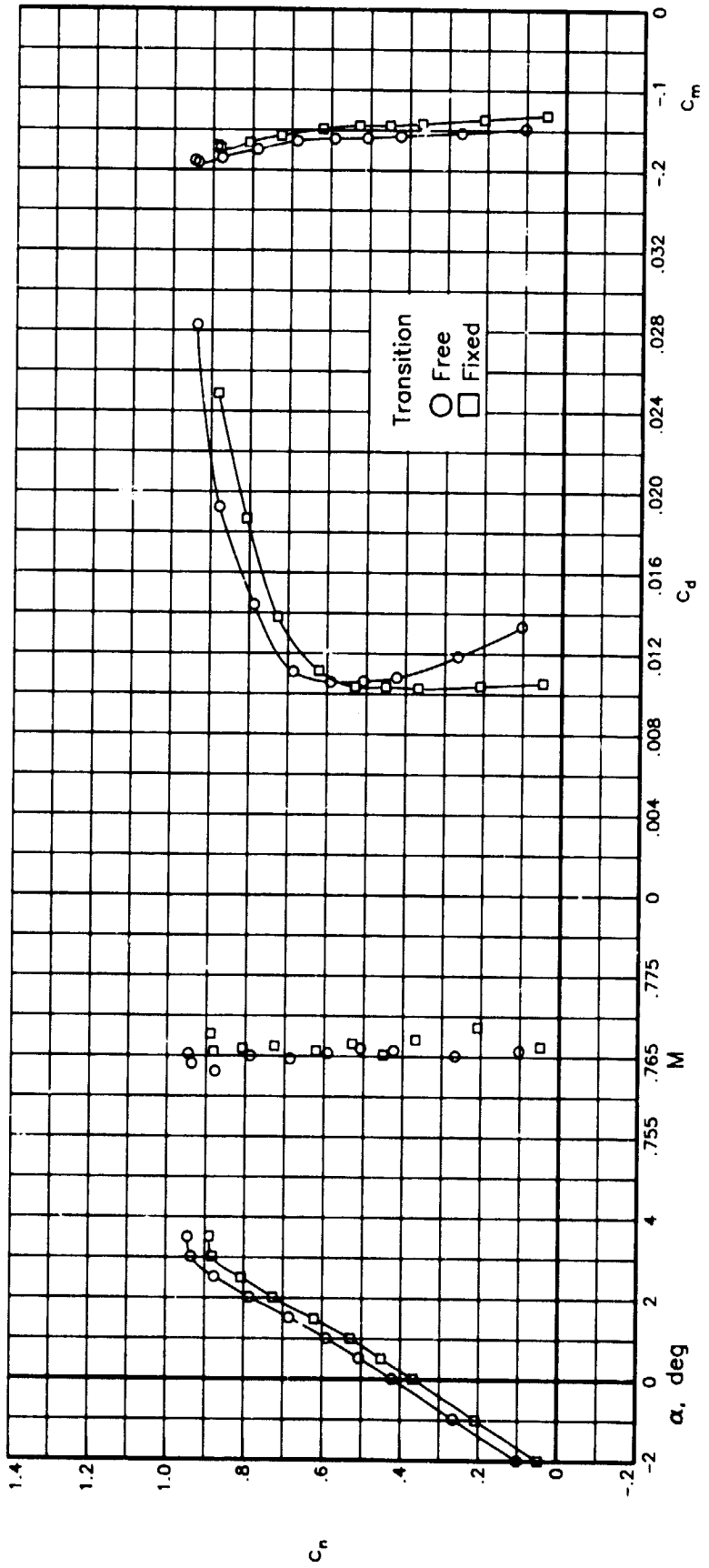

Figure 28.- Effect of fixing transition on aerodynamic characteristics of airfoil at $M \approx 0.765$, $K \approx 6.0 \times 10^6$, and $\bar{m}_{b1} = 0$.

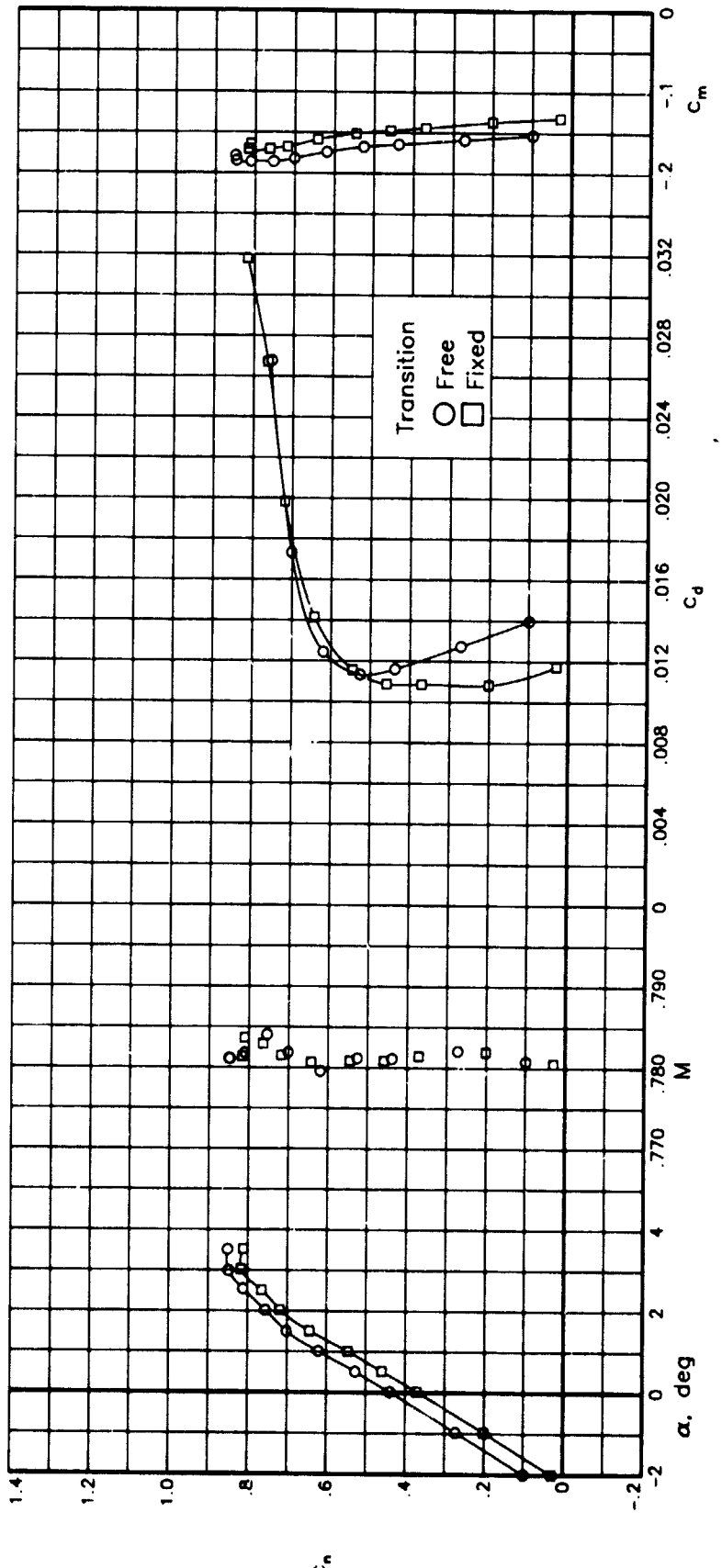

Figure 29.- Effect of fixing transition on aerodynamic characteristics of airfoil at $M = 0.780$, $R = 6.0 \times 10^6$, and $\dot{m}_{bl} = 0$.

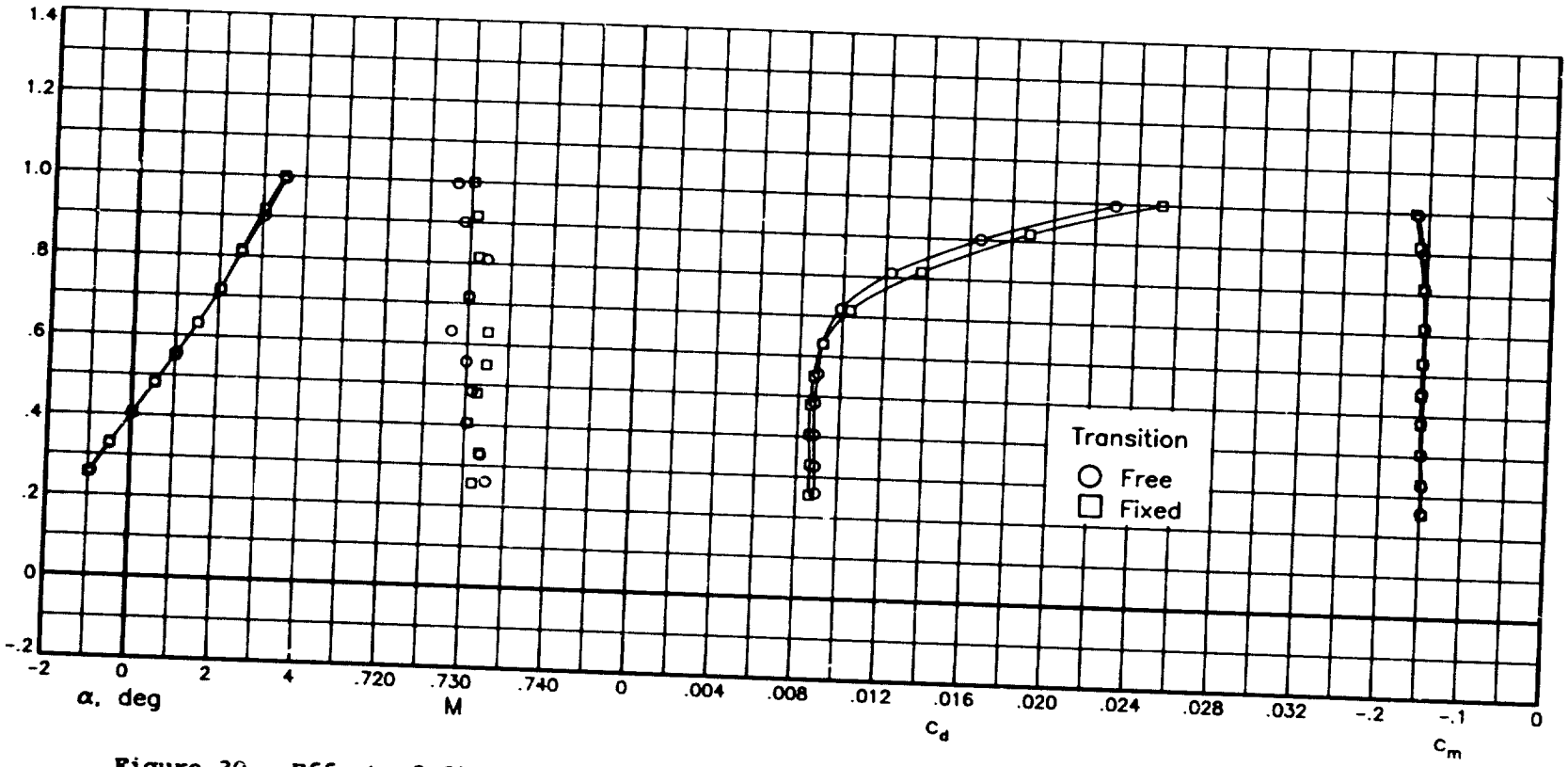

Figure 30.- Effect of fixing transition on aerodynamic characteristics of airfoil at $M \approx 0.730$, $R \approx 15.0 \times 10^6$, and $\dot{m}_{bl} = 0$.

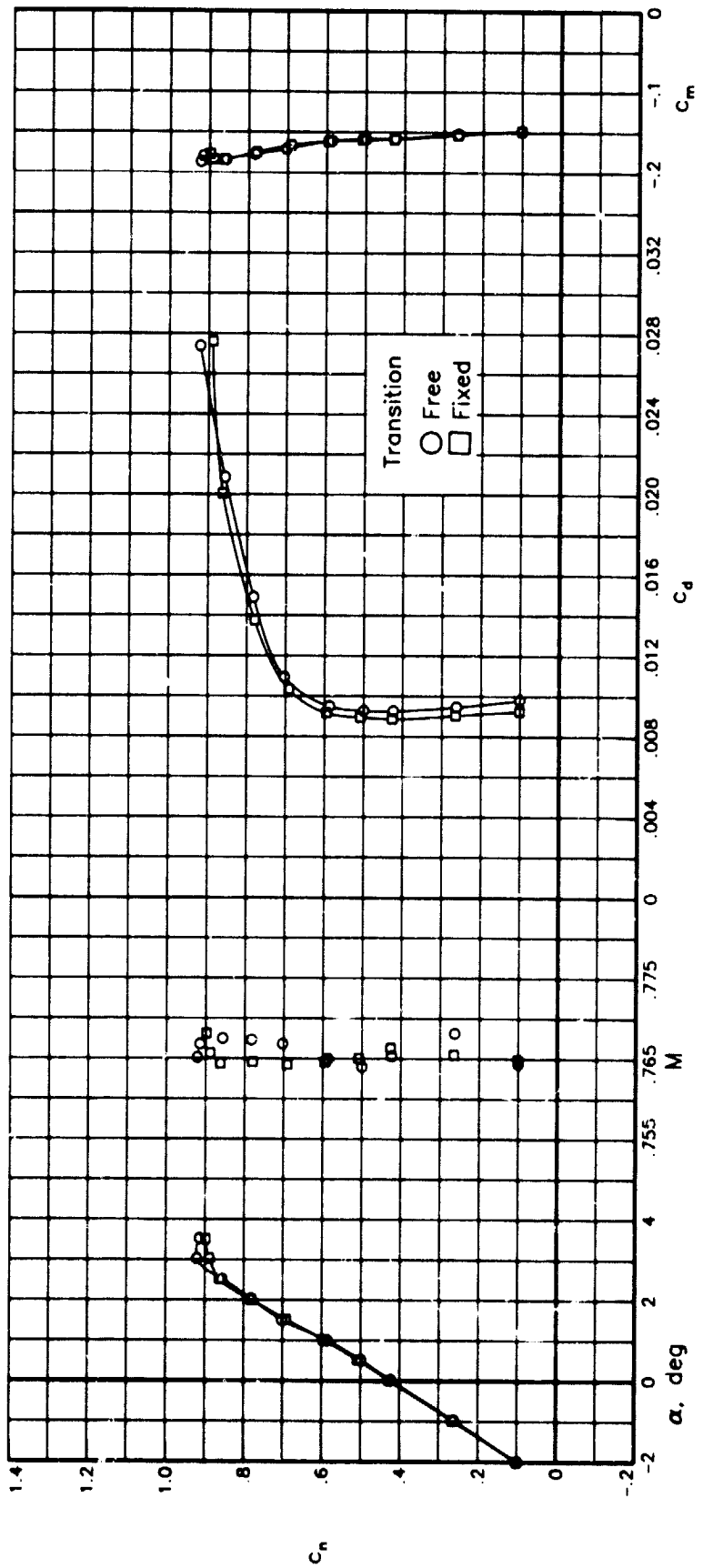

Figure 31.- Effect of fixing transition on aerodynamic characteristics of airfoil at $M = 0.765$, $R = 15.0 \times 10^6$, and $\bar{m}_{b1} = 0$.

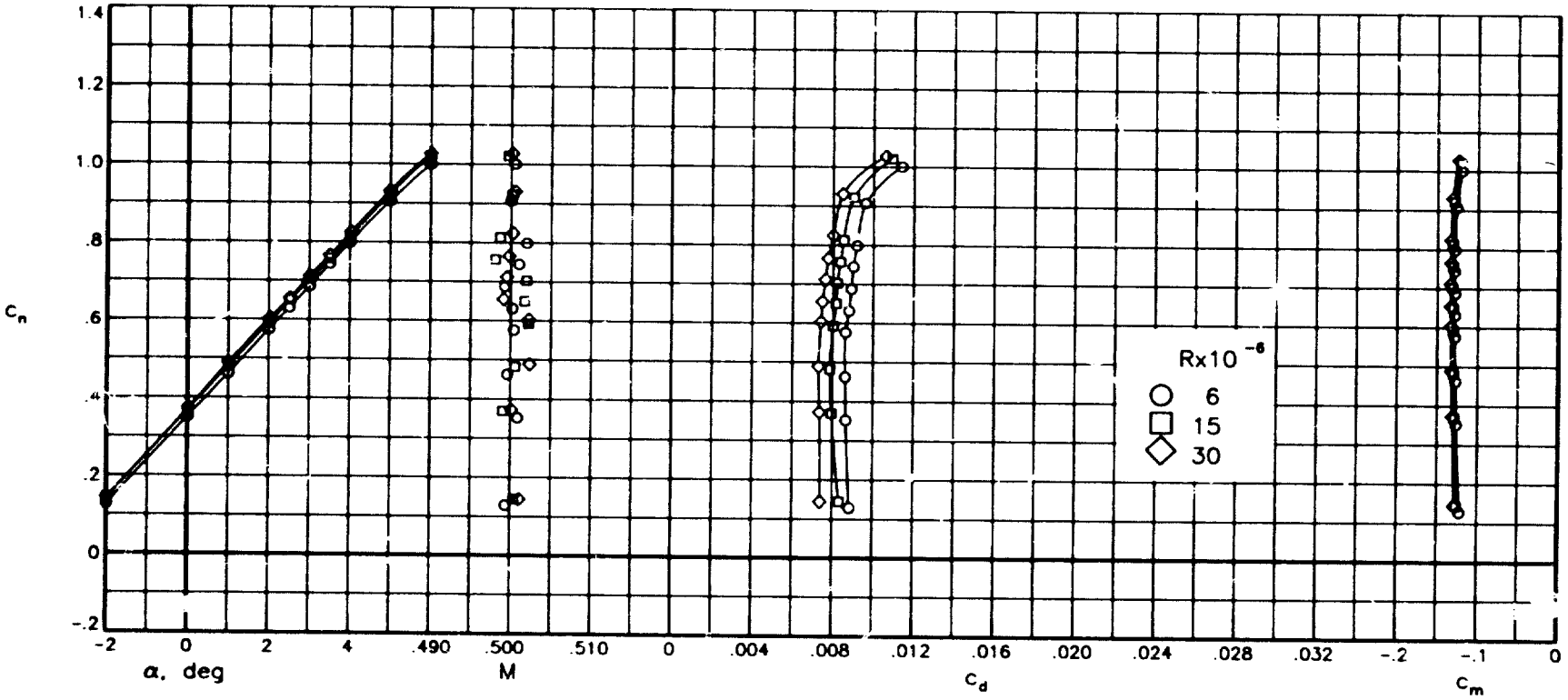

Figure 32.- Effect of Reynolds number on aerodynamic characteristics of airfoil with free transition at $M \approx 0.500$ and $\dot{m}_{bl} = 0$.

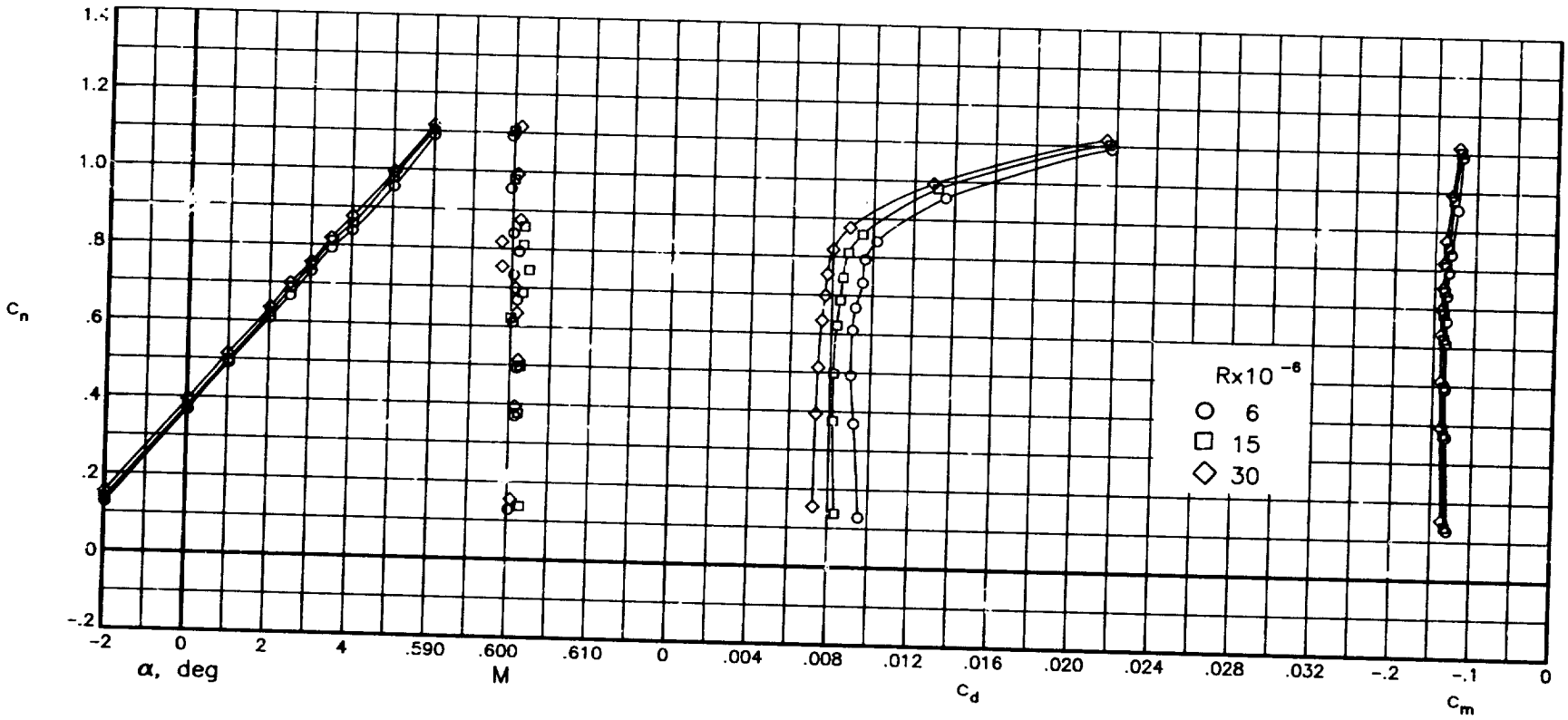

Figure 33.- Effect of Reynolds number on aerodynamic characteristics of airfoil with free transition at $M \approx 0.600$ and $\dot{m}_{bl} = 0$.

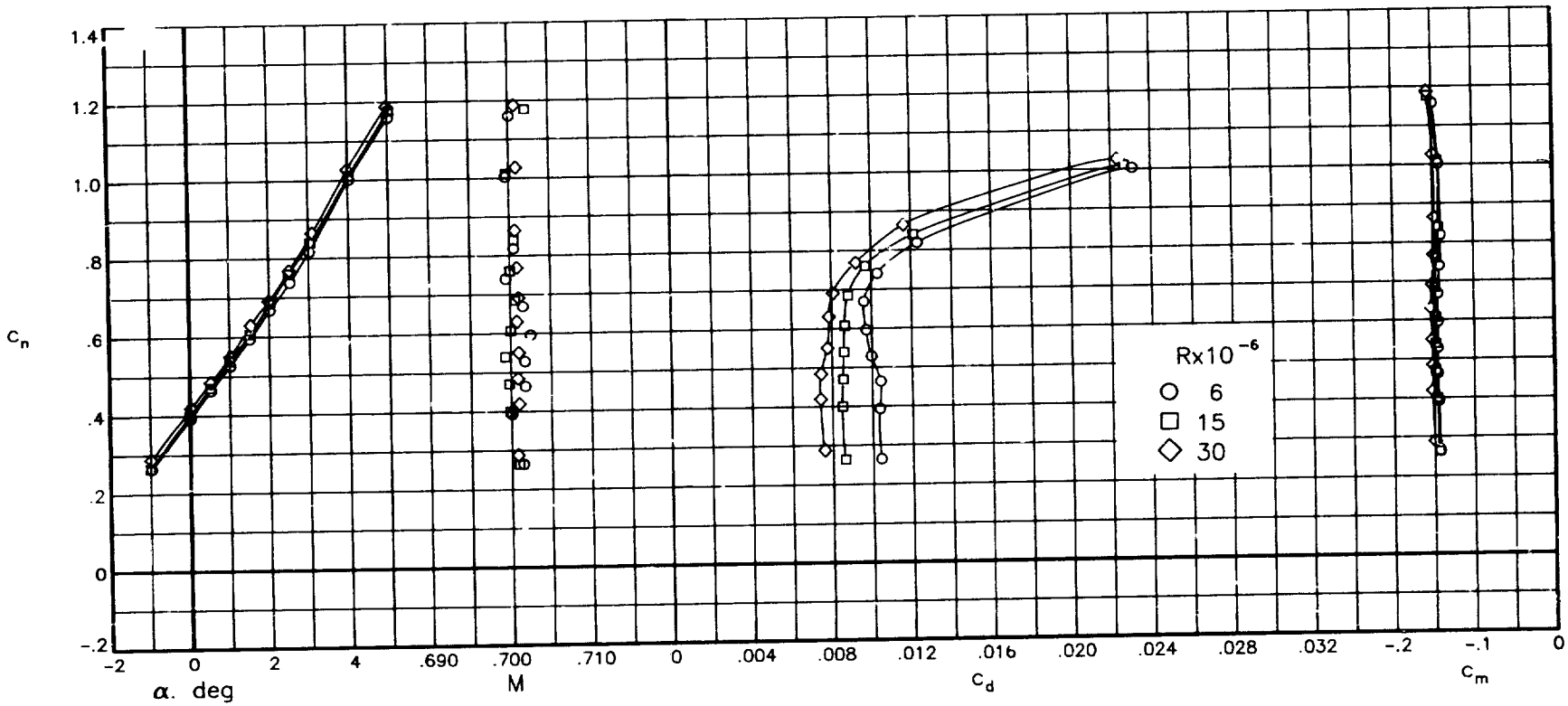

Figure 34.- Effect of Reynolds number on aerodynamic characteristics of airfoil with free transition at $M \approx 0.700$ and $\dot{m}_{bl} = 0$.

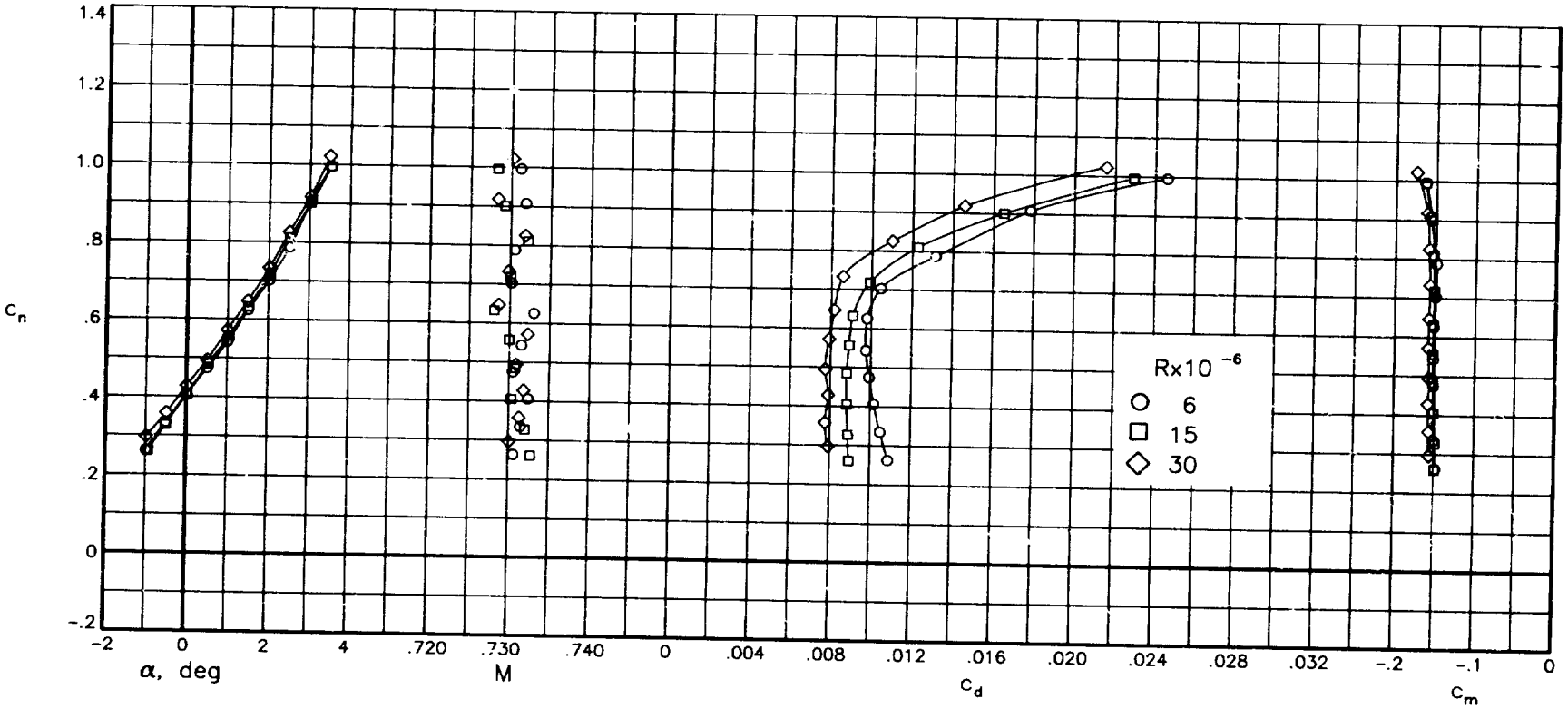

Figure 35.- Effect of Reynolds number on aerodynamic characteristics of airfoil with free transition at $M \approx 0.730$ and $\dot{m}_{bl} = 0$.

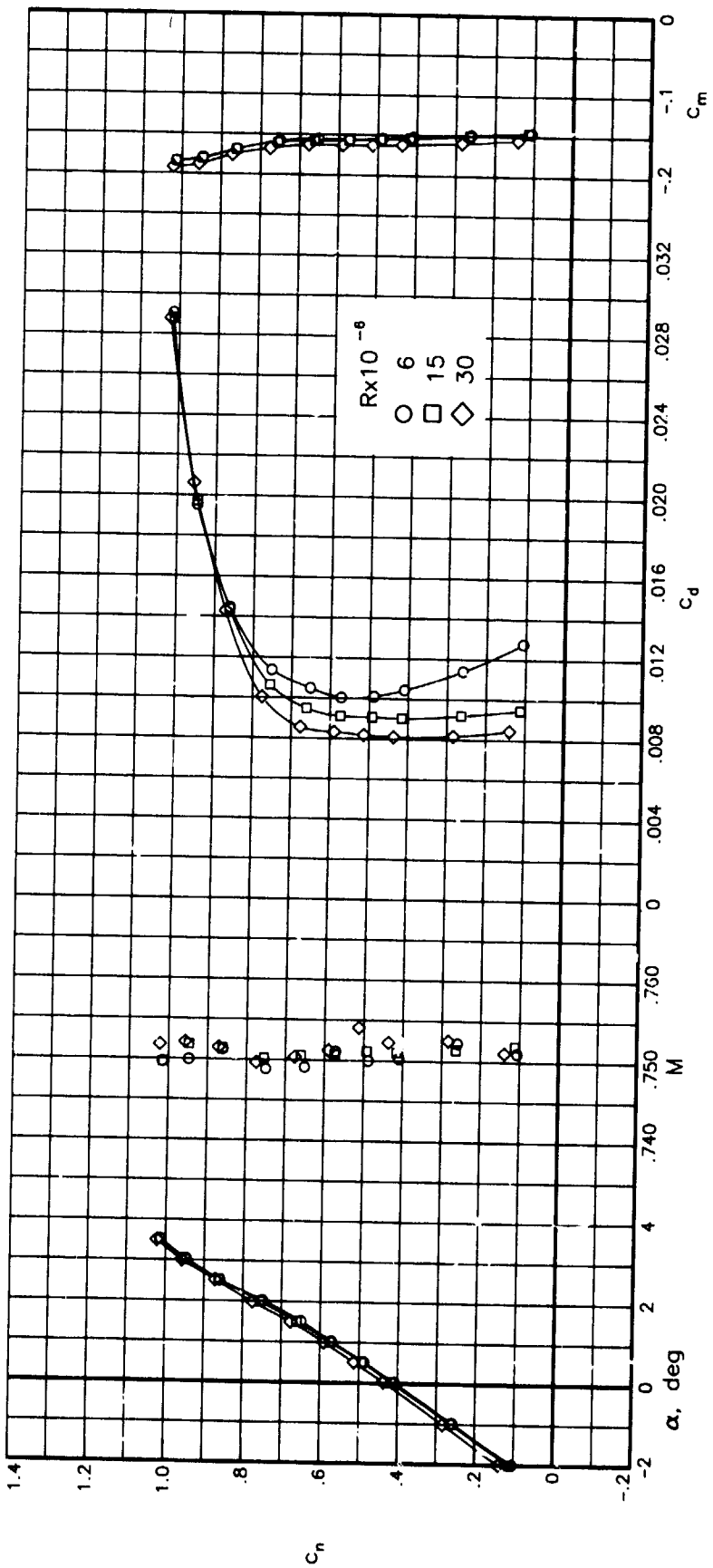

Figure 36.- Effect of Reynolds number on aerodynamic characteristics of airfoil with free transition at M = 0.750 and $\bar{m}_{bl} = 0$.

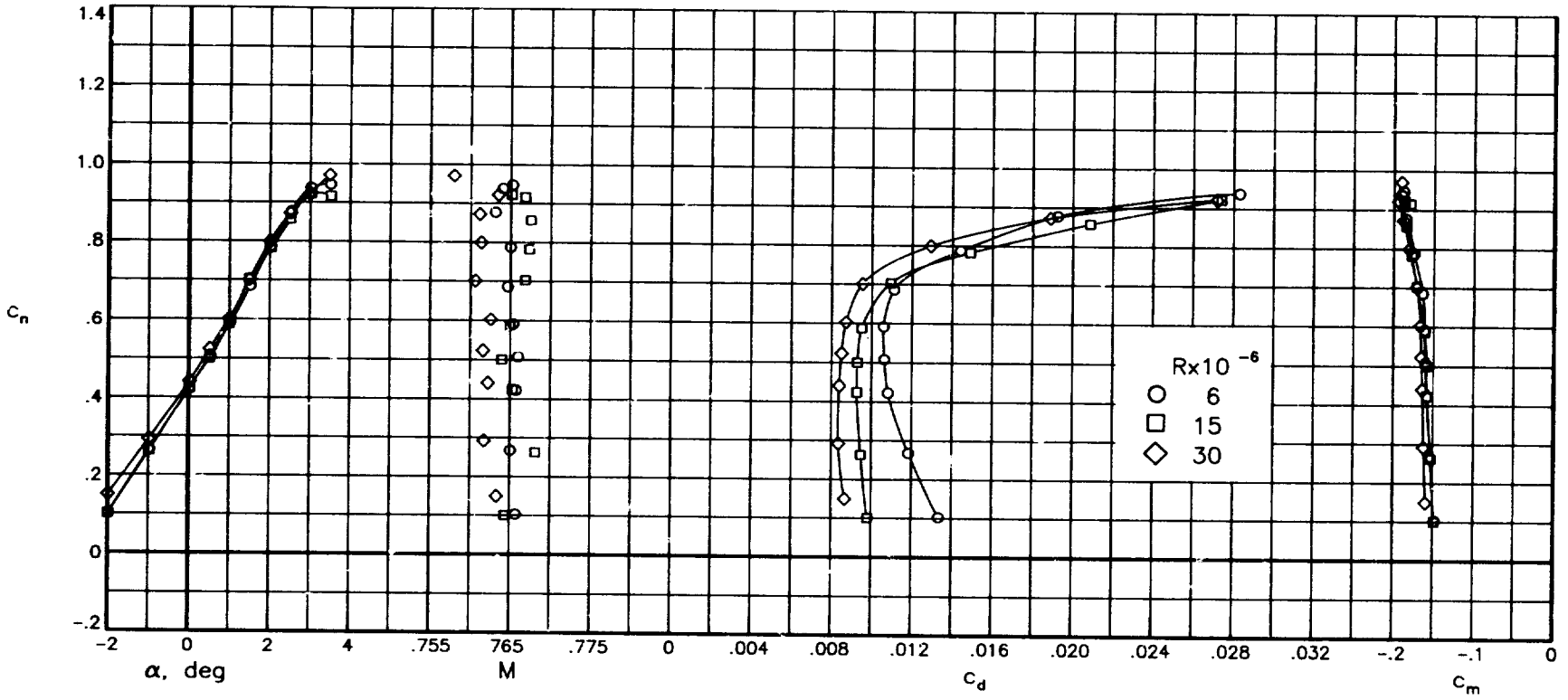

Figure 37.- Effect of Reynolds number on aerodynamic characteristics of airfoil with free transition at $M \approx 0.765$ and $\dot{m}_{bl} = 0$.

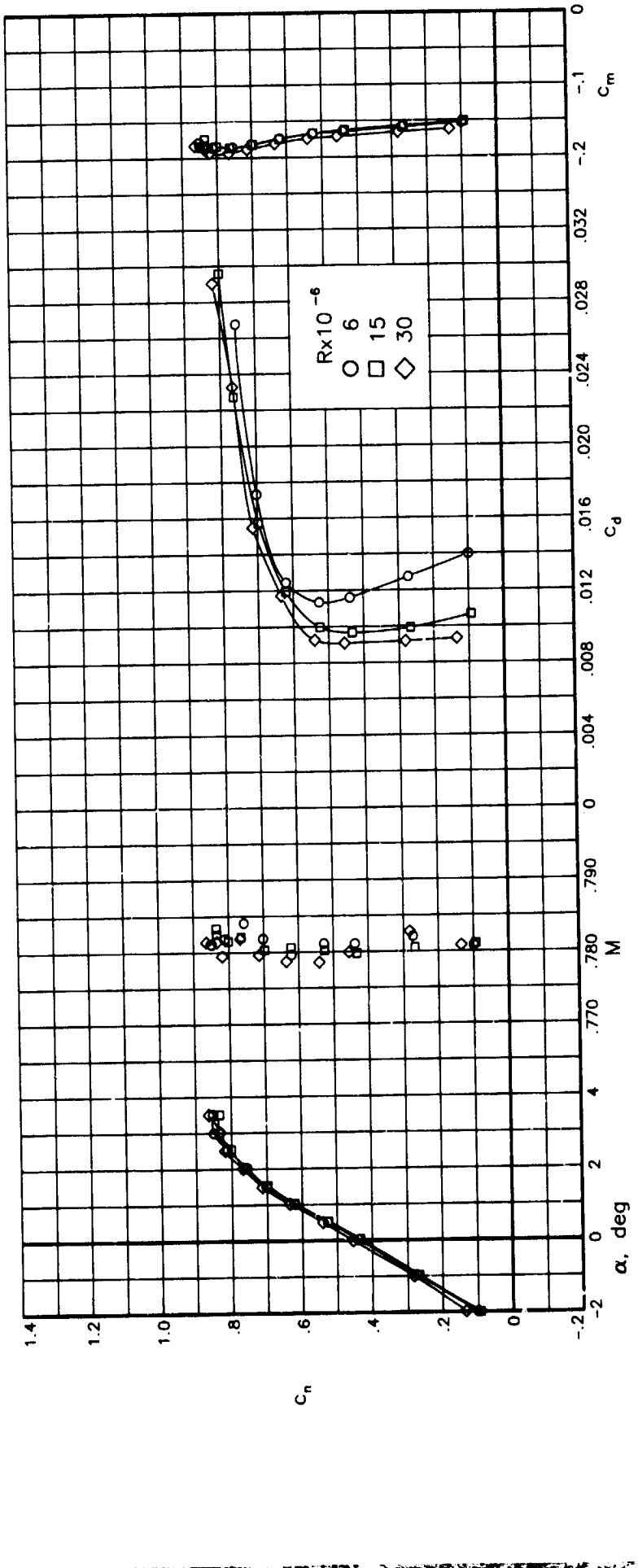

Figure 38.- Effect of Reynolds number on aerodynamic characteristics of airfoil with free transition at M ≈ 0.780 and $\dot{m}_{bl} = 0$.

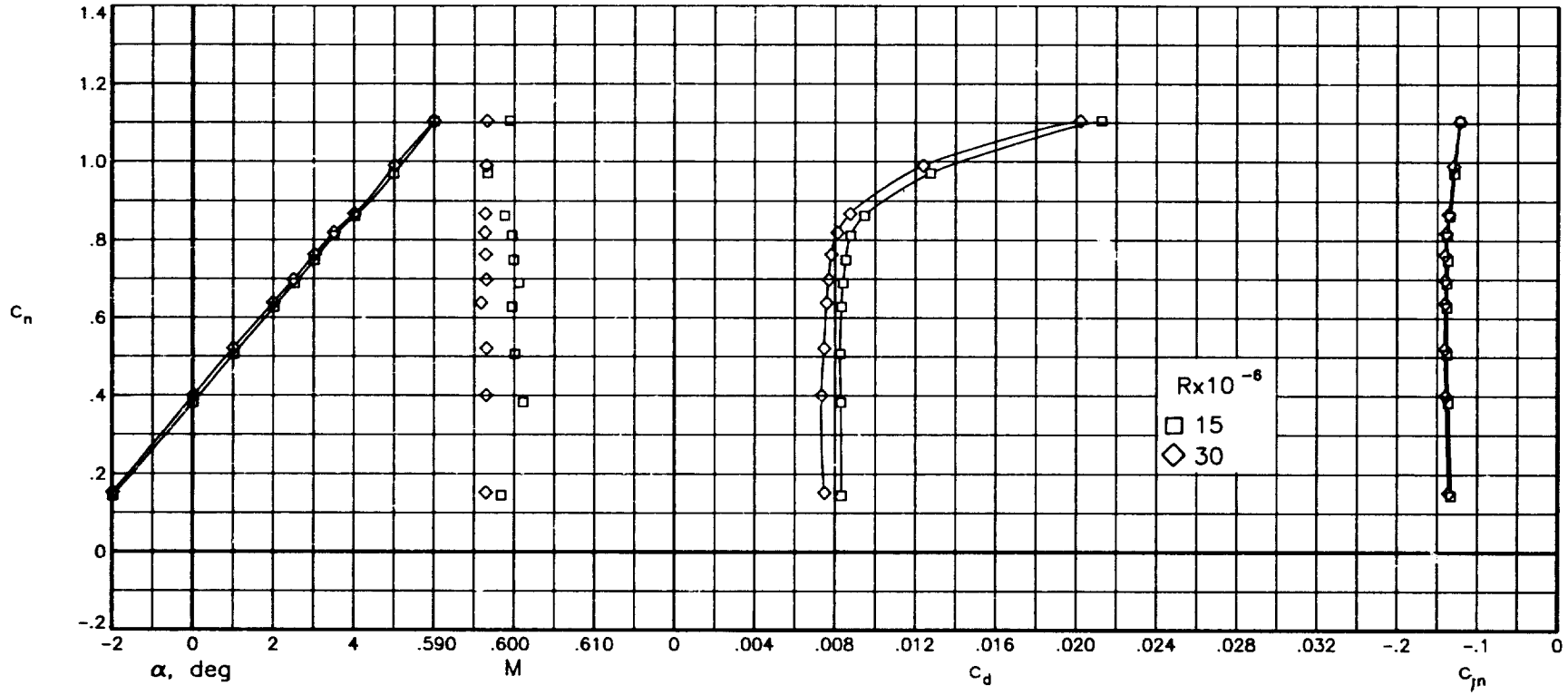

Figure 39.- Effect of Reynolds number on aerodynamic characteristics of airfoil with free transition at $M \approx 0.600$ and $\dot{m}_{bl} = 1.0$.

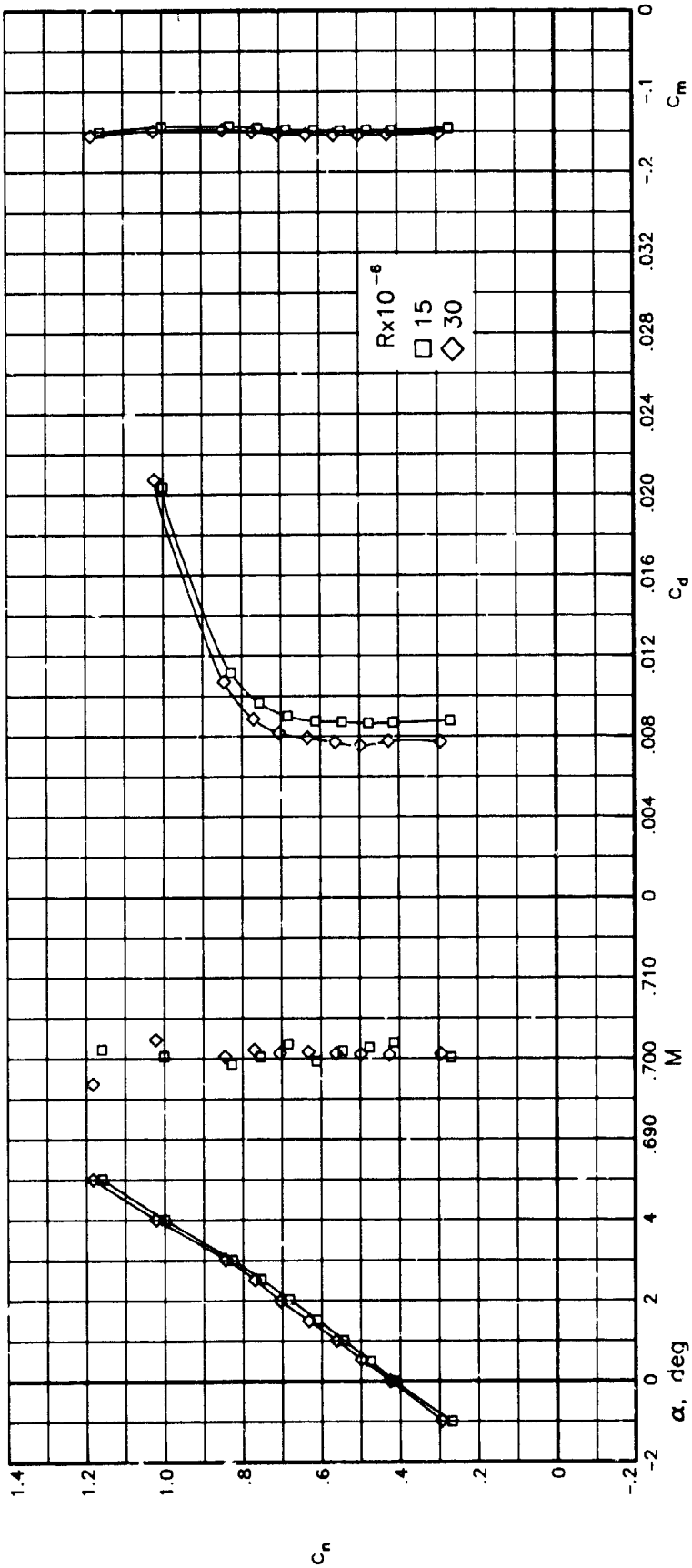

Figure 40.- Effect of Reynolds number on aerodynamic characteristics of airfoil with free transition at M = 0.700 and $\dot{m}_{bl}$ = 1.0.

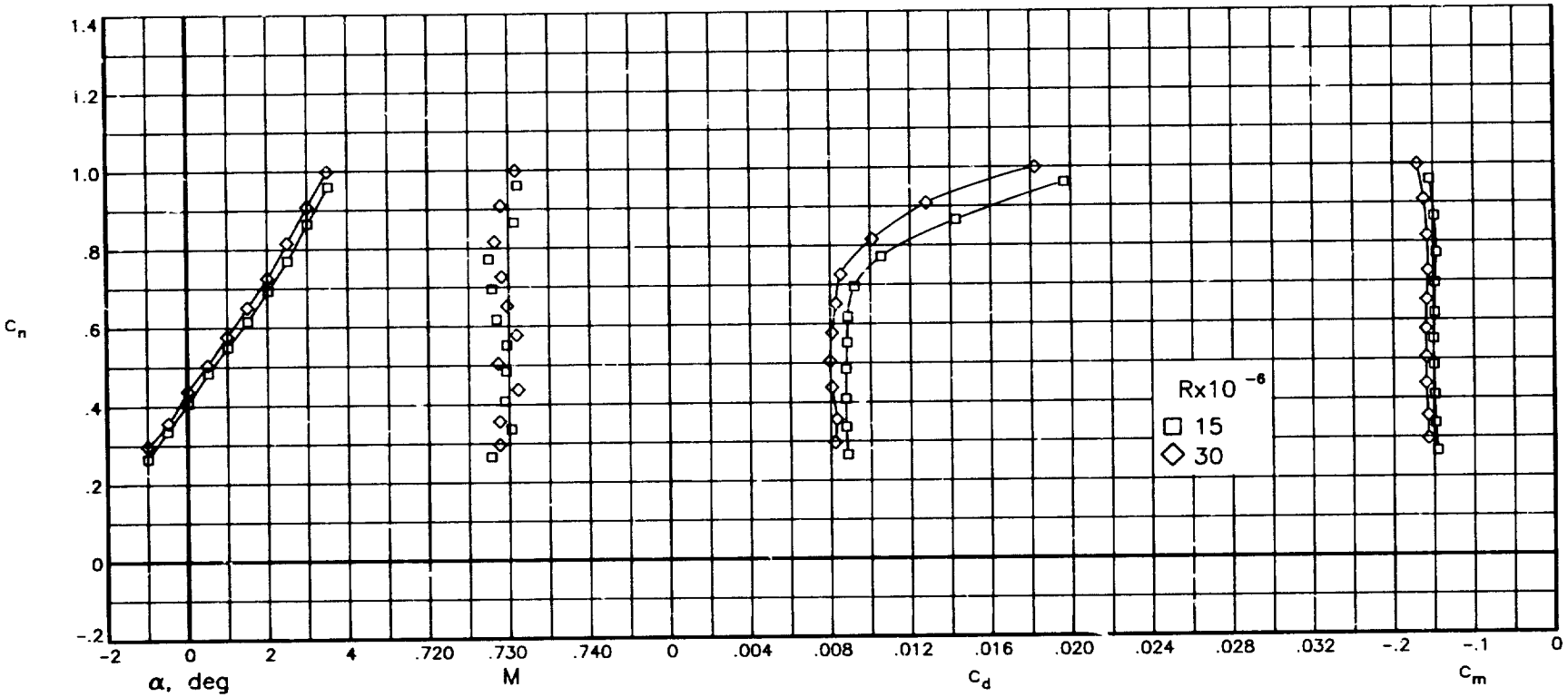

Figure 4i.- Effect of Reynolds number on aerodynamic characteristics of airfoil with free transition at $M \approx 0.730$ and $\dot{m}_{bl} = 1.0$.

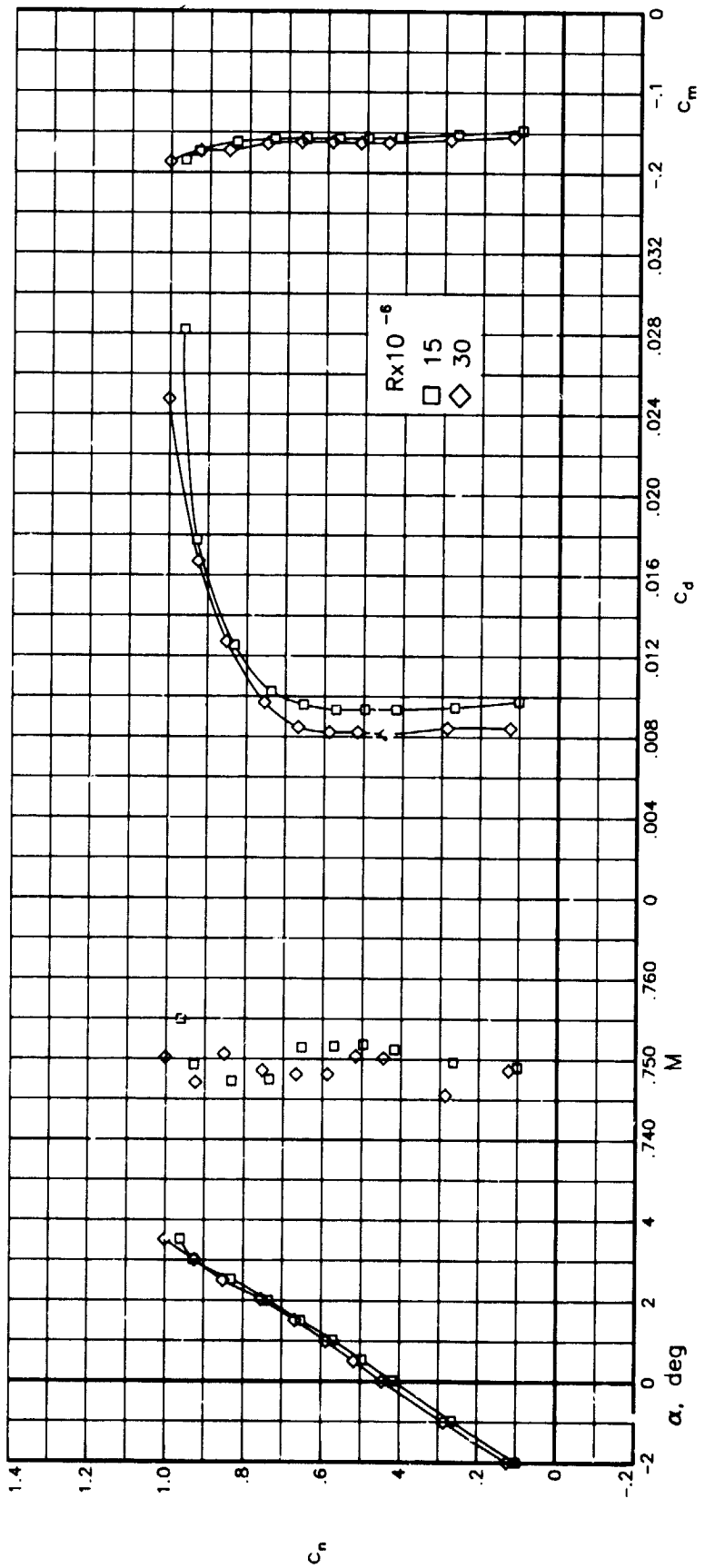

Figure 42.- Effect of Reynolds number on aerodynamic characteristics of airfoil with free transition at M = 0.750 and $\dot{m}_{bl}$ = 1.0.

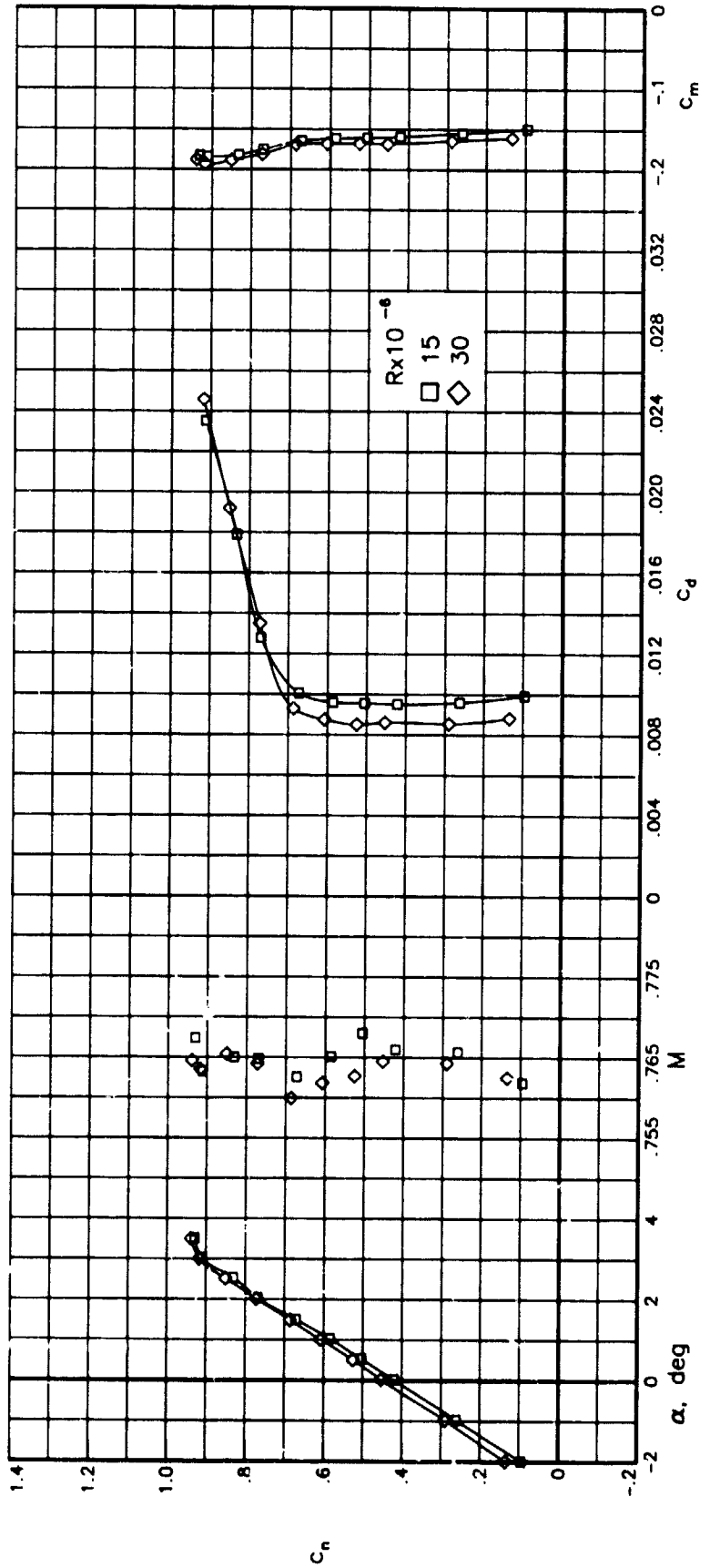

Figure 43.- Effect of Reynolds number on aerodynamic characteristics of airfoil with free transition at M = 0.765 and $\dot{m}_{bl}$ = 1.0.

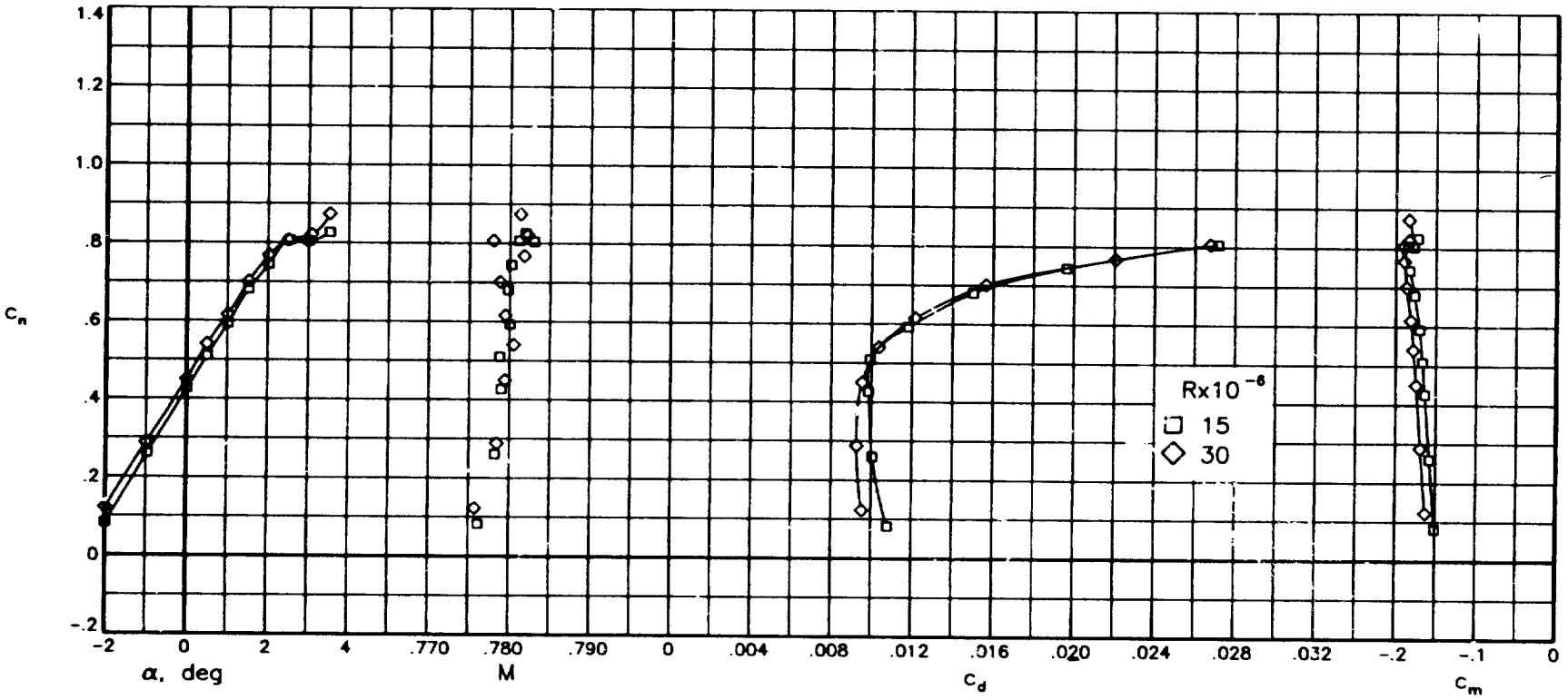

Figure 44.- Effect of Reynolds number on aerodynamic characteristics of airfoil with free transition at $M \approx 0.780$ and $\dot{m}_{bl} = 1.0$.

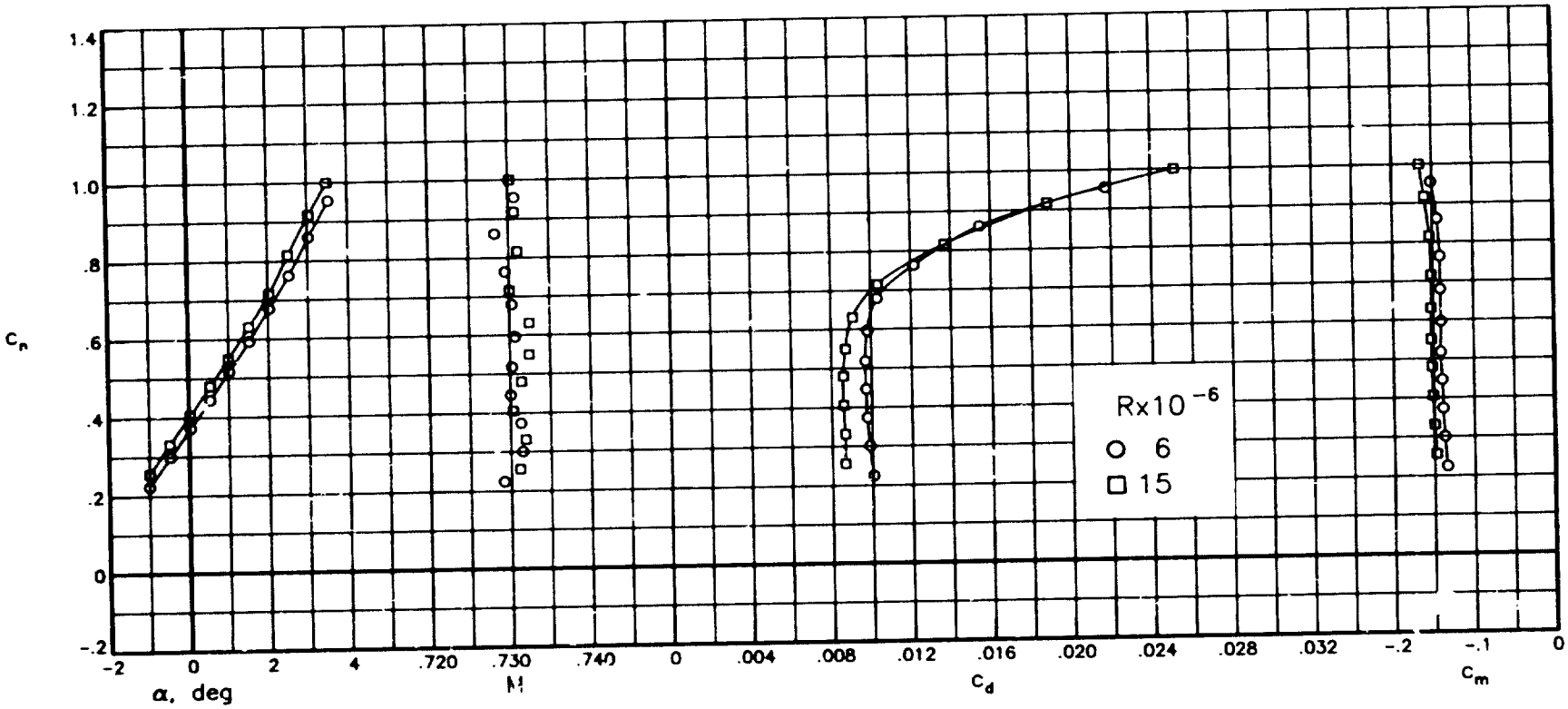

Figure 45.- Effect of Reynolds number on aerodynamic characteristics of airfoil with fixed transition at M ≈ 0.730 and $\dot{m}_{bl} = 0$.

C-2

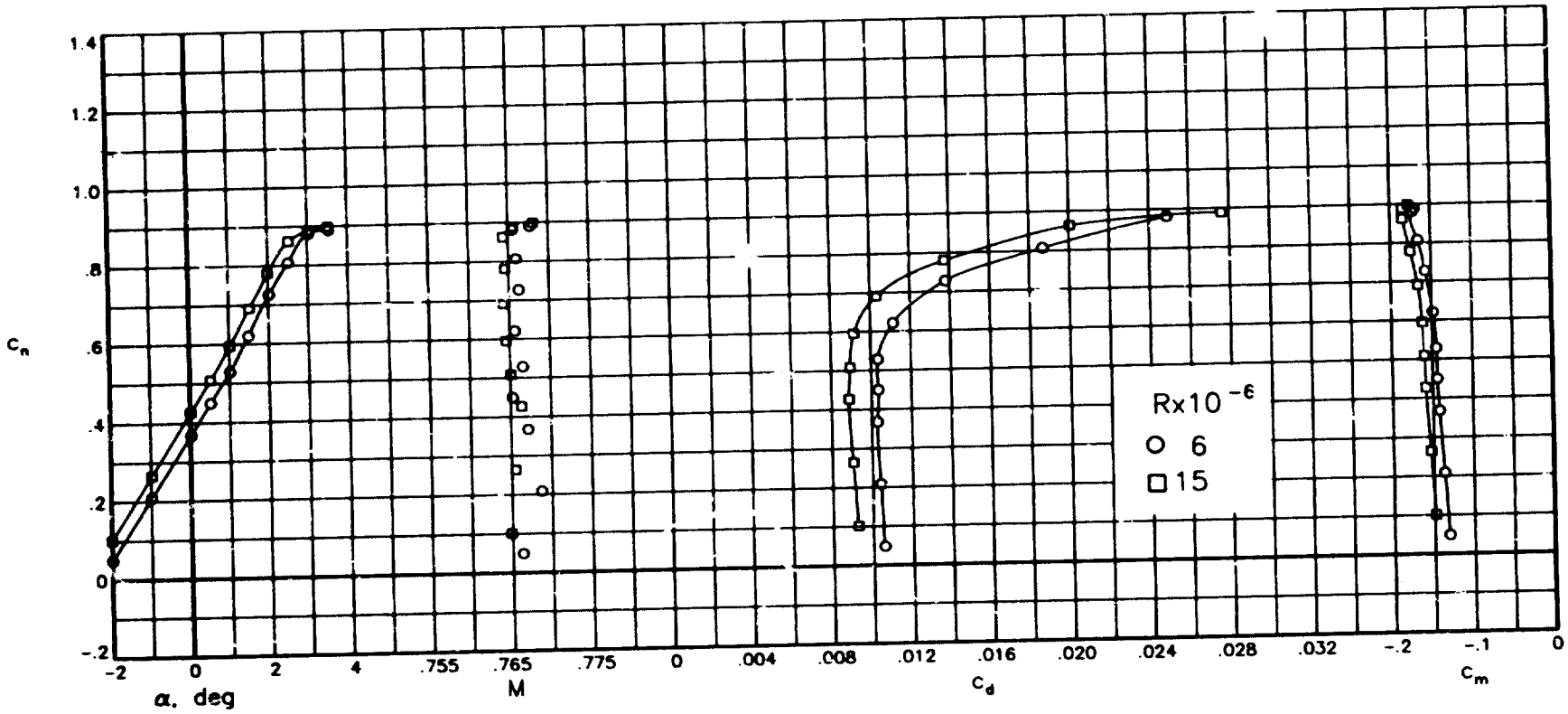

Figure 46.- Effect of Reynolds number on aerodynamic characteristics of airfoil with fixed transition at $M = 0.765$ and $\dot{m}_{bl} = 0$.

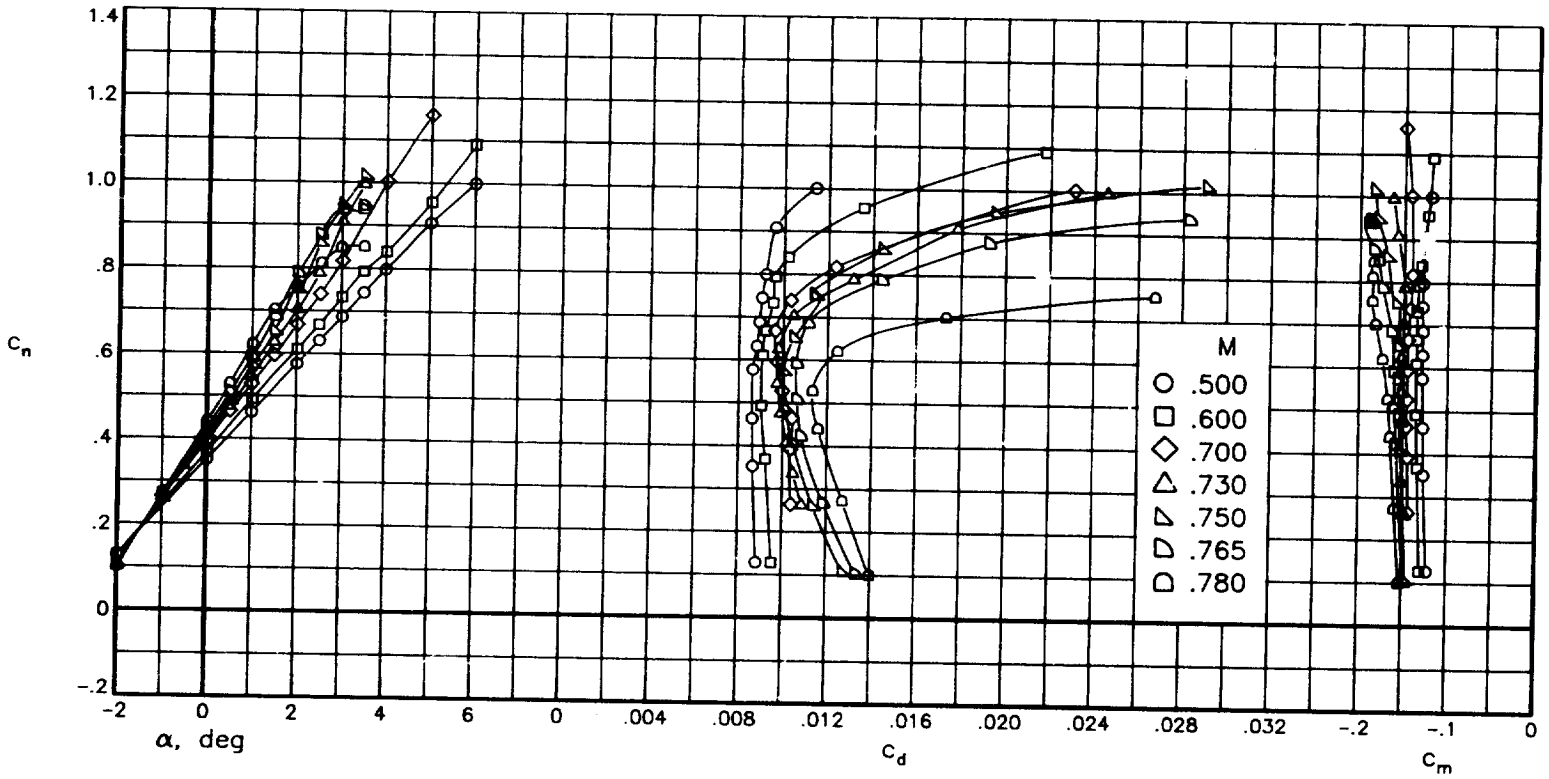

Figure 47.- Effect of Mach number on aerodynamic characteristics of airfoil with free transition at $R \approx 6.0 \times 10^6$ and $\dot{m}_{bl} = 0$.

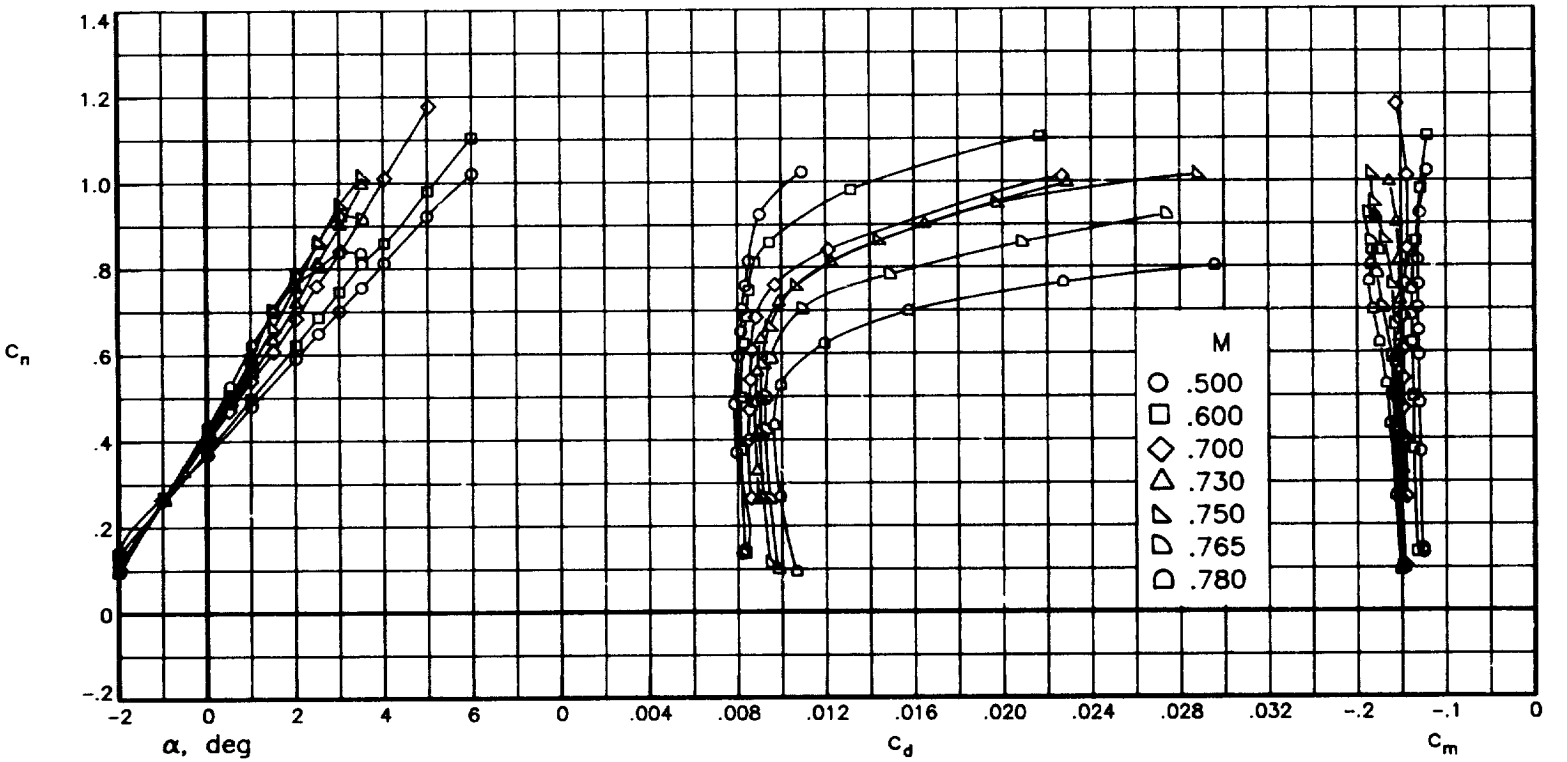

Figure 48.- Effect of Mach number on aerodynamic characteristics of airfoil with free transition at $R \approx 15.0 \times 10^6$ and $\dot{m}_{bl} = 0$.

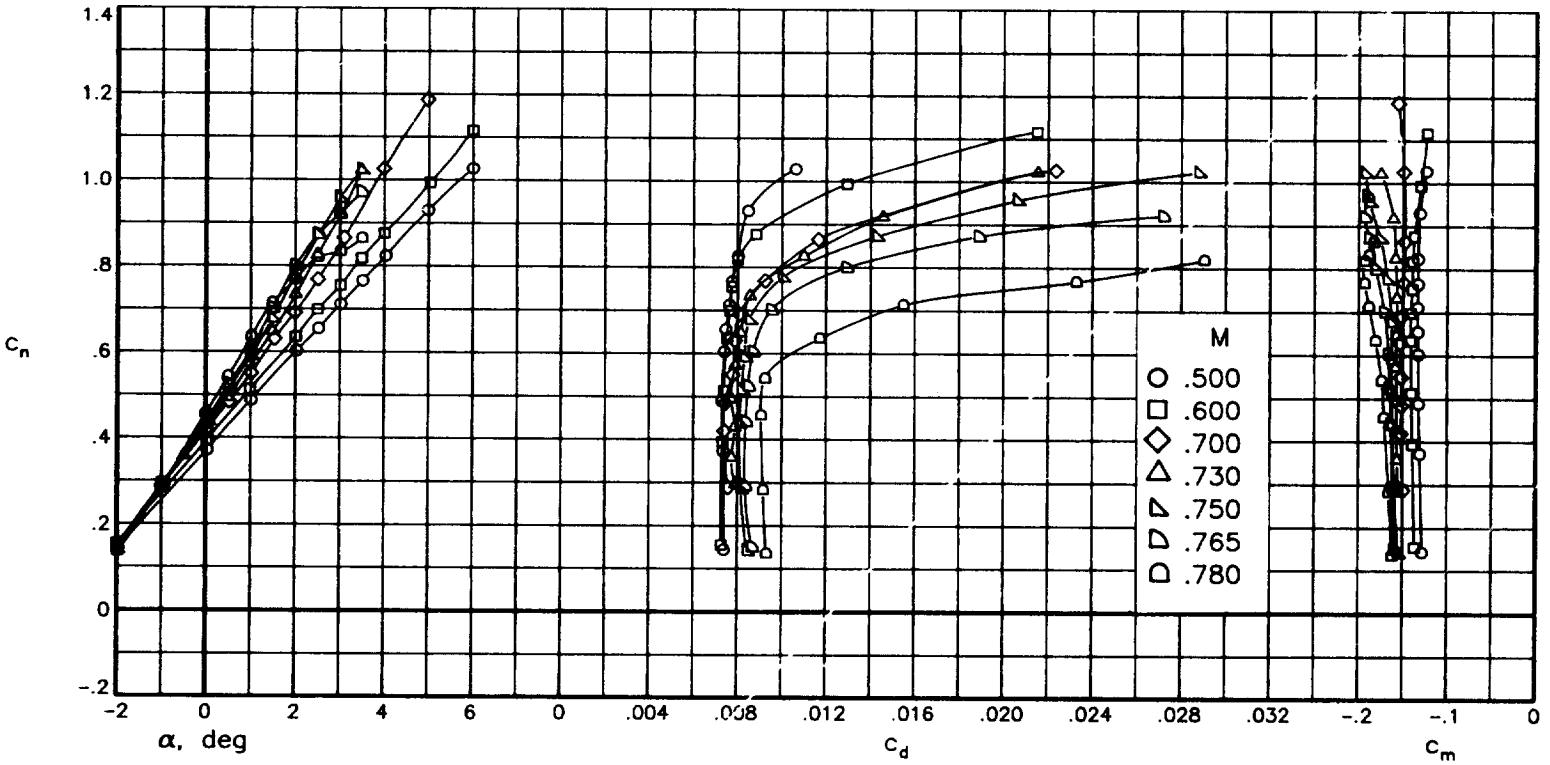

Figure 49.- Effect of Mach number on aerodynamic characteristics of airfoil with free transition at $R \approx 30.0 \times 10^6$ and $\dot{m}_{bl} = 0$.

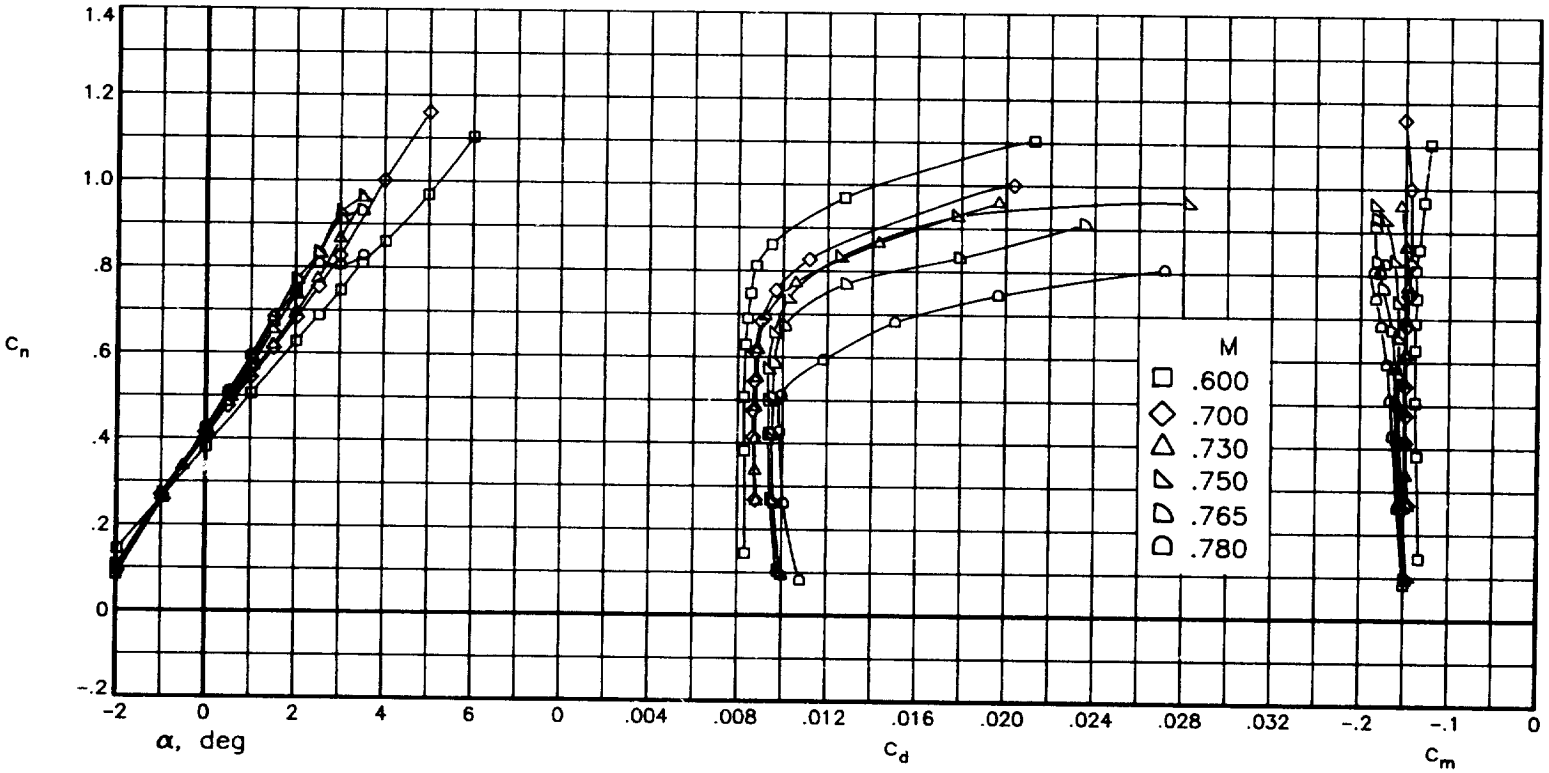

Figure 50.- Effect of Mach number on aerodynamic characteristics of airfoil with free transition at $R \approx 15.0 \times 10^6$ and $\dot{m}_{bl} = 1.0$.

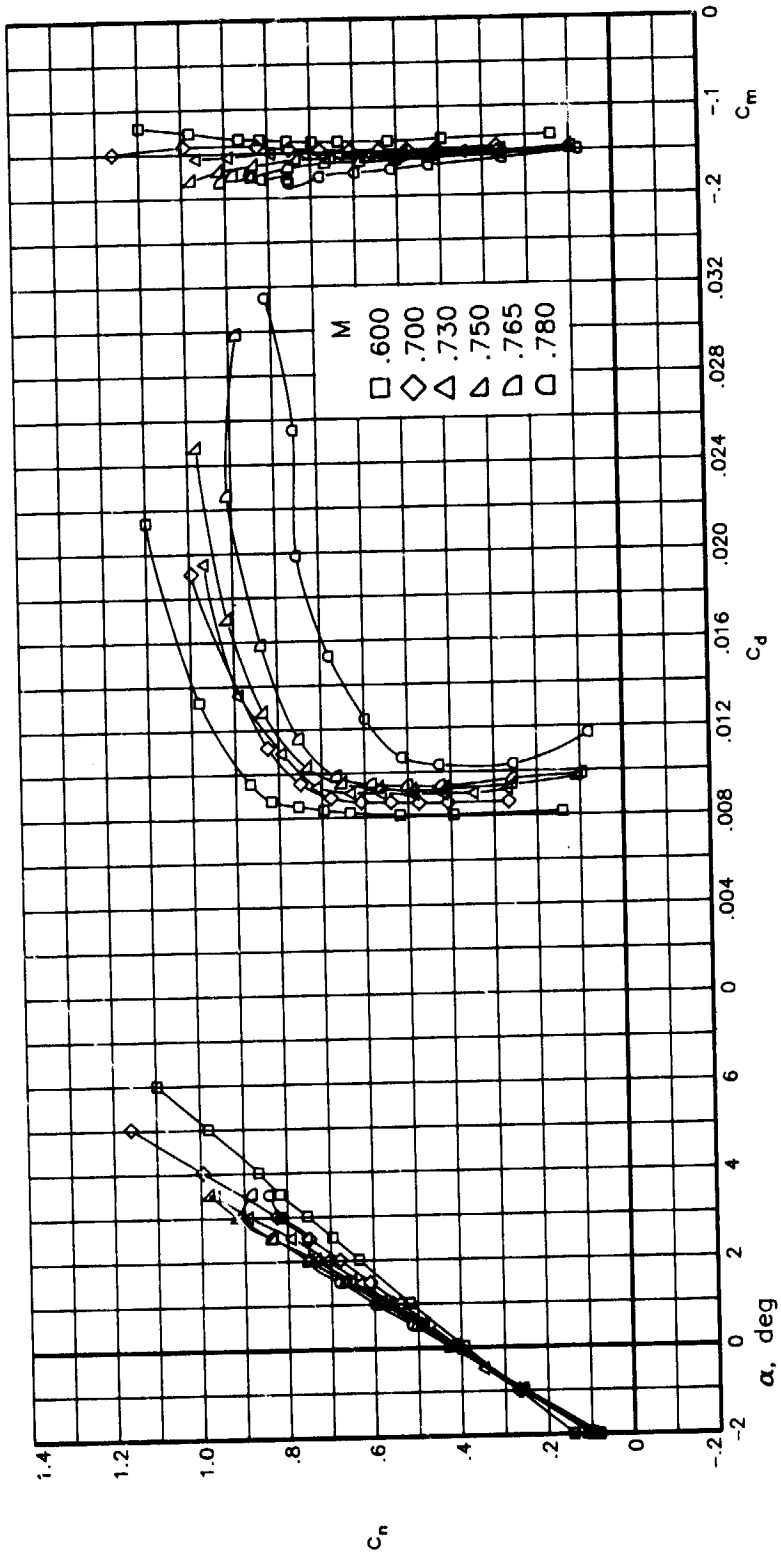

Figure 51.- Effect of Mach number on aerodynamic characteristics of airfoil with free transition at $R = 15.0 \times 10^6$ and $1.1 \leq \bar{m}_{bl} \leq 1.8$.

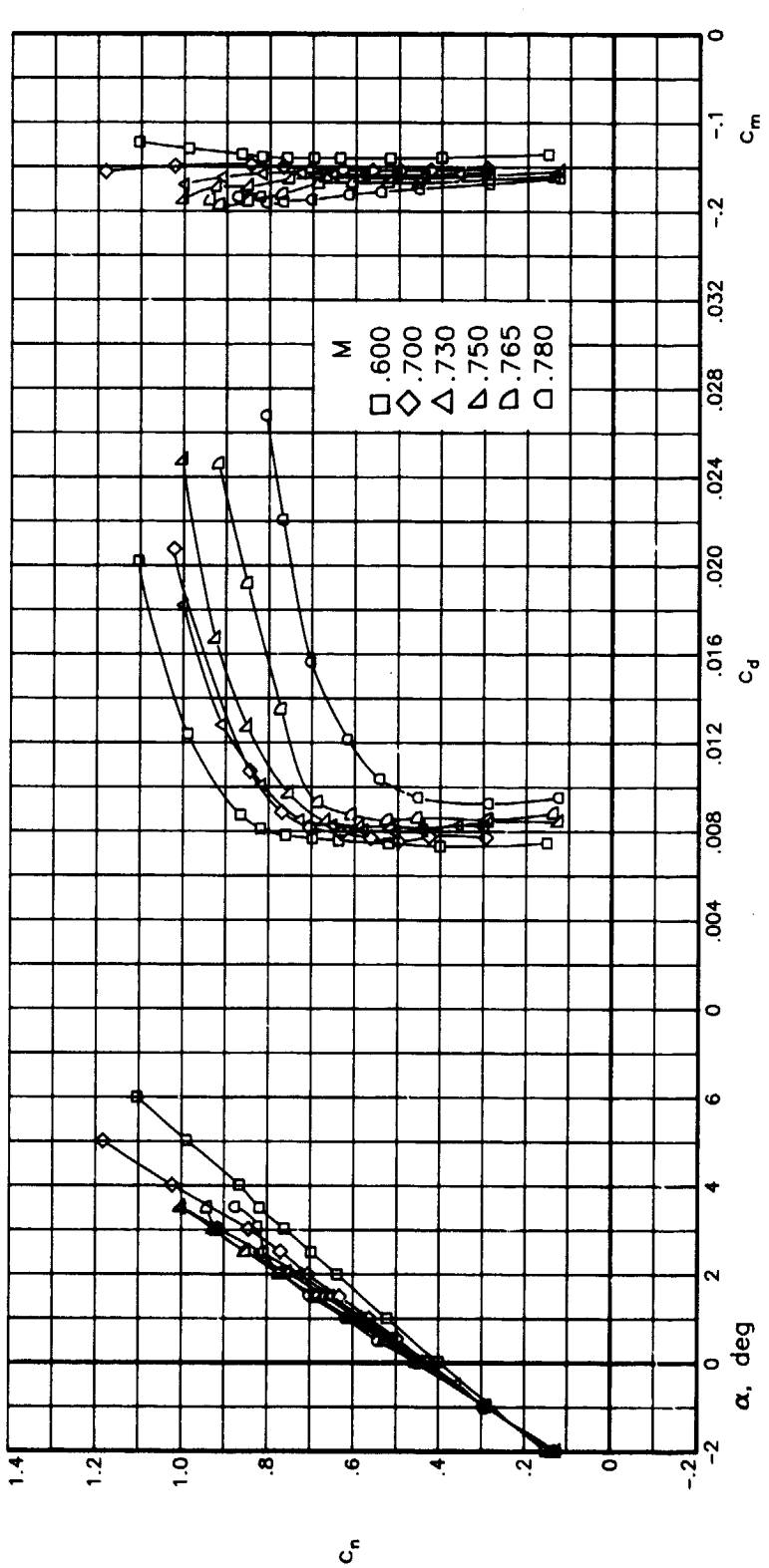

Figure 52.- Effect of Mach number on aerodynamic characteristics of airfoil with free transition at $R \approx 30.0 \times 10^6$ and $\bar{m}_{bl} = 1.0$.

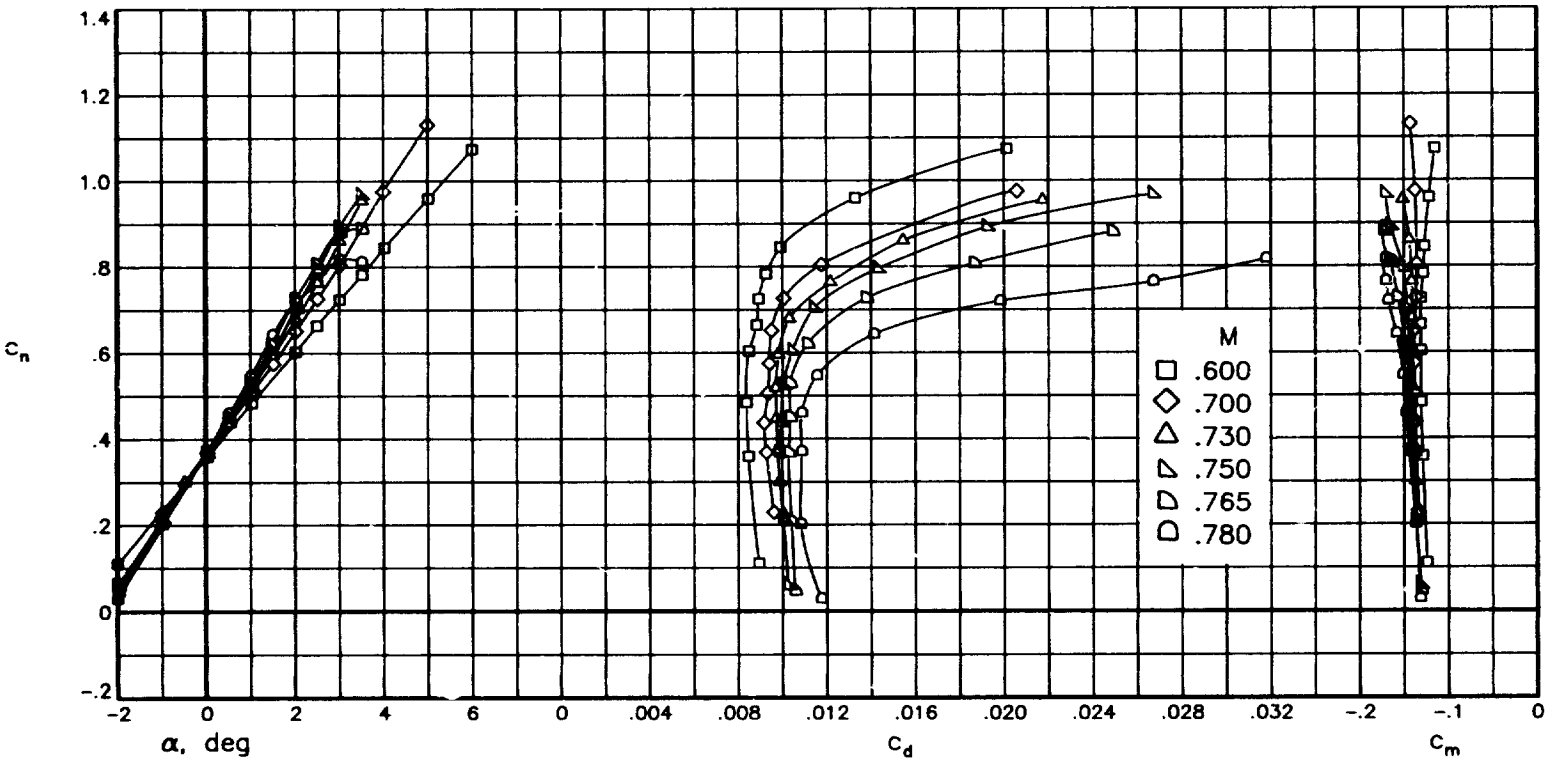

Figure 53.- Effect of Mach number on aerodynamic characteristics of airfoil with fixed transition at $R \approx 6.0 \times 10^6$ and $\dot{m}_{bl} = 0$.

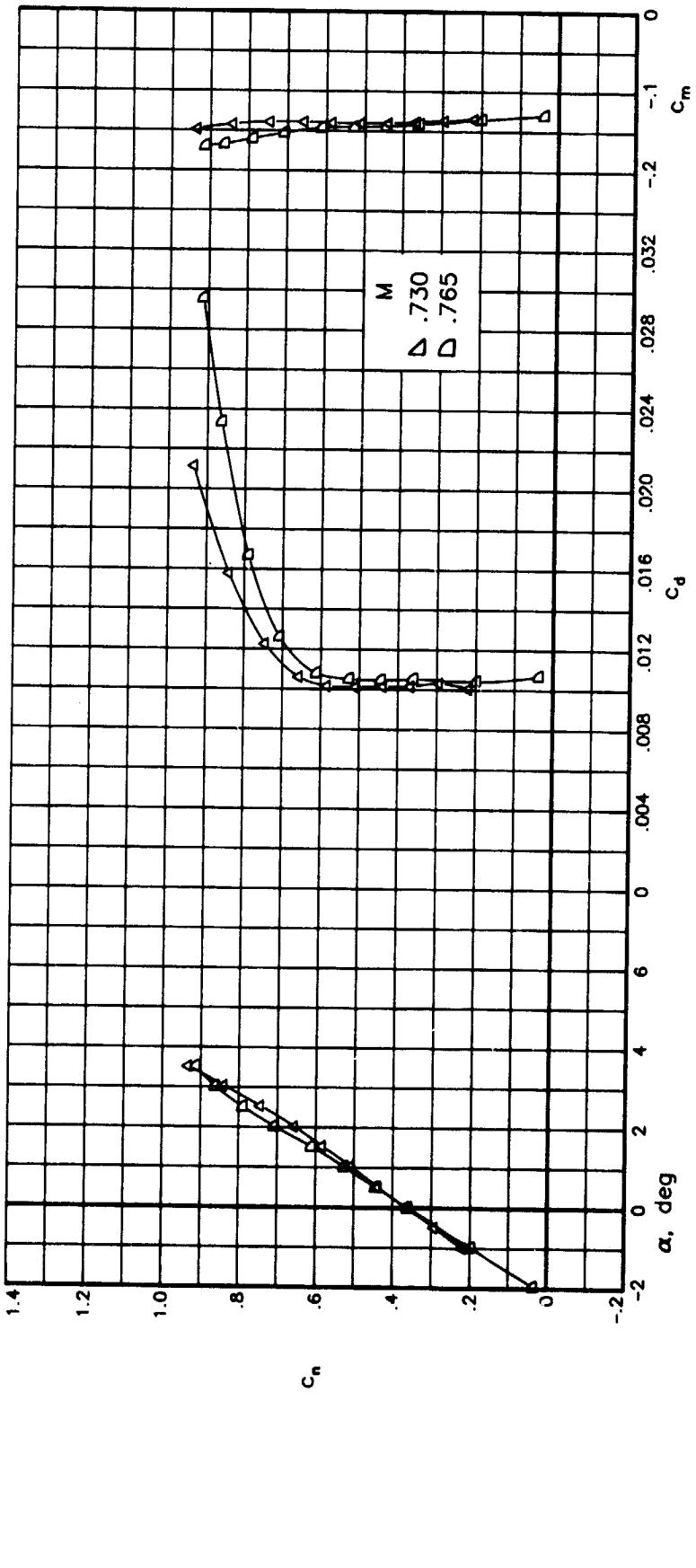

Figure 54.- Effect of Mach number on aerodynamic characteristics of airfoil with fixed transition at $R = 6.0 \times 10^6$ and $\bar{m}_{bl} = 1.0$.

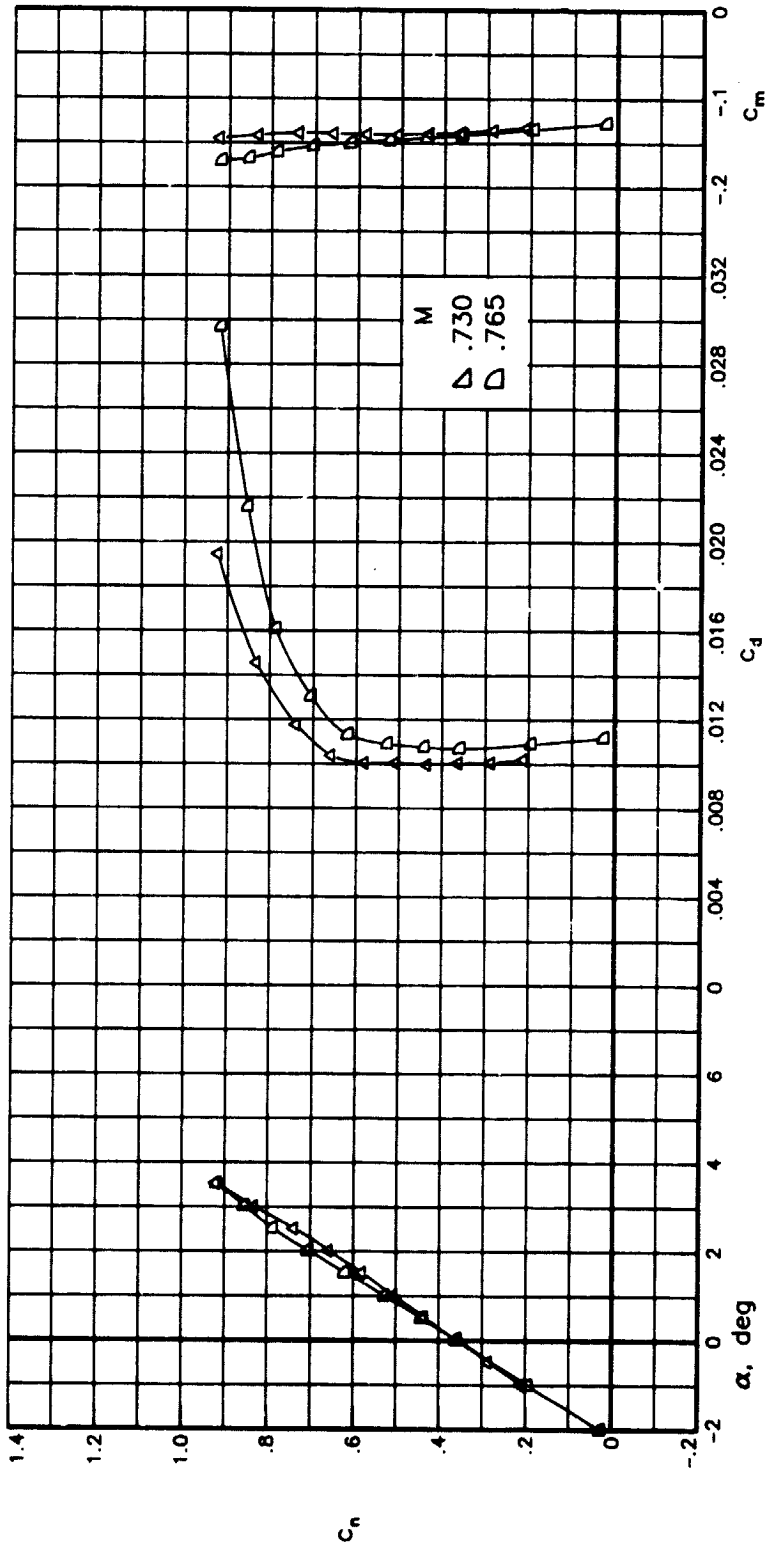

Figure 55.- Effect of Mach number on aerodynamic characteristics of airfoil with fixed transition at $R = 6.0 \times 10^6$ and $\bar{n}_{bl} = 2.0$.

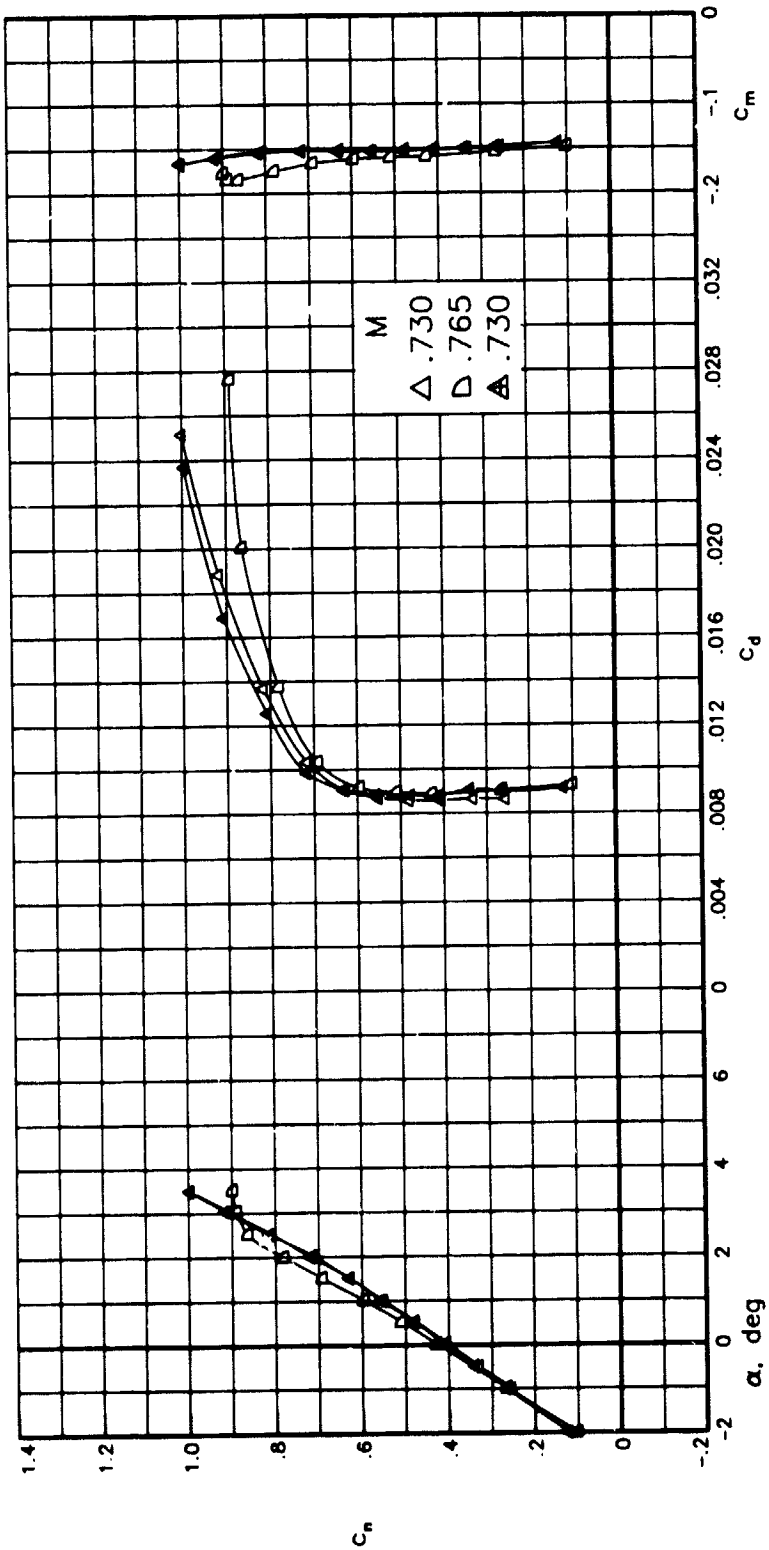

Figure 56.- Effect of Mach number on aerodynamic characteristics of airfoil with fixed transition at $R = 15.0 \times 10^6$ and $\dot{m}_{bl} = 0$.

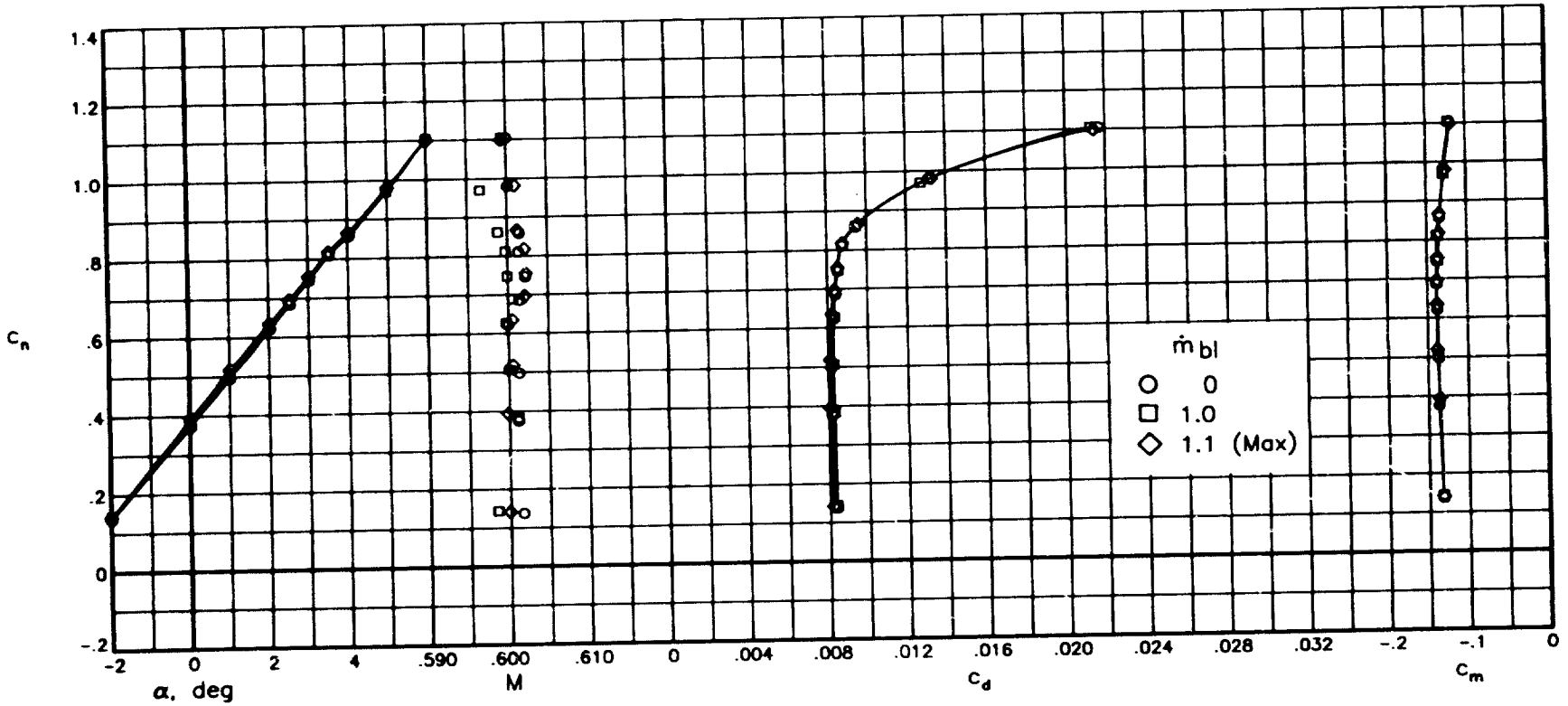

Figure 57.- Effect of sidewall-boundary-layer removal on aerodynamic characteristics of airfoil with free transition at $M \approx 0.600$ and $R \approx 15.0 \times 10^6$.

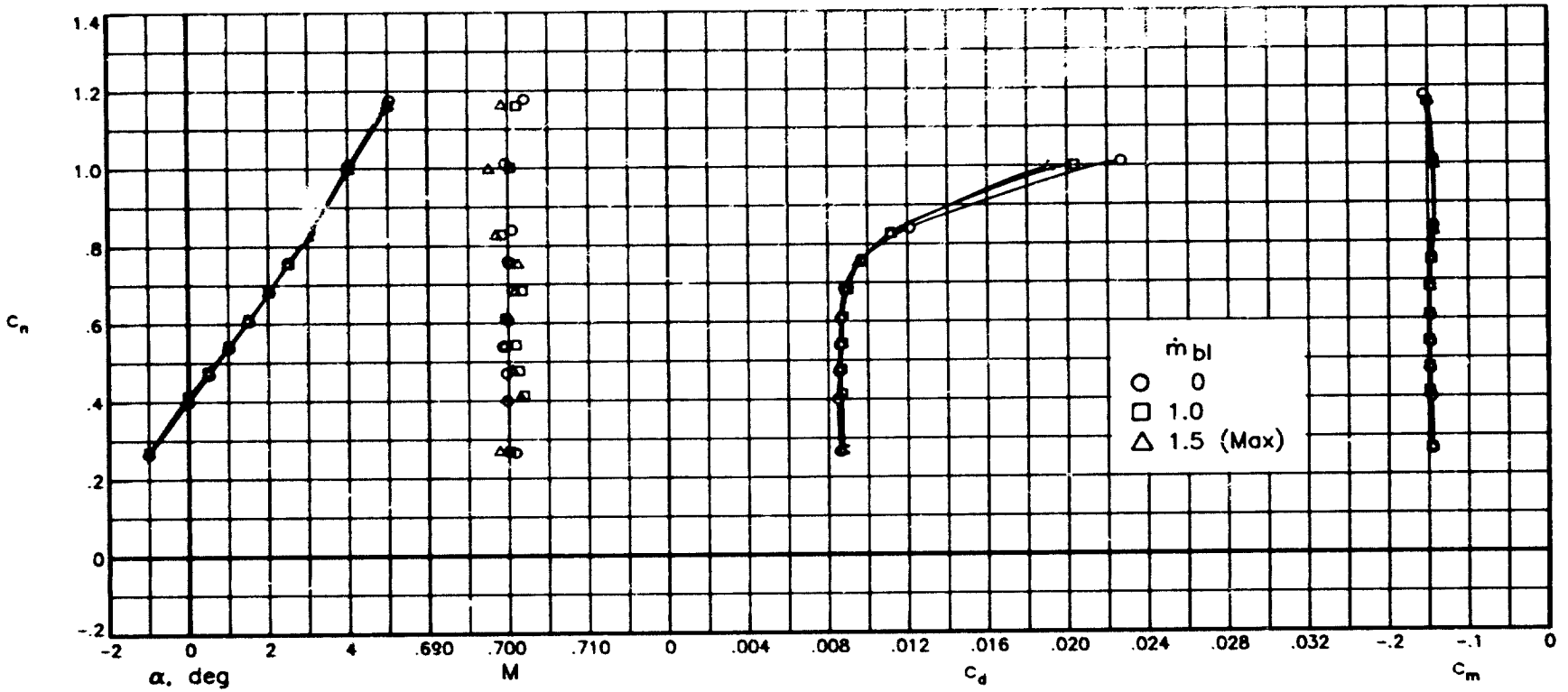

Figure 58.- Effect of sidewall-boundary-layer removal on aerodynamic characteristics of airfoil with free transition at $M = 0.700$ and $R = 15.0 \times 10^6$.

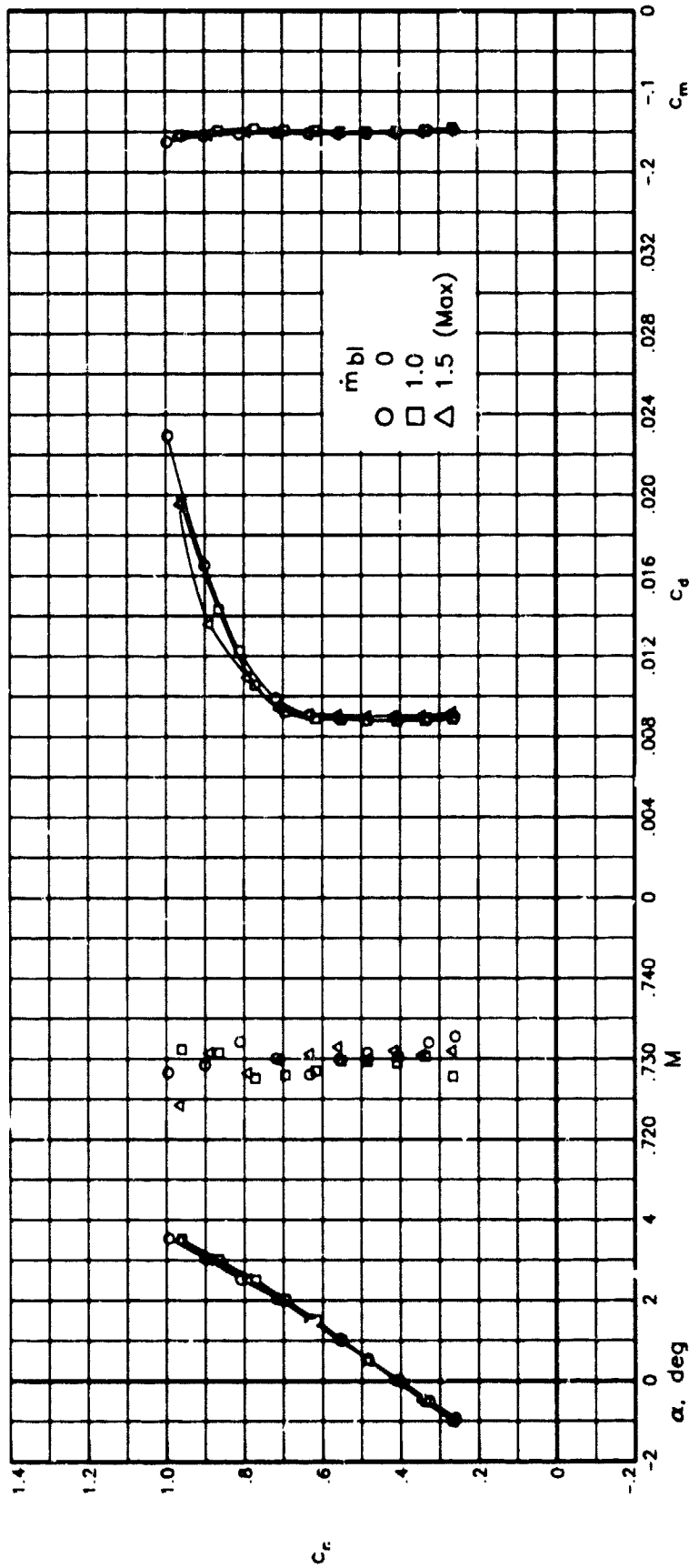

Figure 59.- Effect of sidewall-boundary-layer removal on aerodynamic characteristics of airfoil with free transition at M = 0.730 and R = 15.0 × 10^6.

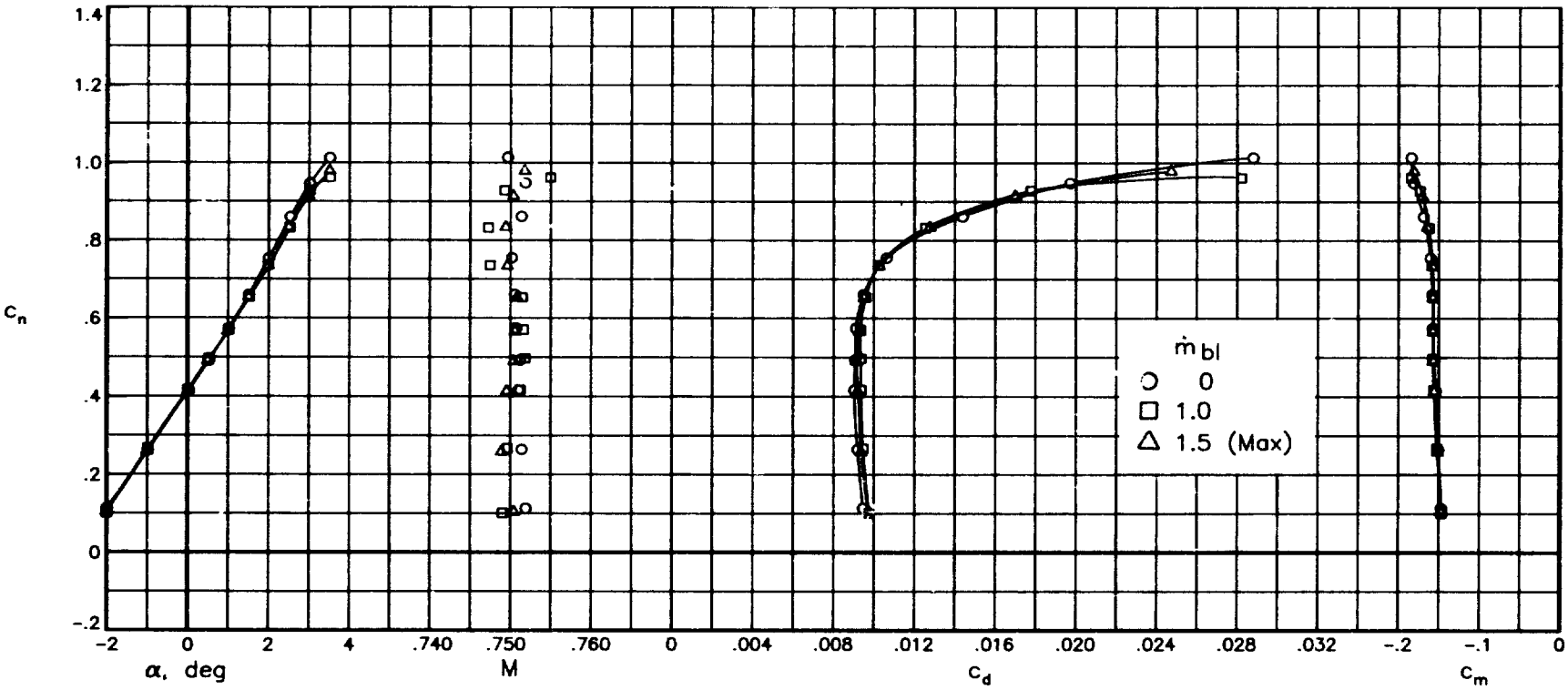

Figure 60.- Effect of sidewall-boundary-layer removal on aerodynamic characteristics of airfoil with free transition at $M \approx 0.750$ and $R \approx 15.0 \times 10^6$.

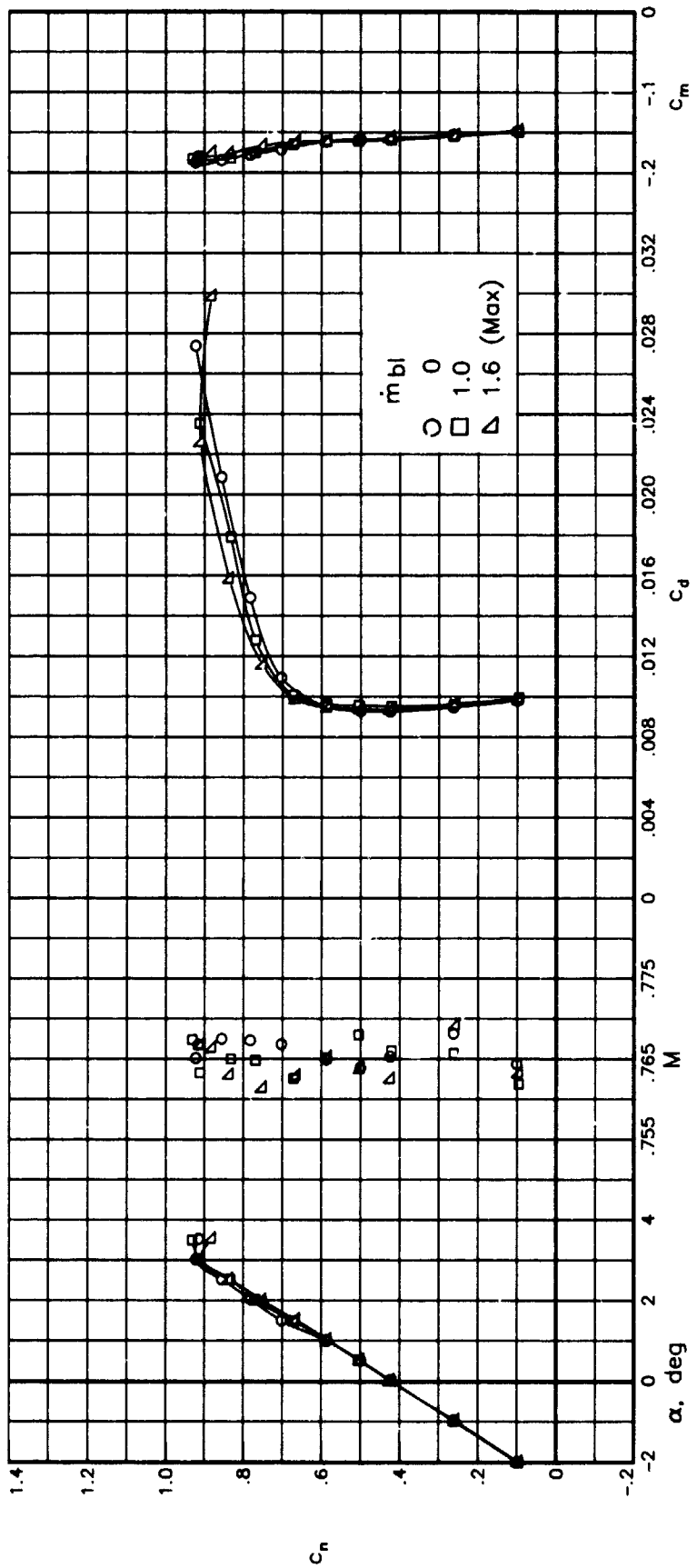

Figure 61.- Effect of sidewall-boundary-layer removal on aerodynamic characteristics of airfoil with free transition at M = 0.765 and R = 15.0 × 10^6.

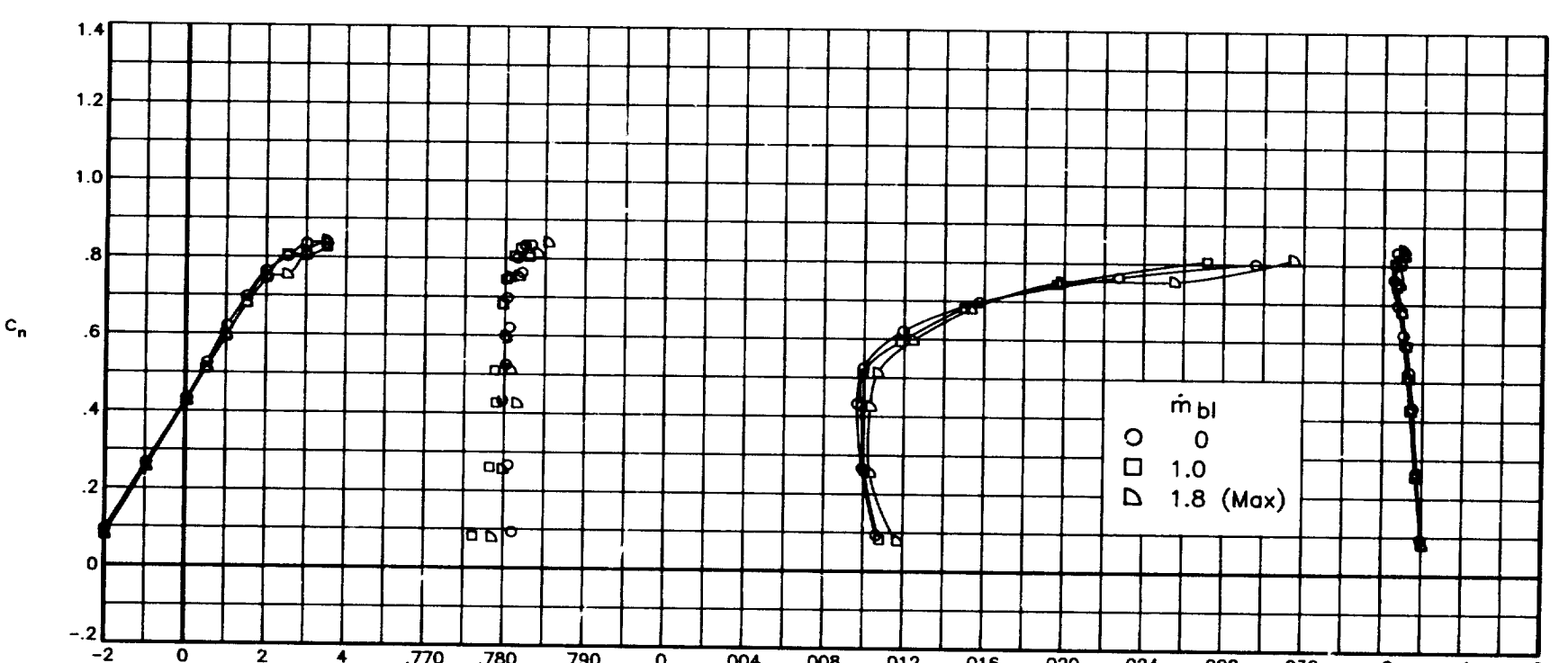

Figure 62.- Effect of sidewall-boundary-layer removal on aerodynamic characteristics of airfoil with free transition at $M \approx 0.780$ and $R \approx 15.0 \times 10^6$.

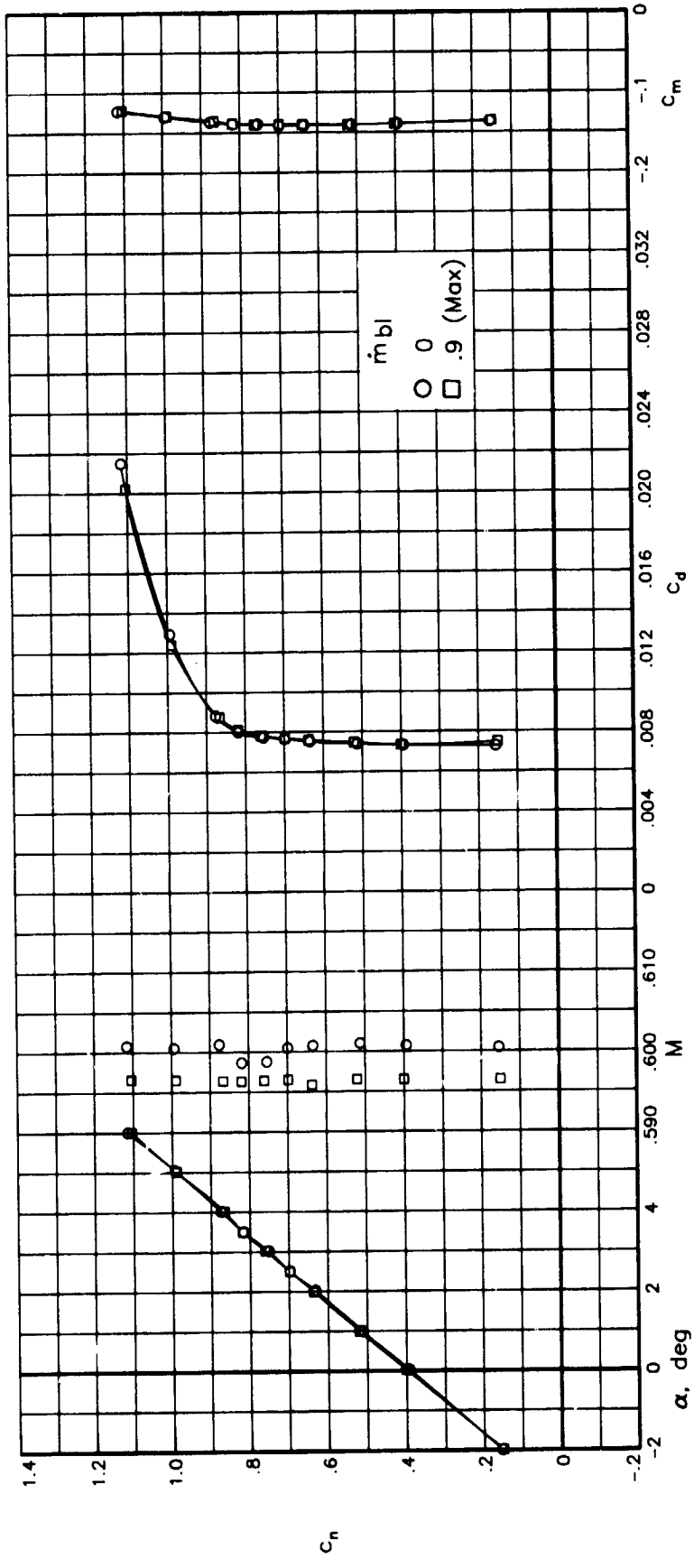

Figure 63.- Effect of sidewall-boundary-layer removal on aerodynamic characteristics of airfoil with free transition at M ≈ 0.600 and R ≈ 30.0 × 10^6.

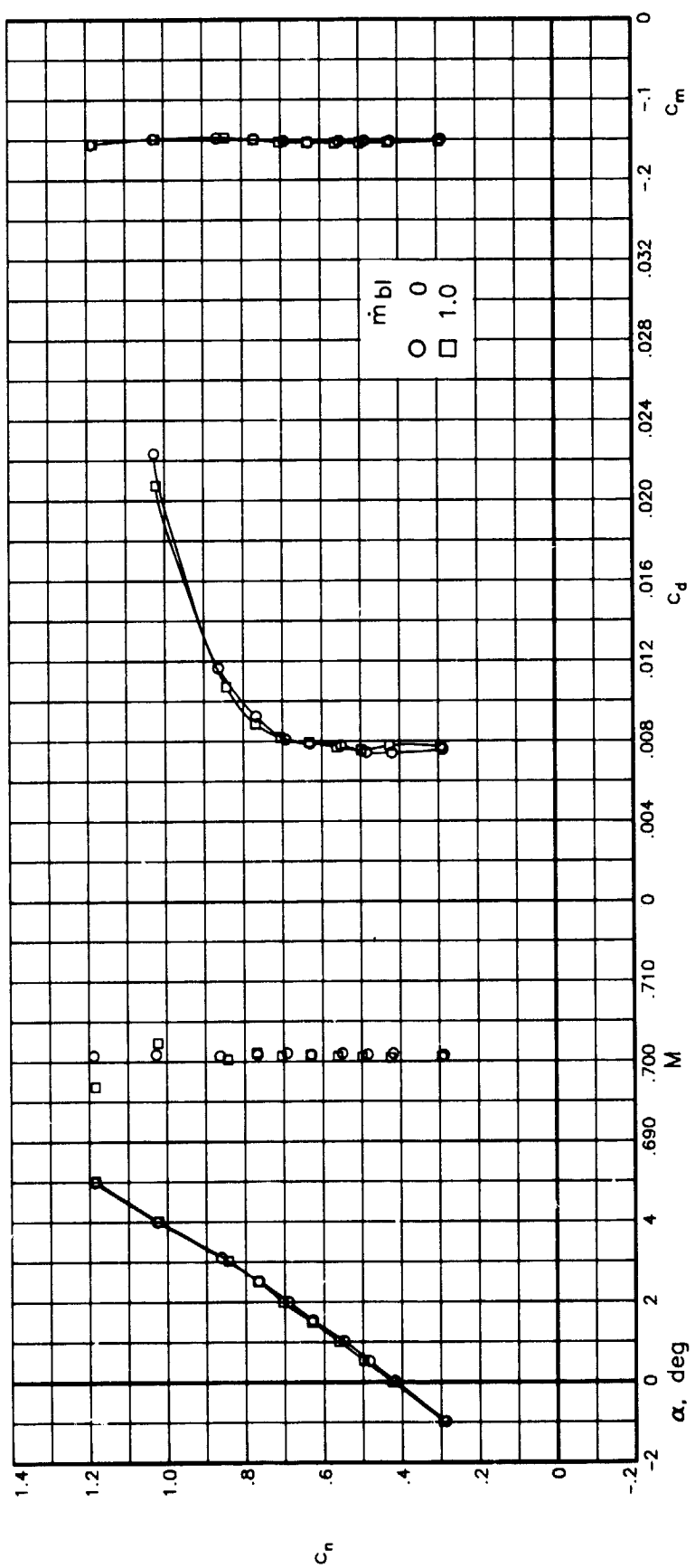

Figure 64.- Effect of sidewall-boundary-layer removal on aerodynamic characteristics of airfoil with free transition at M = 0.700 and R = 30.0 × 10^6.

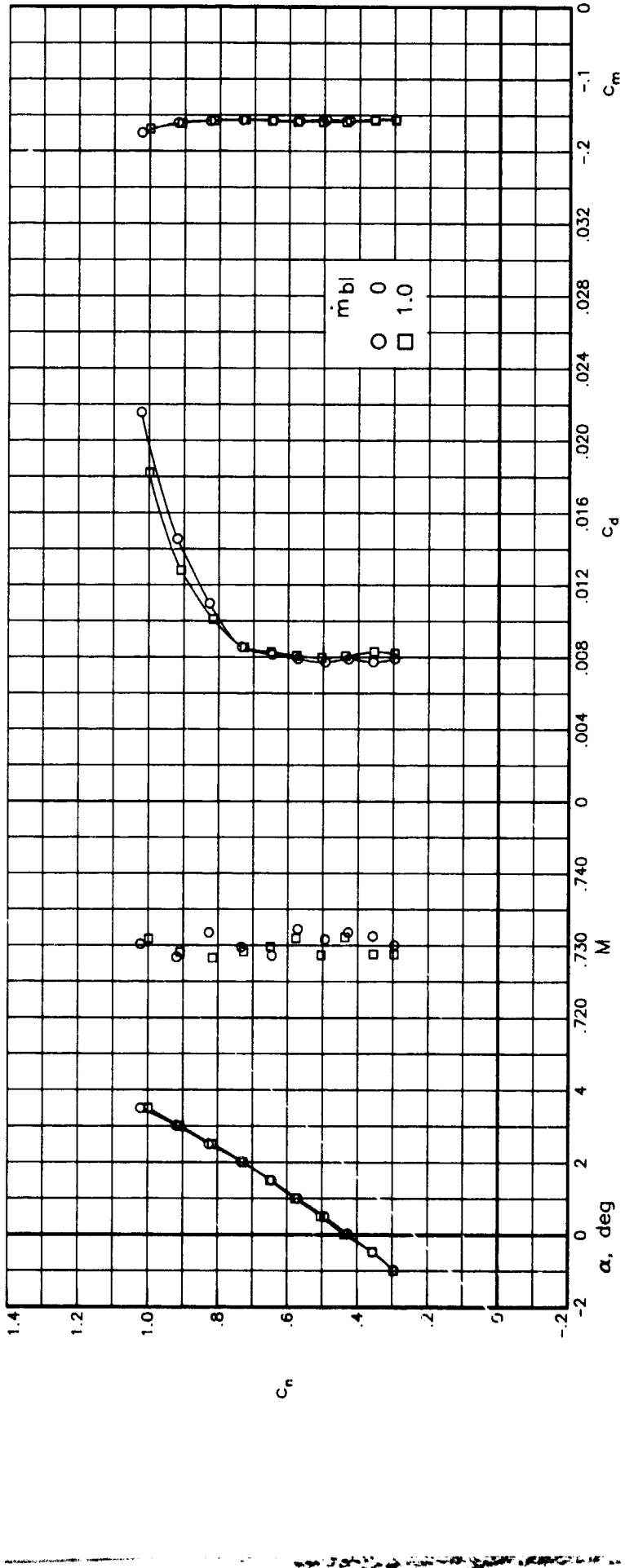

Figure 65.- Effect of sidewall-boundary-layer removal on aerodynamic characteristics of airfoil with free transition at M = 0.730 and R = 30.0 × 10^6.

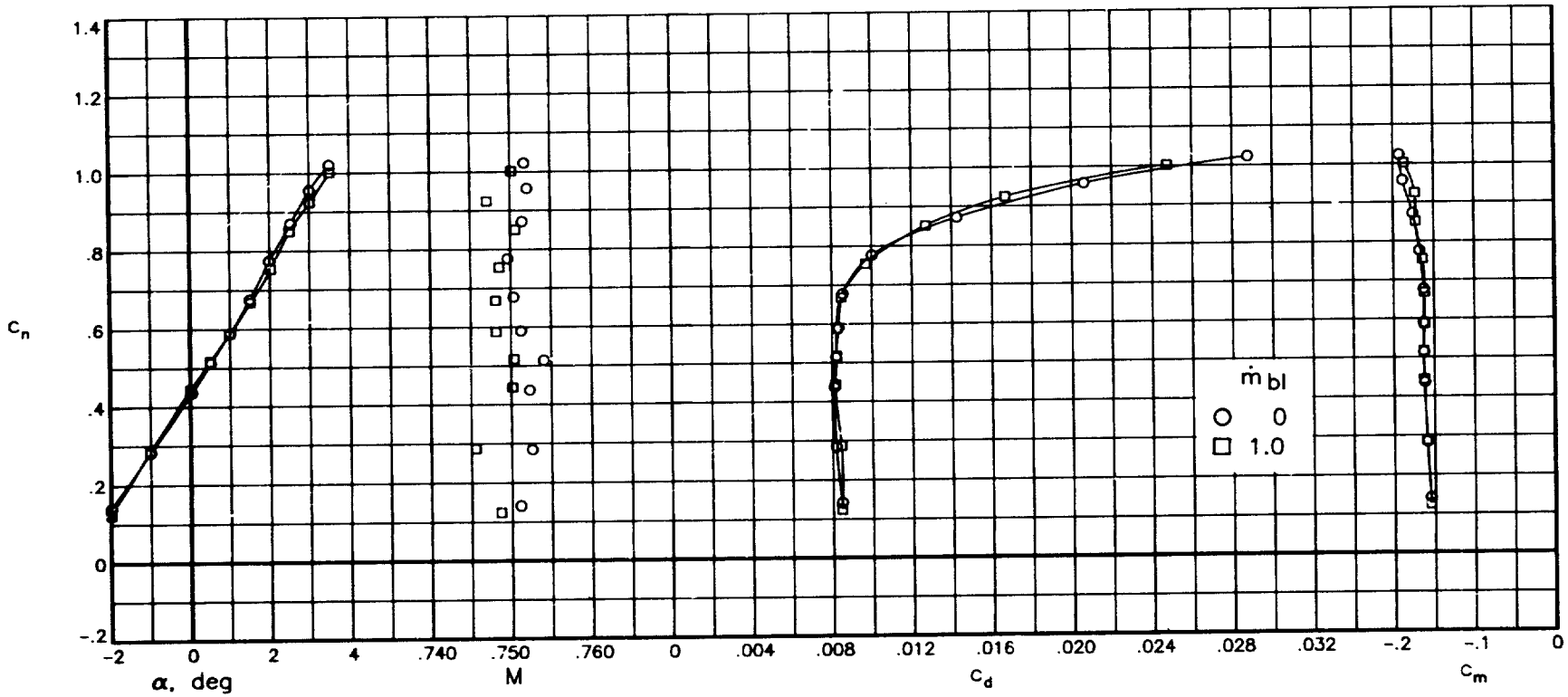

Figure 66.- Effect of sidewall-boundary-layer removal on aerodynamic characteristics of airfoil with free transition at $M \approx 0.750$ and $R \approx 30.0 \times 10^6$.

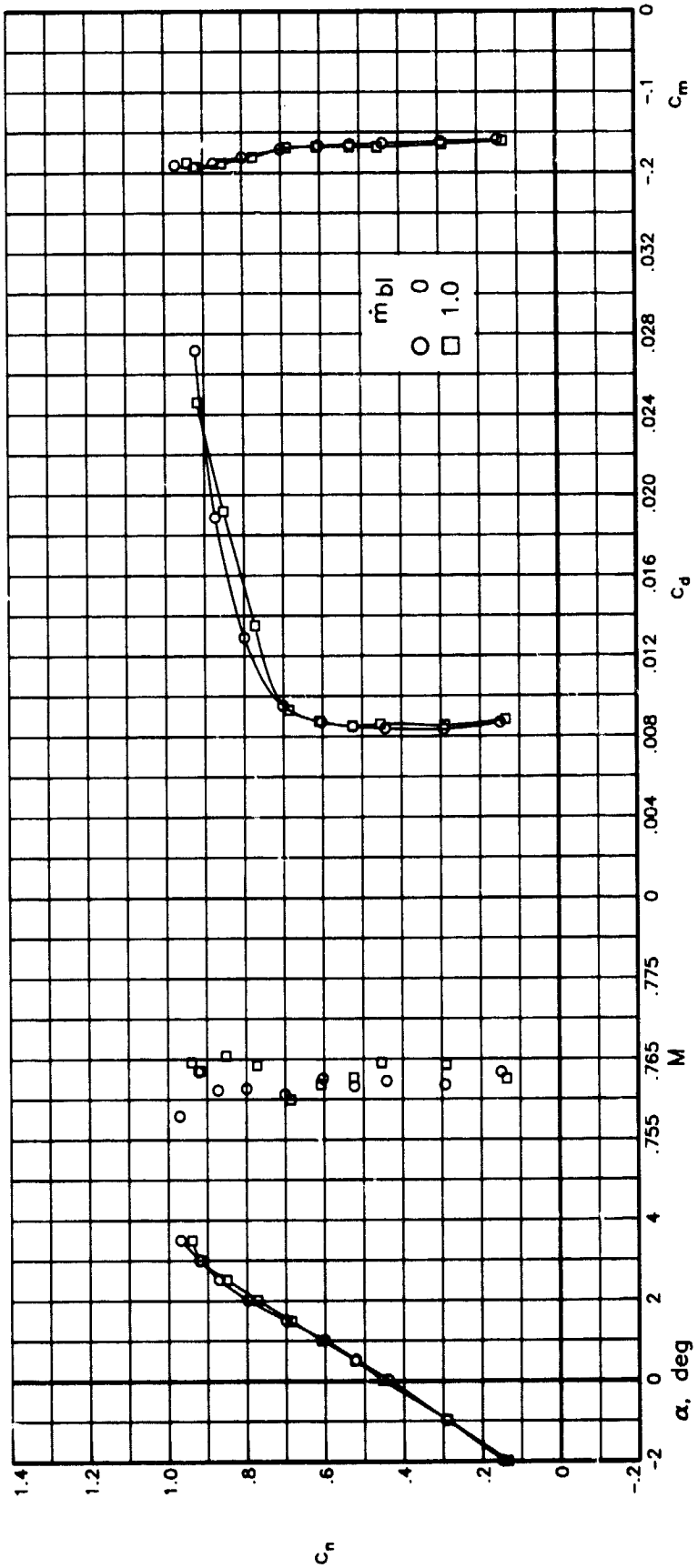

Figure 67.- Effect of sidewall-boundary-layer removal on aerodynamic characteristics of airfoil with free transition at M = 0.765 and R = 30.0 × 10^6.

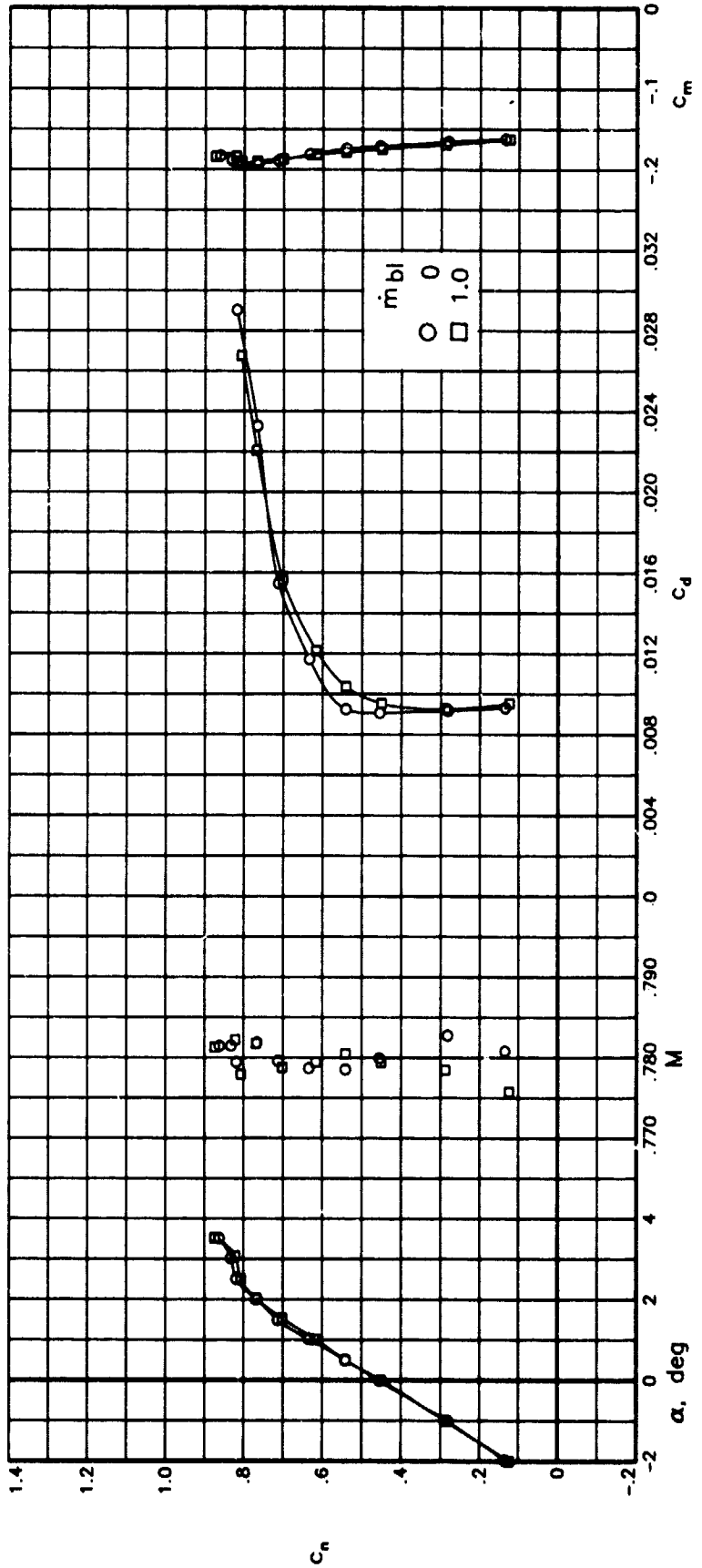

Figure 68.- Effect of sidewall-boundary-layer removal on aerodynamic characteristics of airfoil with free transition at M = 0.780 and R = 30.0 × 10^6.

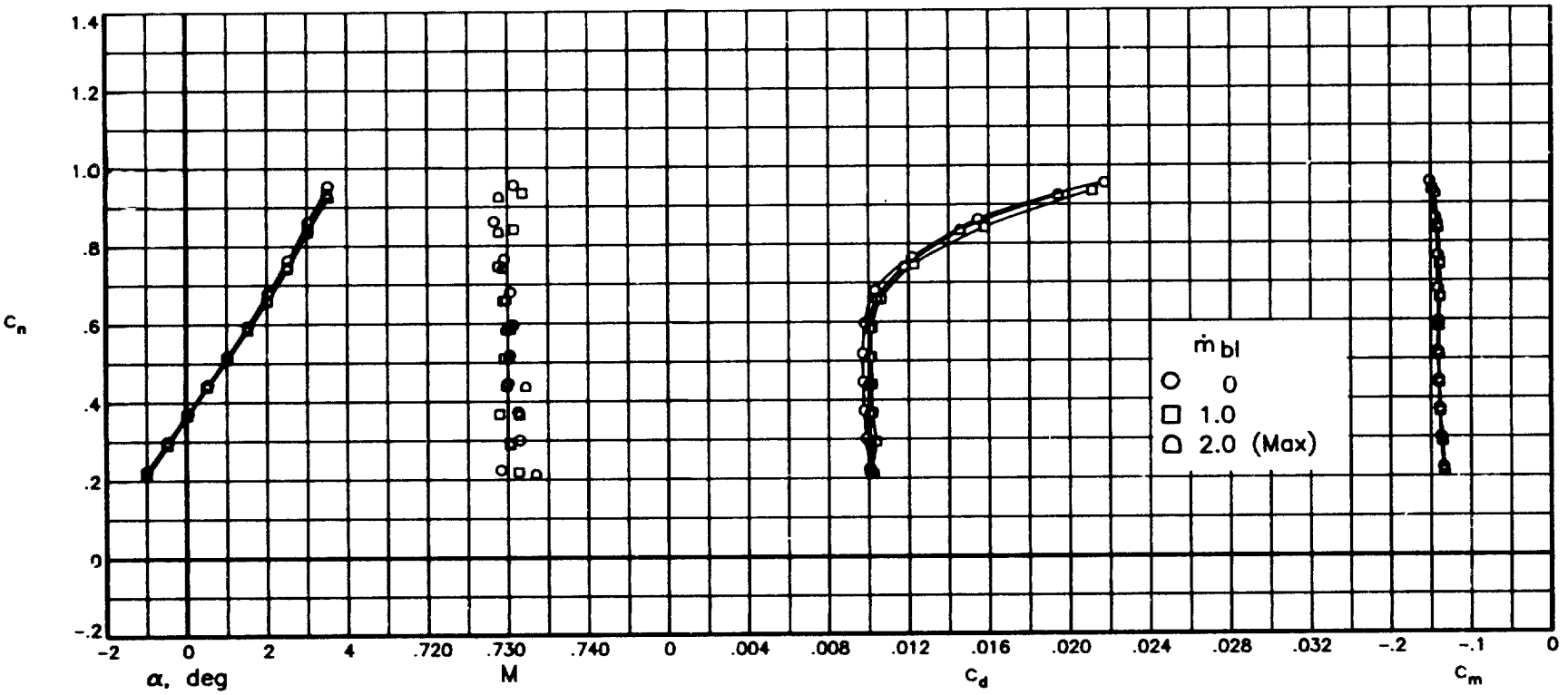

Figure 69.- Effect of sidewall-boundary-layer removal on aerodynamic characteristics of airfoil with fixed transition at $M \approx 0.730$ and $R \approx 6.0 \times 10^6$.

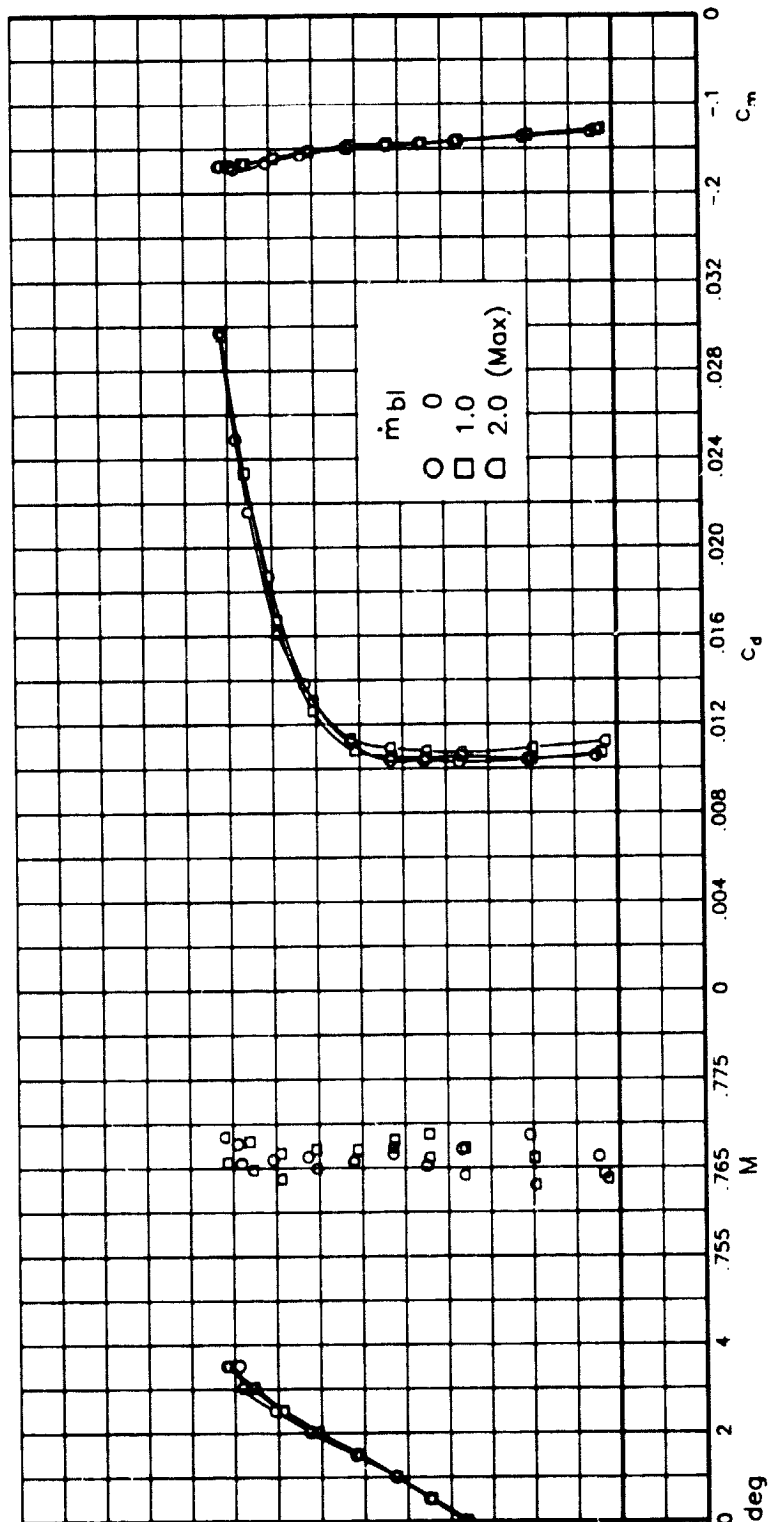

Figure 70.- Effect of sidewall-boundary-layer removal on aerodynamic characteristics of airfoil with fixed transition at M = 0.765 and R = 6.0 × 10^6.

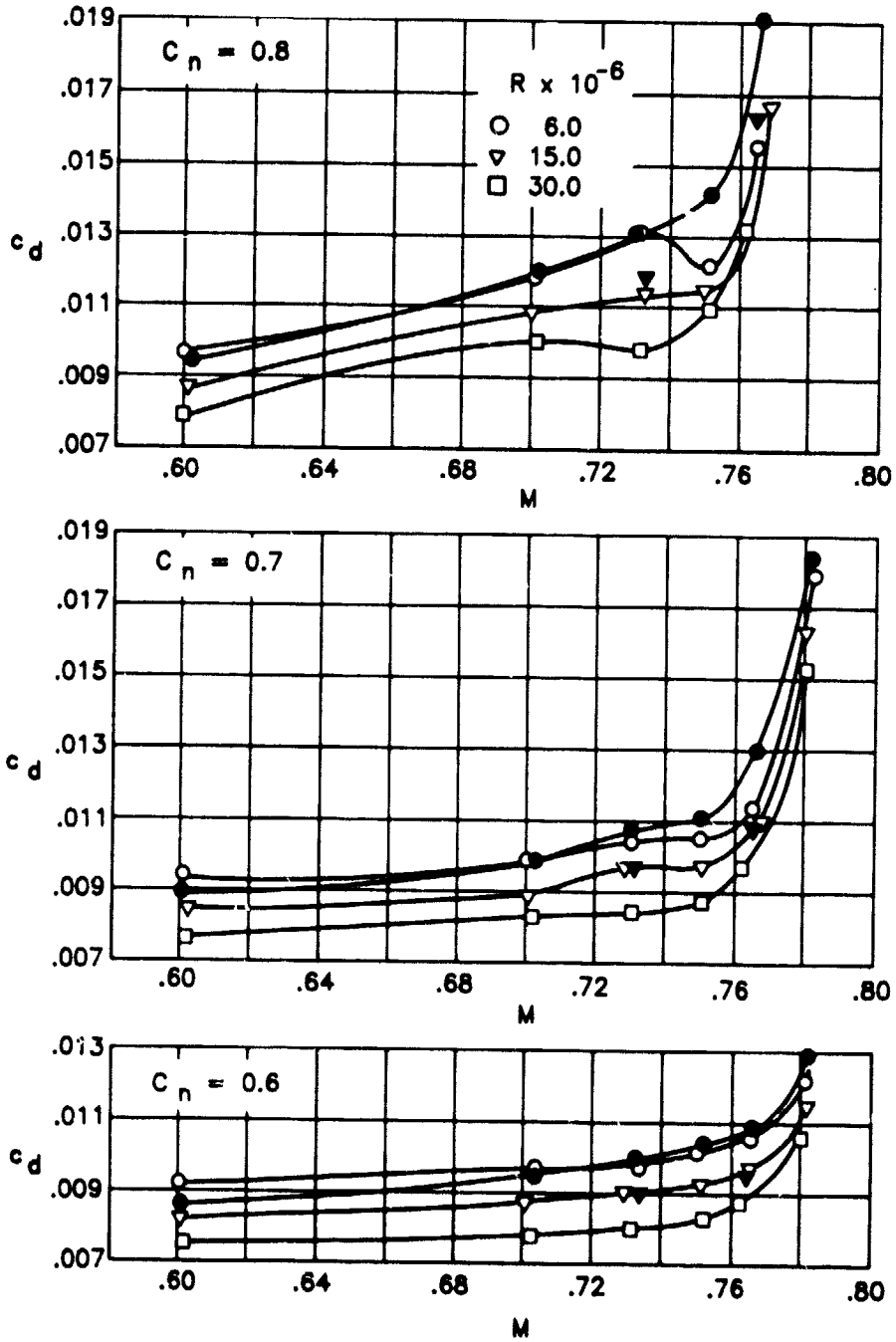

Figure 71.- Effect of Reynolds number on variation of section drag coefficient with Mach number with no sidewall-boundary-layer removal. (Solid symbols indicated fixed transition; open symbols indicate free transition.)

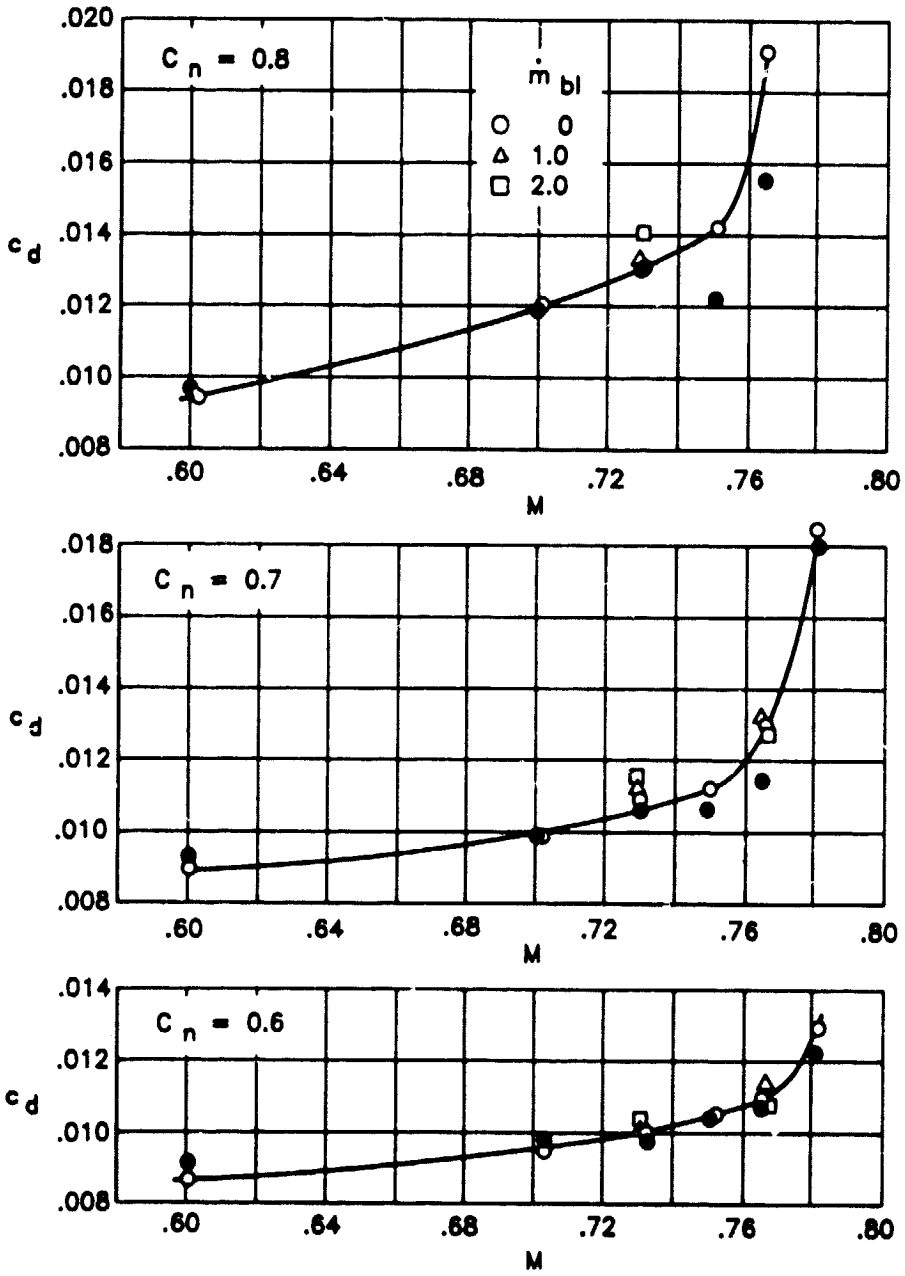

(a) $R = 6.0 \times 10^6$ (solid symbols indicate free transition; open symbols indicate fixed transition).

Figure 72.- Effect of sidewall-boundary-layer removal on variation of section drag coefficient with Mach number.

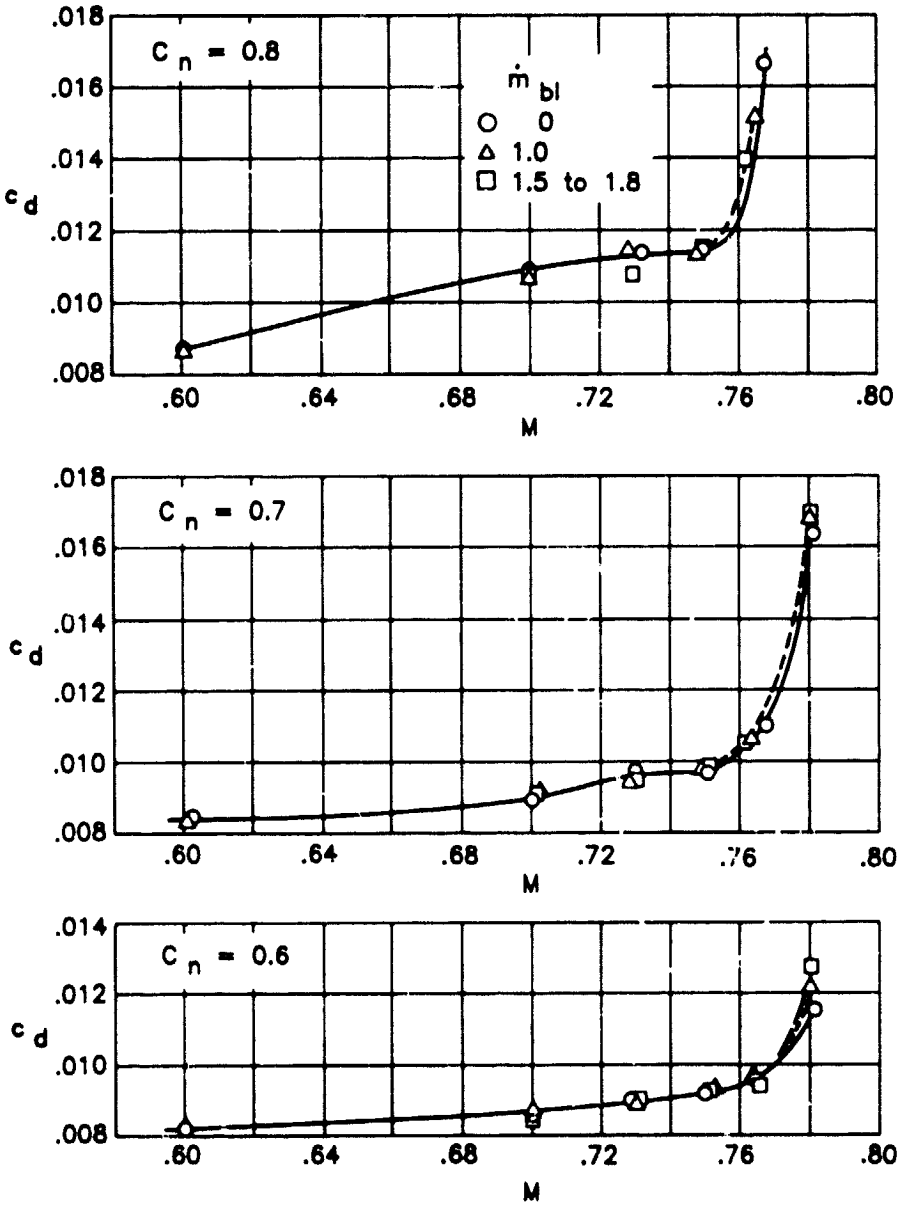

(b) $R = 15.0 \times 10^6$ (free transition).

Figure 72.- Continued.

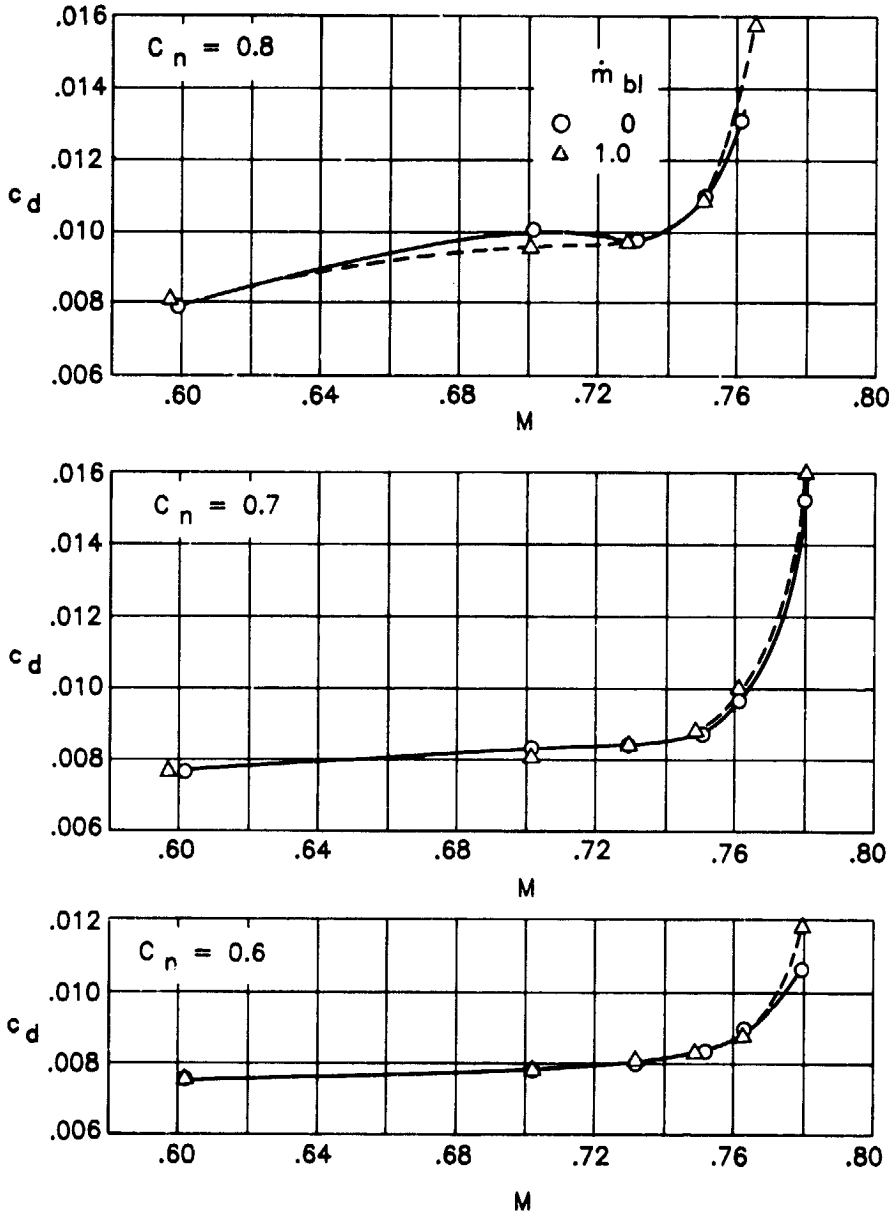

(c) R ≈ 30.0 × 10^6 (free transition).

Figure 72.- Concluded.

1. Report No.	2. Government Accession No.	3. Recipient's Catalog No.
NASA TM-87663		

4. Title and Subtitle	5. Report Date
High Reynolds Number Tests of a Douglas DLBA 032 Airfoil in the Langley 0.3-Meter Transonic Cryogenic Tunnel	May 1986
	6. Performing Organization Code: 505-61-01-02
7. Author(s): Charles B. Johnson, David A. Dress, Acquilla S. Hill, Peter A. Wilcox, and Minh H. Bui	8. Performing Organization Report No.: L-16083
9. Performing Organization Name and Address: NASA Langley Research Center, Hampton, VA 23665-5225	10. Work Unit No.
	11. Contract or Grant No.
12. Sponsoring Agency Name and Address: National Aeronautics and Space Administration, Washington, DC 20546-0001	13. Type of Report and Period Covered: Technical Memorandum
	14. Sponsoring Agency Code

15. Supplementary Notes

Charles B. Johnson, David A. Dress, and Acquilla S. Hill: Langley Research Center, Hampton, Virginia.
Peter A. Wilcox and Minh H. Bui: Douglas Aircraft Company, Long Beach, California.

16. Abstract

A wind-tunnel investigation of a Douglas advanced-technology airfoil was conducted in the Langley 0.3-Meter Transonic Cryogenic Tunnel (0.3-m TCT). This investigation represents the last in a series of NASA/U.S. industry two-dimensional airfoil studies in the Advanced Technology Airfoil Tests program. Test temperature was varied from 227 K (409°R) to 100 K (180°R) at pressures ranging from about 159 kPa (1.57 atm) to about 514 kPa (5.07 atm). Mach number was varied from 0.50 to 0.78. These variables provided a Reynolds number range (based on airfoil chord) from 6.0×10^6 to 30.0×10^6. This investigation was specifically designed to (1) test a Douglas airfoil from moderately low to flight-equivalent Reynolds numbers; and (2) evaluate sidewall-boundary-layer effects on transonic airfoil performance characteristics by a systematic variation of Mach number, Reynolds number, and sidewall-boundary-layer removal. Data are included which demonstrate the effects of fixing transition, Mach number, Reynolds number, and sidewall-boundary-layer removal on the aerodynamic characteristics of the airfoil. Also included are remarks on model design and model structural integrity. Airfoil pressure distributions are not included.

17. Key Words (Suggested by Authors(s))	18. Distribution Statement
Sidewall-boundary-layer removal Two-dimensional airfoil Cryogenic wind tunnel High Reynolds number	[redacted] Subject Category 02

19. Security Classif.(of this report)	20. Security Classif.(of this page)	21. No. of Pages	22. Price
Unclassified	Unclassified	123	

NASA-Langley, 1986